OPTIMISATION SOFTWARE, INC.

F I N A L R E P O R T

OPTIMIZATION AND SIMULATION OF FLIGHT CONTROL LAWS UNDER PARAMETER UNCERTAINTY AND EXTERNAL DISTRUBANCES.

Contract No. NASW-3158

Dec. 1, 1979

Optimization Software Inc.,
1100 Glendon Ave.,
Los Angeles,Calif. 90024

CONTENTS

LIST OF FIGURES

LIST OF TABLES

SUMMARY

Several tasks pertinent to flight control in parameter uncertainty and wind-gust loading have been successfully completed.

Identification Algorithms for extracting stability and control derivatives from flight data taking gust loading into account have been developed. They have been verified by simulation and evaluated throughly on actual flight data taken on a Lockheed Jet Star flying in turbulence. In particular the need for automatically generated dither-like inputs has been studied.

Criteria for performance evaluation using stochastic models have been developed for gust alleviation as well as handling qualities. Algorithms for assessing degradation in performance due to parameter uncertainty have been developed and evaluated using flight test data (Lockheed Jet Star).

INTRODUCTION

This report deals with the general problem of flight control taking into account parameter uncertainty and wind gust loading. The following specific tasks were undertaken:

Task A. Develop criteria for assessment of control performance for uncertain systems with particular reference to flight control under parameter uncertainty and gust loads.

Task B. Develop identification algorithms for stability and control derivatives from flight data taking gust loading into account, and assessing the need for automatically generated dither-like inputs.

Task C. Evaluate the performance of identification algorithms for typical flight conditions.

The report is organized generally in order of these tasks.

We begin in section 1 with the problem of control performance assessment. We consider two kinds of performance evaluation: Windgust Alleviation and Handling Quality Improvement. We develop a general theory

in section 1.1 which embraces indices of performance for both categories, and present formulas for assessing degradation in performance due to parameter uncertainty. In section 1.2 we illustrate the theory by evaluating the degradation in gust alleviation for typical flight conditions using Lockheed Jet Star data. In particualr we use stability and control parameters obtained with dither-like inputs as reflecting uncertainty in parameters, and in this way assess the efficacy of dither-like inputs for parameter identification in flight test data containing gust loading. A new handling quality criterion is developed in section 1.3 using a stochastic pilot input model (see L. W. Taylor [1]) as well as the corresponding optimal feedback control.

Section 2 is devoted to Task B. Using a continous-time white noise theory developed by the Principal Investigator, a maximum likelihood identification algorithm for flight test data containing wind gust response is developed in sections 2.1 and 2.2. The first results using this theory were reported by K. W. Iliff in his UCLA thesis [2]. The specifics of the algorithms employed in the present work are quite different however. The algorithms were verified by simulating longitudinal short period motion accounting for vertical wind gust modelled by the Dryden Spectrum. The simulation results are presented in section 2.3.

The bulk of the results presented in this report is contained in section 3 where we evaluate the performance of identification algorithms (developed in section 2.2) for typical flight conditions, as required under task C. Flight test data taken on a Lockheed Jet Star flying in heavy turbulence (obtained courtesy of DFRC) was used. The time-history of about 60 seconds was divided into several sections and the data in each

section analysed separately. The stability and control derivatives were extracted as well as the gust intensity. Moreover the vertical gust velocity wave-form has been reconstructed and the corresponding power density spectrum plotted. The results generally agree with those of [2], and provide a thorough and extensive evaluation of the identification algorithms for typical flight conditions.

Section 4 utilized the Jet Star flight data to study the efficacy of using dither-like inputs in place of conscious pilot inputs. Two meneuvers not containing pilot input were used for this purpose and the algorithms used to determine the derivatives. The extracted values are compared with the derivatives obtained during an adjacent maneuver with a significant pilot input.

All the tasks, A, B, and C have been successfully completed, as the report will indicate.

Finally, and Appendix (Appendix I) examines a basic question in flight-test data processing: whether system models should be time-discrete or time-continuous. It is shown that for type of flight-test data considered the continuous-time model is to be preferred.

1. ASSESSMENT OF CONTROL PERFORMANCE UNDER PARAMETER UNCERTAINTY AND GUST LOADING

1. ASSESSMENT OF CONTROL PERFORMANCE UNDER PARAMETER UNCERTAINTY AND GUST LOADING.

1.1 The Basic Formulas

In this section we develop some general formulas for the assessment of the degradation in control performance due to parameter uncertainty. As we shall show in Section 3, it is general enough in formulation to include both gust alleviation and handling quality criteria.

We begin with the linearized state equations of motion:

$$\left.\begin{aligned} \dot{x}(t) &= Ax(t) + Bu(t) + F\,n(t) \\ y(t) &= Cx(t) + G\,n(t) \end{aligned}\right\} \qquad (1.1)$$

where $x(t)$ is the state (enhanced as necessary to take care of the wind gust model with the Dryden or similar rational spectrum), and $y(t)$ represents the sensor data available. The matrix A represents the stability derivatives, and the matrix B contains the control derivatives,

$$G\,G^* = I$$

$$F\,G^* = 0,$$

and $n(t)$ is white Gaussian with unit spectral density. The performance criterion is:

$$(1/T)\int_0^T (E(||Lx(t)||^2 + \lambda||u(t)||^2)\,dt \qquad (1.2)$$

where L is a matrix that determines the variable to be minimised (e.g. the

normal acceleration), and λ is a suitably chosen positive number to yield the appropriate level of control constraint. E denotes expected value. We are interested primarily in the case where T is large (or, $T \to \infty$, in theory).

We know that the optimal control that minimises the performance criterion chosen is given by:

$$u_o(t) = -B^* P_c \hat{x}_o(t) / \lambda \tag{1.3}$$

where P_c satisfies the Control Riccatti Equation:

$$\dot{P}_c(t) + A^* P_c(t) + P_c(t)A + L^*L - P_c(t)BB^*P_c(t) / \lambda = 0$$
$$P_c(T) = 0$$

As we have indicated, we are primarily interested in the case of 'large' T, so that we may use the 'steady state' version, setting the time derivative to be zero:

$$A^*P_c + P_cA + L^*L - P_c B B^* P_c / \lambda = 0 \tag{1.4}$$

The Kalman estimate $\hat{x}(t)$ is defined by:

$$\dot{\hat{x}}(t) = A\hat{x}(t) + B u_c(t) + P_f C^*(y(t)-C\hat{x}(t)) \tag{1.5}$$

where, consistent with out steady state view-point, we shall take the initial estimate $\hat{x}(0)$ to be zero, and P_f the filter matrix satisfies:

$$A P_f + P_f A^* + FF^* - P_f C^* C P_f = 0 \tag{1.6}$$

For the optimal system, the performance functional

$$J = \lim_{T \to \infty} \left(\frac{1}{T}\right) \int_o^T ||L x(t)||^2 dt \tag{1.7}$$

$$= Tr\,(L^* L P_f + L^* L J_a)$$

where

$$\left(\frac{A-BB^*P_c}{\lambda}\right) J_a + J_a \left(\frac{A-BB^*P_c}{\lambda}\right) + P_f C^* C P_f = 0$$

Of course, to achieve the value of the performance criterion given by (1.7) we will need to know the systems parameter values exactly. Our task now is to determine what happens when the parameters are unknown, and have to be estimated by an identification algorithm, or other means. Let us denote the estimated parameter matrices by the subscript e. Then the feedback control will be determined as:

$$u_o(t) = -B_e^*(P_{c,e}/\lambda)\,\hat{x}(t) \tag{1.8}$$

where

$$A_e^* P_{c,e} + P_{c,e} A_e + L_e^* L_e - (1/\lambda) P_{c,e} B_e B_e^* P_{c,e} = 0 \tag{1.9}$$

$$\left.\begin{aligned} \dot{\hat{x}}(t) &= A_e \hat{x}(t) + B_e u_o(t) + P_{f,e} C_e^* (y(t) - C_e \hat{x}(t)) \\ \hat{x}(0) &= 0. \end{aligned}\right\} \tag{1.10}$$

$$A_e P_{f,e} + P_{f,e} A_e^* + F_e F_e^* - P_{f,e} C_e C_e^* P_{f,e} = 0 \qquad (1.11)$$

The problem now is to calculate the functional J for this choice of optimal control. We know of course that it will be larger than that given by (1.7). We can calculate it as follows. Let

$$z(t) = \begin{bmatrix} x(t) \\ \hat{x}(t) \end{bmatrix} \qquad (1.12)$$

Under the choice (1.8) thru (1.11), we have:

$$\dot{x}(t) = A\,x(t) - (1/\lambda)\, B\, B_e^*\, P_{c,e}\, \hat{x}(t) + F\, n(t) \qquad (1.13)$$

$$\dot{\hat{x}}(t) = (A_e - P_{f,e}\, C_e^*\, C_e)\, \hat{x}(t) + P_{f,e}\, C_e^* (C\,x(t) + G\,n(t)) - B_e\, B_e^*\, P_{c,e}\, \hat{x}(t)/\lambda \qquad (1.14)$$

where we substituted for y(t) from (1.1). We can rewrite these equations in the form:

$$\dot{z}(t) = A_e z(t) + H_e\, n(t)$$

where A_e is the compound matrix:

$$A_e = \begin{bmatrix} A & -B B_e^*\, P_{c,e}/\lambda \\ P_{f,e}\, C_e^* C & A_e - P_{f,e} C_e^*\, C_e - B_e B_e^* P_{c,e}/\lambda \end{bmatrix} \qquad (1.15)$$

$$H_e = \begin{bmatrix} F \\ P_{f,e}\, C_e^*\, G \end{bmatrix}$$

Then letting K denote the compound matrix:

$$K = L \quad 0$$

and

$$M = 0 \quad I$$

so that:

$$L\,x(t) = K\,z(t)$$

$$M\,z(t) = x(t)$$

and defining

$$R_e = \text{Lim}\, E(\ z(t)\ \ z(t)^*)$$

we have

$$J = \lim\ (1/T) \int_0^T ||Lx(t)||^2 dt \quad = \text{Tr.}\ K^*K\ R_e \quad (1.17)$$

Of course this simplifies to (1.7) when the parameters are correct. We note that R_e may be computed by solving the linear equation:

$$A_e R_e + R_e A_e^* + H_e H_e^* = 0$$

The actual degradation in performance is of course the difference between (1.17) and (1.7). The calculation however can be made more efficient by noting that the difference will be small and is well approximated by the linear terms only. In other words, denoting the

difference by ΔN, we have:

$$\Delta N = \text{Tr.} \quad (K^* K \, \Delta R_e)$$

where ΔR_e can be calculated by the linear approximation equation:

$$A \Delta R + (\Delta R) A^* + (\Delta A) R + R(\Delta A)^* + H(\Delta \Xi)^* + (\Delta H) H^* = 0 \quad (1.20)$$

And ΔP_c is calculated from:

$$(A^* - (1/\lambda) P_c \; B \, B^*)(\Delta P_c) + \text{Adjoint} + L^* \Delta L + (\Delta L)^* L$$
$$+ (\Delta A)^* P_c + P_c \, \Delta A - P_c (\Delta B) B^* P_c / \lambda - \text{Adjoint} = 0 \quad (1.21)$$

Similarly, ΔP_f is obtained from the liner equation:

$$(A - P_f \, C \, C^*) \Delta P_f + \text{Adjoint} + ((\Delta \Gamma)^* + \Gamma (\Delta \Gamma)^* - P_f (\Delta C) \, C^* P_f - \text{Adjoint}$$
$$+ (\Delta A) P_f + P_f (\Delta A)^* = 0 \quad (1.22)$$

1.2 Application to Jet Star

We now specialise the formulas of the previous section to calculate the degradation in control performance due to uncertainty in the parameters to the case of the Lockheed Jet Star. We consider the linearised longitudinal short period motion equations:

$$\dot{\alpha} = Z_\alpha \alpha + \dot{\theta} + Z_{\delta e}\ \delta_e + Z_\alpha\ \frac{w_g}{v}$$

$$\ddot{\theta} = M_\alpha \alpha + M_{\dot{\theta}} \dot{\theta} + M_{\delta e}\ \delta_e + M_\alpha\ \frac{w_g}{v}$$

$$\dot{\delta}_e = -20\ \delta_e + 20\ \delta_\rho$$

where δ_e is the elevetor deflection due to the pilot input δ_ρ (we are neglecting the servo-actuator non-linearity), and the other quantities are as before. We assume a Dryden spectrum for the vertical component of the gust velocity, and hence we can write:

$$\alpha_g = \frac{w_g}{v},$$

$$\dot{\alpha}_g = \frac{-v}{L_1}\ \alpha_g + \sigma_1\ \left(\sqrt{2|vL_1}\right)\ N(t)$$

where $N(\cdot)$ is white Gaussian with unit spectral density, L_1 is the scale lenght of the turbulance. The break frequency (radians|sec) is:

$$\omega_c = \frac{v}{L_1}$$

and the intensity is:

$$\frac{\sigma_1^2}{v^2}$$

We take

$$L_1 = 1000$$

in this section.

The sensor measurements are:

$q \sim$ Pitch Rate

$\theta \sim$ Pitch angle

$n_z \sim$ Normal acceleration

$\alpha_v \sim$ α-Vane deflection angle

we note that

$$n_z = \frac{v}{g} [\dot{\theta} - \dot{\alpha}]$$

$$\alpha_v = K_\alpha (\alpha + \frac{w_g}{v}) - \frac{K_\alpha \ell_\alpha}{v} \dot{\theta}$$

We can put these relations in State Space form, allowing for sensor measurement errors at the same time. We take the errors to be white Gaussian.

Let

$$x = \begin{bmatrix} \alpha \\ \theta \\ \dot{\theta} \\ \alpha_g \\ \delta_e \end{bmatrix}$$

Let

$$v = \begin{bmatrix} q_m \\ \theta_m \\ n_{z_m} \\ \alpha_{v_m} \end{bmatrix}$$

where the subscrip m denotes the sensor measurement corrupted by noise.

Then we can write

$$v = C\,x + G\,N$$

$$\dot{x} = A\,x + B\,u + F\,N$$

where

$$A = \begin{bmatrix} Z_\alpha & 0 & 1 & Z_\alpha & Z_{\delta_e} \\ 0 & 0 & 1 & 0 & 0 \\ M_\alpha & 0 & M_q & M_\alpha & M_{\delta_e} \\ 0 & 0 & 0 & -v/L & 0 \\ 0 & 0 & 0 & 0 & -20 \end{bmatrix}$$

$$B = \begin{bmatrix} 0 \\ 0 \\ 0 \\ 0 \\ 20 \end{bmatrix}$$

$$C = \begin{bmatrix} 0 & 0 & 1 & 0 & 0 \\ 0 & 1 & 0 & 0 & 0 \\ \dfrac{\ell_z M_\alpha - VZ_\alpha}{g} & 0 & \dfrac{\ell_z M_q}{g} & \dfrac{\ell_z M_\alpha - V Z_\alpha}{g} & \dfrac{\ell_z M_{\delta_e} - V Z_{\delta_e}}{g} \\ k_\alpha & 0 & \dfrac{-1_k k_\alpha}{v} & k_\alpha & 0 \end{bmatrix}$$

$$F = \begin{bmatrix} 0 & 0 & 0 & 0 & 0 \\ 0 & 0 & 0 & 0 & 0 \\ 0 & 0 & 0 & 0 & 0 \\ 0 & 0 & 0 & 0 & \sigma_1 \quad \sqrt{2|vL_1} \end{bmatrix}$$

$$G = \begin{bmatrix} g_1 & 0 & 0 & 0 & 0 \\ 0 & g_2 & 0 & 0 & 0 \\ 0 & 0 & g_3 & 0 & 0 \\ 0 & 0 & 0 & g_4 & 0 \end{bmatrix}$$

where g_1^2, g_2^2, g_3^2, g_4^2 are white noise spectral densities corresponding to the corresponding sensors.

We take our performance criterion to be that of minimising the normal acceleration due to gust. Hence

$$L = \frac{v}{g} \begin{bmatrix} -Z_\alpha, & 0, & 0, & -Z_\alpha, & -Z_{\delta_e} \end{bmatrix}.$$

and is 1 x 5.

The nominal parameter values will be taken to be those listed below, corresponding to those extracted from maneuver A.

$$Z_\alpha = -1.45$$

$$M_\alpha = -9.79$$

$$M_q = -1.43$$

$$Z_{\delta_e} = -0.098$$

$$M_{\delta_e} = -8.15$$

$$\sigma_1^2 = 25.2$$

The corresponding value of m.s. normal acceleration J was calculated for two values of λ : $\lambda = 1$ (large control), $\lambda = 10$ (small control). For $\lambda = 1$, J = .007985; for $\lambda = 10$, J = .008264. It may be noted that in the absence of any feedback control, J = .01185. The reduction is not spectacular for the particular control configuration, but our purpose here is to illustrate the techniques. To calculate the performance degradation (due to wrong parameter choice) we shall take the parameter values extracted from maneuver X corresponding to the 'dither' input. In other words, we are determining the adequacy of parameters extracted using only a dither input (in gust, of course). The parameter values corresponding to maneuver X are.

$$Z_\alpha = -1.41$$

$$M_\alpha = -9.42$$

$$M_q = -0.53$$

$$Z_{\delta_e} = -0.029$$

$$M_{\delta_e} = -6.04$$

$$\sigma_1^2 = 26.84$$

The corresponding values of m.s. normal acceleration were:

$$\lambda = 1, \quad J = \cdot 008668$$

$$\lambda = 10, \quad J = .008973$$

The percent degradation is

$$\lambda = 1 \qquad \frac{\Delta J}{J} = 8.55\ \%$$

$$\lambda = 10 \qquad \frac{\Delta J}{J} = 8.58\ \%$$

Thus the percent degradation is relatively insensitive to control effort constraint.

The degradation due to change in each individual parameter was calculated using the linear approximation theory, and the results are shown in Table 1.1; only the case $\lambda = 1$ is considered. Note that the largest change in parameter occurs for M_q but the performance degradation due to this change is relatively small being only 0.2%. Of course, as is only to be expected, the largest performance degradation was due to uncertainty in the control variable Z_{δ_e}. It is interesting that the various parameter changes cancel out; in particular the particular change in M_{δ_e} actually causes a performance improvement! The net degradation in performance of the linear approximation basis yields 10.96% which should be compared to the actual value of 8.55% The linear approximation thus

tends to slightly exaggerate the degradation, at least for this particular case.

It would appear that uncertainties in the control derivatives result in greatest degradation while the uncertainties in the stability derivatives play a much less significant role. Fortunately in the overall parameter estimation technique the control derivatives are usually the most accurately determinable.

TABLE 1.1

Performance Degradation (Jet Star Data)
Due to Parameter Uncertainty

M.S. Normal Acceleration: No Control: 0.01185

$\lambda = 1$

	Nominal Parameters (Maneuver A)	Dither Input Estimates (Maneuver X)	ΔPerf.	Performance Degradatio (ΔJ/J)
Z_α	-1.45	-1.41	0.04	-5.0%
M_α	-9.79	-9.42	0.37	-0.08%
M_q	-1.43	-0.53	0.90	-0.24%
Z_{δ_e}	-0.098	-0.029	0.069	-7.0%
M_{δ_e}	-8.15	-6.04	2.11	+1.43%
σ^2	25.2	26.84	1.64	-0.07%

Total -10.9%

1.3 HANDLING QUALITY AND GUST ALLEVIATION.

In this section we develop a new criterion for handling-quality improvement and gust alleviation. Following usual practice, we interpret handling-quality as the ability of the aircraft to respond closely to the pilot input (signal). For this purpose we use a stochastic model for the pilot input, and a quadratic error criterion. We asume a Dryden or similar rational spectrum model for the gust, and a quadratic minimisation criterion as well for gust alleviation. Finally we add a soft constraint on the control effort.

Mathematically, the problem can then be stated as follows. We begin with the linearised rigid body perturbation equations of motion of the aircraft:

$$\dot{x}(t) = A_1 x(t) + B_1 u(t) + F_1 n(t)$$

$$y(t) = C_1 x(t) + G_1 n(t)$$

where $x(\cdot)$ is the state, enhanced to include the gust generation model, $y(\cdot)$ is the sensor output, $u(\cdot)$ is the control to be optimised, and $n(t)$ is white Gaussian with unit spectral density,

$$F_1 G_1^* = 0$$

to reflect the fact that gust and sensor noise processes are independent, and

$$G_1 G_1^* > 0 \quad \text{(Nonsingular)}.$$

Let $v(t)$ denote the pilot input . Then we can formulate the performance criterion as:

$$Pr = \frac{1}{T} E \int_0^T ||Lx(t) - v(t)||^2 \, dt + \frac{1}{T}\int_0^T E(||Qx(t)||^2) \, dt + \frac{\lambda}{T}\int_0^T E(||u(t)||^2) \, dt$$

Here L and Q are appropriately chosen rectangular matrices, and λ is a positive constant reflecting the degree of control effort constraint desired.

To proceed further we need to specify the model to be assumed for the representation of the pilot input. Thus let:

$$v(t) = C_2 z(t) + G_2 N(t)$$

$$\dot{z}(t) = A_2 z(t) + F_2 N(t)$$

where $N(t)$ is white Gaussian with unit spectral density, with

$$F_2 G_2^* = 0$$

$$G_2 G_2^* > 0 \quad \text{(Nonsingular)}$$

In what follows we shall specialise to

$$G_2 G_2^* = \varepsilon I \quad , \quad I = \text{Identity matrix.}$$

where

$$\varepsilon \geq 0$$

as being general enough. If $\varepsilon > 0$, this is tantamount to saying that we allow for some error in the sensor ; we shall consider the case where ε is zero, separately below.

The key step in our theory is to recast the performance criterion, making essential use of the pilot input model, into the "stochastic regulator" form, from which the optimal feedback control can be readily deduced.

It is convenient to specify the dimensions of the various vectors and matrices we shall use to clarify the notation . Thus let:

$$x \sim n \times 1$$
$$z \sim m \times 1$$
$$B_1 \sim n \times j$$
$$C_1 \sim r \times n$$
$$C_2 \sim p \times m$$
$$L \sim p \times n$$
$$Q \sim q \times n$$

Let X denote the $(m+n) \times 1$ matrix:

$$X = \begin{bmatrix} x \\ z \end{bmatrix}$$

Then

$$||L x - C_2 z||^2 + ||Q x||^2 = \text{Tr. } R\, X X^*$$

where

$$R = \begin{bmatrix} L^*L + Q^*Q & -L^* C_2 \\ -C_2^* L & C_2^* C_2 \end{bmatrix}$$

Note that R is $(m+n) \times (m+n)$ and is of course non-negative definite.

Using $X(t)$ as the compound state space, and R as defined above, the performance criterion Pr. can now be rewritten as:

$$\text{Pr.} = (1/T) \int_0^T E([R\,X(t), X(t)] + \lambda[u(t),u(t)]\ )\,dt$$

where $[\ ,\ ]$ denotes inner product, and where $X(t)$ satisfies the 'state' equation:

$$\dot{X}(t) = A\,X(t) + B\,u(t) + F\,\eta(t)$$

where

$$A = \begin{bmatrix} A_1 & 0 \\ 0 & A_2 \end{bmatrix}$$

$$B = \begin{bmatrix} B_1 \\ 0 \end{bmatrix}_{(n+m)xj}$$

$$F = \begin{bmatrix} F_1 & 0 \\ 0 & F_2 \end{bmatrix}$$

$$\eta(t) = \begin{vmatrix} n(t) \\ N(t) \end{vmatrix}$$

The control $u(t)$ is now to be based on the "observation" vector:

$$\begin{bmatrix} y(t) \\ v(t) \end{bmatrix}$$

where of course:

$$\begin{matrix} y(t) \\ v(t) \end{matrix} = \begin{bmatrix} C_1 & 0 \\ 0 & C_2 \end{bmatrix} \begin{matrix} x(t) \\ z(t) \end{matrix} + \begin{bmatrix} G_1 & 0 \\ 0 & G_2 \end{bmatrix} \begin{matrix} n(t) \\ N(t) \end{matrix}$$

The optimal feedback control $u_o(t)$ can then be expressed as:

$$u_o(t) = (-1/\lambda)\ B_1^*\ (\ P_c^{11}\ \hat{x}(t) + P_c^{12}\ \hat{z}(t)\ )$$

where

$$\dot{\hat{x}}(t) = A_1\ \hat{x}(t) + P_f^1\ C_1^*\ (\ y(t) - C_1\ \hat{x}(t)) + B\ u_o(t)$$

$$\dot{\hat{z}}(t) = A_2\ \hat{z}(t) + P_f^2\ C_2^*\ (\ v(t) - C_2\ \hat{z}(t))\ \varepsilon^{-1}$$

$$\dot{P}_f^1(t) = A_1 P_f^1(t) + P_f^1(t)\ A_1^* + F_1\ F_1^* - P_f^1(t) C_1^*\ C_1\ P_f^1(t)$$

$$\dot{P}_f^2(t) = A_2 P_f^2(t) + P_f^2(t)\ A_2^* + F_2\ F_2^* - P_f^2(t)\ C_2^*\ C_2\ P_f^2(t)\ \varepsilon^{-1}$$

Finally

$$P_c = \begin{bmatrix} P_c^{11} & P_c^{12} \\ P_c^{21} & P_c^{22} \end{bmatrix}$$

and

$$\dot{P}_c(t) + A^*\ P_c(t) + P_c(t)\ A - \frac{P_c(t)\ B\ B^*\ P_c(t)}{\lambda} + R = 0\ ;\quad P_c(T) = 0.$$

As in most applications, we may use the 'steady state' versions of the solutions to the Riccatti equations.

Either the handling quality criterion or the gust alleviation criterion (or both) can be expressed in the form:

$$\lim_{T\to\infty}\ \frac{1}{T}\int_0^T \| N\ X(t)\|^2\ dt$$

which can be calculated as:

$$\text{Tr.}\ \ M^{*}\ M\ P_f \ +\ \text{Tr.}\ M^{*}\ M\ J$$

where J is the solution of the linear equation:

$$0 \ = \ (A - B\ B^{*}\ P_c\ |\lambda)\ J \ + \ J\ (A - B\ B^{*}\ P_c\ |\lambda) \ + P_f C^{*} C\ P_f$$

where

$$P_f \ = \begin{bmatrix} P_f^1 & 0 \\ 0 & P_f^2 \end{bmatrix}$$

$$C \ = \begin{bmatrix} C_1 & 0 \\ 0 & C_2 \end{bmatrix}$$

Example

As a specific example we shall take the one-dimensional pilot model:

$$\dot{z}(t) \ = \ A_2\ z(t) \ + \ F_2 N(t)$$

where

$$A_2 \ = \ -\left(1/1.11\right)$$

$$F_2 \ = \ \text{Identity}$$

we shall also take the observation to be noise free [c=0]. In this case

[and more generally where the full state is observed noise-free, or C_2 is non singular and $\varepsilon=0$]

$$z(t) = \hat{z}(t)$$

and the combined system of equations for $\hat{x}(t)$ and $\hat{z}(t)$ is given by:

$$\dot{\hat{x}}(t) = A_1 \hat{x}(t) + P_f^1 C_1^* (y(t) - C_1\hat{x}(t)) + B_1 u_o(t)$$

$$\dot{\hat{z}}(t) = A_2\hat{z}(t) + F_2N(t)$$

We shall also specialize to the case where we are not interested in gust alleviation but only in handling-quality so that

$$Q = 0$$

We shall further take $\lambda = 1$ for simplicity.

The main thing is the calculation of P_c^{11} and P_c^{12}. For this we must solve the Steady State Riccatti equation for P_c which in the present case is (dropping the subscript c):

$$A_1^* P^{11} + P^{11}A_1 - P^{11}B_1B_1^*P^{11} + L L^* = 0$$

$$P^{21} A_1 + A_2^* P^{21} - P^{21}B_1B_1^*P_{11} - C_2^*L = 0$$

$$A_2^*P^{22} + P^{22}A_2 - P^{21}B_1B_1^* P^{12} + C_2^* C_2 = 0$$

Because A_2 is 1 x 1 we can express P^{22} and P^{21} in terms of P^{11}. Thus we have

$$P^{21}(A_1 + A_2^* I - B_1B_1^*P_{11}) = C_2^*L$$

or

$$P_{12}^{*} = P^{21} = C_2^{*} L(A_1 + A_2^{*} - B_1 B_1^{*} P_{11})^{-1}$$

$$P^{22} = (A_2 + A_2^{*})^{-1}\left(P^{21} B_1 B_1^{*} P^{12},\ -C_2^{*} C_2\right)$$

Because $\varepsilon=0$, J is now given by:

$$(A - BB^{*}P_c)J + J(A-BB^{*}P_c)^{*} + \begin{bmatrix} P_f^1 C_1^{*} C_1 P_f^1 & 0 \\ 0 & F_2 F_2^{*} \end{bmatrix} = 0$$

And finally the minimal value of

$$\lim_{T\to\infty} \frac{1}{T} \int_0^T E||L\,x(t) - v(t)||^2\, dt$$

$$= \mathrm{Tr}\, M M^{*} J + \mathrm{Tr}.\, M M^{*} \begin{bmatrix} P_f^1 & 0 \\ 0 & 0 \end{bmatrix}$$

where

$$M M^{*} = \begin{bmatrix} L L^{*} & -L^{*} C_2 \\ -C_2^{*} L & C_2^{*} C_2 \end{bmatrix}$$

Decomposing J as:

$$J = \begin{bmatrix} J_{11} & J_{12} \\ J_{21} & J_{22} \end{bmatrix}$$

we have:

$$A_2 J_{22} + J_{22} A_2^* + F_2 F_2^* = 0$$

$$(A_1 - B_1 B_1^* P^{11}) J_{12} - B_1 B_1^* P^{12} J_{22} + J_{12} A_2^* = 0$$

$$(A_1 - B_1 B_1^* P^{11}) J_{11} - B_1 B_1^* P^{12} J_{22}$$

$$+ J_{11} (A_1 - B_1 B_1^* P^{11})^* - J_{22} P^{21} B_1 B_1^*$$

$$+ P_f^1 C_1 C_1^* P_f^1 = 0$$

Taking advantage of the fact that in our example A_2 is one-dimensional, we have

$$J_{22} = -(A_2 + A_2^*)^{-1} F_2 F_2^*$$

etc., and thus expressing J_{11}, J_{12} in terms of J_{22}.

Finally

$$\text{Tr. } M M^* J = \text{Tr. } (L L^* J_{11} - L^* C_2 J_{21} - C_2^* L J_{12} + C_2^* C_2 J_{22})$$

Taking $C_2 = 4$ and the longitudinal Jet-Star equation at the nominal values (p. 57) we have:

For the Jet-Star

$$A_1 = \begin{bmatrix} Z_\alpha & 0 & 1 & Z_\alpha & Z_{\delta_e} \\ 0 & 0 & 1 & 0 & 0 \\ M_\alpha & 0 & M_q & M_\alpha & M_{\delta_e} \\ 0 & 0 & 0 & -\omega_c & 0 \\ 0 & 0 & 0 & 0 & -k_A \end{bmatrix}$$

$$B_1 = \left[\begin{array}{c|c|c} 0 & & 0 \\ 0 & & 0 \\ 0 & F & 0 \\ 0 & & \frac{\sigma}{v}\sqrt{2\omega_c} \\ k_A & & 0 \end{array}\right] \qquad L = \left|\begin{array}{ccccc} 0 & 0 & 0 & 0 & 1 \end{array}\right|$$

$$G = \text{diag.}\ (5 \times 10^{-4},\ 1 \times 10^{-4},\ 1 \times 10^{-2},\ 5 \times 10^{-5})$$

$$C_1 = \begin{bmatrix} 0 & 0 & 1 & 0 & 0 \\ 0 & 1 & 0 & 0 & 0 \\ \frac{-vZ_\alpha}{g} & 0 & 0 & \frac{-vZ_\alpha}{g} & \frac{-vZ_{\delta_e}}{g} \\ K_\alpha & 0 & \frac{-\ell_\alpha K_\alpha}{v} & K_\alpha & 0 \end{bmatrix}$$

The control gain matrix P_c is calculated to be:

$$P_c^{11} = (10^{-7}) \begin{bmatrix} 1.32 & -1.63 & -.224 & 0 & .0811 \\ -1.63 & 2.02 & 0.277 & 0 & -.100 \\ -0.224 & 0.277 & .033 & 0 & -.0138 \\ 0 & 0 & 0 & 0 & 0 \\ .0811 & -0.1 & -.0138 & 0 & 2.07 \times 10^5 \end{bmatrix}$$

$$P_c^{12} = (10^{-7}) \; [4.935, -6.11, -.8393, 0, -1.371 \times 10^6]$$

$$P_c^{22} = 4.710$$

$$-B_1^* P_c^{11} = 10^{-7} \; [-1.622, 2.008, .2759, 0, (-20)\,(2.07)\,10^5]$$

Hence we see that with good approximation

$$u_o(t) = (-20)\,(2.07)\,10^{-2}\hat{x}_5 + (20)\,(1.37)10^{-1}\,\hat{z}$$

$$= (20)(10^{-2})(2.07\,\hat{x}_5 - 13.7\,\hat{z})$$

where $x_5 = \delta_e(t)$, the actuator output. As expected, the controller virtually ignores all other states. Note that the control gains are independent of the gust intensity.

The corresponding value of the steady-state mean quadratic deviation

$$= \text{Tr.}\ MM^{*}J + \text{Tr}\ MM^{*}P_f$$

$$= 2.58 + 0$$

$$= 2.58$$

The matrix J is

2.13	5.37	3.01	0	-1.62	0
5.37	4.59×10^{4}	4.59	0	-5.07	-2.03
3.01	4.59	9.40	0	-3.64	-1.83
0	0	0	0	0	0
-1.62	-4.07	-3.64	0	2.02	1.04
-0.08	-2.03	-1.83	0	1.04	0.0556

2: IDENTIFICATION OF DERIVATIVES FROM FLIGHT DATA: THEORY, ALGORITHMS AND SIMULATION RESULTS.

In this section we report on Task B: development of an algorithm for extracting stability and control derivatives from flight data taking gust into account. Section 2.1 deals with the essential background theory. The algorithm itself is developed in Section 2.2. Section 2.3 details of verification of the algorithm on simulated flight data.

2.1 THEORY

The theory will be presented in a degree of generality that can handle the linearised model of any rigid-body aircraft motion, longitudinal-and-lateral, and taking gust loading into account.

We use a 'continous-time' model rather than a 'discrete-time model (as in most of the engineering literature) primarily because the data sampling rate (50 samples/sec) is much higher that the Nyquist rate corresponding to the noise bandwidth [5 Hertz at most], so that the usual assumption of independence of noise samples on the output is not valid. On the other hand, time-continuous model 'integrals' are well approximated by 'sums'. A fuller discussion of the trade-offs in the choice between the two models may be found in Appendix I.

It is convenient to rewrite the motion equations and sensor data in state-space form. Thus we have:

$$\dot{x}(t) = A\,x(t) + B\,u(t) + F\,n(t)$$

for the 'state' equation, where the matrix A contains the stability derivatives, and B contains control derivatives, u(t) being the input

(δ_e, δ_a, δ_r etc.) and n(t) is white Gaussian noise with unit spectral density matrix. The term F n(t) characterises the gust, as we shall see below. We denote by the column vector Y(t), the various sensor outputs (observed data) and can be expressed as

$$Y(t) = CX(t) + D\,u(t) + G\,n(t).$$

The 'state' noise F n(t) and "observation noise" G n(t) are independent:

$$F G^{*} = 0$$

and

$$GG^{*} = \text{diag.}\,[d_i]$$

with all d_i positive - corresponding to the fact that we do not assume that any sensor is noise-free.

We denote by θ the (vector of) various unknown parameters in all the matrices A, B, C, D, F, we estimate 'θ' by minimising with respect to θ, the unknown initial state X_0 and possibly unknown noise matrix diag. $\{d_i\}$, as well as bias :

$$q(\theta;T) = \text{Tr. Log } GG^{*} + \frac{1}{T}\int_0^T [(Y(t) - C\hat{x}(t) - D\,u(t)),$$
$$(GG^{*})^{-1}\,(Y(t) - C\hat{x}(t) - Du(t))]\,dt$$
$$+ \text{Tr. } (GG^{*})^{-1}\,C\,P\,C^{*} \qquad (2.1)$$

where $\hat{x}(t)$ is the Kalman state estimate defined by:

$$\dot{\hat{x}}(t) = (A - P C^*(GG^*)^{-1} C)\,\hat{x}(t) + B\,u(t) + PC^*(GG^*)^{-1}\,Y(t) \qquad (2.2)$$

$$\hat{x}(0) = \hat{x}_0$$

and P is determined by:

$$0 = A P + P A^* + F F^* - P C^* (GG^*)^{-1} C P \qquad (2.3)$$

Let us next calculate the C - R bound matrix, assuming that (GG^*) is known. Let

$$\hat{Y}(t) = C\hat{x}(t) + D\,u(t)$$

$$R(\theta;T) = \left\{ E \int_0^T \left[(GG^*)^{-1} \frac{\partial}{\partial \alpha_i} \hat{Y}(t), \frac{\partial}{\partial \alpha_j} \hat{Y}(t) \right] dt \right\} \qquad (2.4)$$

where $\{\alpha_i\}$ denote the components of θ. Then letting θ_o denote the true value of θ, the C. R. bound matrix is

$$R(\theta_o ; T)^{-1}$$

where θ_o is the true-value of θ (no model error).

we approximate this by

$$(T\,\bar{R}\,(\hat{\theta}_T\,;\,T)\,)^{-1}$$

where $\hat{\theta}_T$ is our estimate for θ and

$$\bar{R}\,(\,\theta;\,T\,) = \left\{\frac{1}{T}\int_0^T [(G\,G^*)^{-1}\,\frac{\partial}{\partial\alpha_i}\hat{Y}\,(t),\,\frac{\partial}{\partial\alpha_j}\hat{Y}\,(t)\,]\,dt\right\}. \quad (2.5)$$

Note that the approximation depends on the observed data directly (in addition to the dependence via $\hat{\theta}_T$, the estimate).

2.2 ALGORITHMS

In this section we develop the algorithms for parameter estimation in the generality of the formulation of Section 2.1.

In minimising (2.1) we first use nominal values for the stability derivatives, and take $G\,G^*$ as the identity matrix, unless there is à priori values of $\{d_i\}$ available from previous flight test data in clear air. In the first iteration step we vary only the Control derivatives (in B and D) as well as the biases. Note that in this process A, C, F, and P remain fixed. A first estimate for $(G\,G^*)$ is then obtained using:

$$\hat{d}_i = \frac{1}{T}\int_0^T (Y\,(t) - \hat{Y}\,(t)\,)_i^2\,dt$$

where $(\,)_i$ denotes i^{th} component.

using this value of $(G\,G^*)$ we now iterate with respect to all the parameters, θ, ζ and the biases, using the following formula:

$$\theta_{n+1} = \theta_r - \bar{R}(\theta_n;T)^{-1}\ \bar{G}(\theta_n;T)$$

where $\bar{G}(0;T)$ is the vector with components

$$\left\{ \frac{1}{T} \int_0^T [(GG^*)^{-1} \frac{\partial}{\partial \alpha_i} \hat{Y}(t), \hat{Y}(t) - Y(t)\ ]\, dt \right.$$

$$\left. + \mathrm{Tr.}\ (G\,G^*)^{-1} \frac{\partial}{\partial \alpha_i} C\,P\,C^* \right\}$$

and $\bar{R}(0;T)$ as defined already in (2.5)

A few words on the details of the computer calculation of relevant quantities may be in order. The main step is the calculation of the partial derivaties of dynamic variables:

$$\frac{\partial}{\partial \alpha_i} \hat{x}(t)$$

For this, we take the first order variation on the Kalman equation:

$$\frac{d}{dt}\left(\frac{\partial}{\partial \alpha_i} \hat{x}(t) \right) = (A - P\,C^*\,C) \frac{\partial}{\partial \alpha_i} \hat{x}(t) + \frac{\partial}{\partial \alpha_i} (A - P\,C^*\,C)\, \hat{x}(t)$$

$$+ \left(\frac{\partial}{\partial \alpha_i} B \right) u(t)$$

$$+ \left(\frac{\partial}{\partial \alpha_i} P\,C^* \right) (G\,G^*)^{-1}\, Y(t)$$

$$\frac{\partial}{\partial \alpha_i} \hat{x}(0) = 0$$

Also

$$\frac{\partial P}{\partial \alpha_i}$$

is determined from the linear equation:

$$0 = (A - P C^* (G G^*)^{-1} C) \frac{\partial P}{\partial \alpha_i}$$

$$+ \frac{\partial P}{\partial \alpha_i} (A - P C^* (G G^*)^{-1} C)^*$$

$$+ \frac{\partial}{\partial \alpha_i} (F F^*)$$

We also note that the integration of the time continous linear equation

$$\dot{x}(t) = A x(t) + B u(t)$$

is performed as:

$$x((n+1)\Delta) = e^{A\Delta} x(n\Delta) + \int_0^{\Delta} e^{As} ds\, b\, \frac{1}{2} [u((n+1)\Delta) + u(n\Delta)]$$

where Δ is the sampling interval (0,02 sec. in our case).

The Riccati matrix P is computed by the following algorithm:
[we assume A-Stable, A - F controllability and C - A observability]:
compute Λ from:

$$A^* \Lambda + \Lambda A + C^* C = 0$$

then solve (the linear equation)

$$0 = (A - P_n C^* C) P_{n+1} + P_{n+1} (A - P_n C^* C)^* + F F^* + P_n C^* C P_n$$

with

$$P_0 = \Lambda^{-1}$$

2.3 VERIFICATION OF ALGORITHMS: SIMULATION RESULTS.

The algorithms developed in the previous section were verified by simulating the longitudinal short-period motion dynamics. The equations used in State Space form were:

$$\begin{cases} \dot{x}(t) = Ax(t) + Bu(t) + Fn_s(t) \\ v(t) = Cx(t) + Du(t) + Gn(t) \end{cases}$$

where

$$x = \begin{bmatrix} \alpha_s \\ \theta \\ \dot{\theta} \\ \alpha_g \end{bmatrix} \qquad v = \begin{bmatrix} \dot{\theta}_m \\ \theta_m \\ a_{n_m} \\ \alpha_m \end{bmatrix} \qquad u = \begin{bmatrix} \delta_e \\ 1 \end{bmatrix}$$

$$A = \begin{bmatrix} Z_\alpha & 0 & 1 & Z_\alpha \\ 0 & 0 & 1 & 0 \\ M_\alpha & 0 & M_{\dot{\theta}} & M_\alpha \\ 0 & 0 & 0 & -v/1000 \end{bmatrix} \qquad B = \begin{bmatrix} Z_{\delta_e} & Z_0 \\ 0 & 0 \\ M_{\delta_e} & M_0 \\ 0 & 0 \end{bmatrix}$$

$$C = \begin{bmatrix} 0 & 0 & 1 & 0 \\ 0 & 1 & 0 & 0 \\ \dfrac{\ell_z M_\alpha - V z_\alpha}{g} & 0 & \dfrac{\ell_z M_{\dot\theta}}{g} & \dfrac{\ell_z M_\alpha - V z_\alpha}{g} \\ k_\alpha & 0 & \dfrac{-\ell_\alpha k_\alpha}{v} & k_\alpha \end{bmatrix}$$

$$D = \begin{bmatrix} 0 & 0 \\ 0 & 0 \\ \dfrac{\ell_z M_{\delta_e} - V Z_{\delta_e}}{g} & \dfrac{\ell_z M_0 - V Z_0}{g} \\ 0 & 0 \end{bmatrix}$$

$$F = \begin{bmatrix} 0 \\ 0 \\ 0 \\ \dfrac{\sigma_{\alpha_g}}{v} \sqrt{2\omega_c} \end{bmatrix} \qquad G = \begin{bmatrix} g_1 & 0 & 0 & 0 \\ 0 & g_2 & 0 & 0 \\ 0 & 0 & g_3 & 0 \\ 0 & 0 & 0 & g_4 \end{bmatrix}$$

and $n(t)$ and $n_s(t)$ are scalar and vector valued independent Gaussian white noise processes with zero mean and unit spectral densities, respectively.

We assume that G is known, and estimate Z_α, M_α, $M_{\dot\theta}$, Z_{δ_e}, M_{δ_e} and $\sigma^2_{w_g}$ from sensor measurements $v(t)$ and known control input $\delta_e(t)$.

Input valves for the simulation are listed in Table 2.1. The control input δ_e is taken to be a square wave of amplitude 0.02 rad. and of frequency 0.4 hertz.

The Power Spectral Density (PSD) based on 512 points of simulated measurement noises are shown in Figure 2.1. The horizontal line is the desired spectral density assuming the noise process in white. The noise processes shown in the figure are seen to be reasonable approximations of white noise.

Figure 2.2 shows the PSD of α_g, and its theoretical asymptote. Since the turbulence is direct proportional to α_g, its PSD will also have the same shape. 512 points were used in the computation.

The rate of convergence of the Riccati matrix, P, to its steady value is examined. The diagonal elements are plotted in Figures 2.3 and 2.4. Note that P converges to its steady state value after approximately 12 iterations.

Figure 2.5 is a comparison of the simulated time-history and the estimated time-history obtained from the identification algorithms. The solid lines are simulated data and the broken lines are the estimated data. The fit is observed to be excellent.

The residuals are plotted in Figure 2.6 and their PSD's are plotted in Figure 2.7. The residual PSD's are essentially flat over all frequencies.

The convergence of the estimated parameters based on 5.12 seconds of data shown in Table 2.2. All parameters converged in six iterations. The final estimates of all parameters with the exception of the last one are

very close to the true parameter values. Since the last parameter σ^2 is the turbulence power, it should measured in decibels. Here the difference is less than 2 db.

Finally, the identification algorithm is applied to other simulated data records. Each record has the same control input but the state and measurement noises are independent from those of the record. The mean and variance of estimated parameters are then computed. Tables 2.3 thru 2.6 mean and variance with the true parameter value and the Cramer-Rao bound. The mean values are very close to the true parameter value. The variances are reasonable close to the Cramer-Rao bound, for the small number of samples.

Table 2.1. Data for Simulation

θ°

$Z_{\alpha} = -1.65$ rad/sec

$M_{\alpha} = -54.0$ rad/sec^2

$M_{\dot{\theta}} = -1.65$ rad/sec

$Z_{\delta_e} = -0.45$ rad/sec

$M_{\delta_e} = -52.5$ rad/sec^2

$\sigma^2_{w_g} = 25.0$ ft^2/sec^2

$Z_o = 0$

$M_o = 0$

$V = 1670$ ft/sec

$\ell_z = 10$ ft

$\ell_{\alpha} = 32$ ft

$K_{\alpha} = 1.7$

$\Delta = 0.01$ sec

$g_1 = 0.0005$ rad/sec

$g_2 = 0.0001$ rad/sec

$g_3 = 0.01$ g

$g_4 = 0.00005$ rad

Table 2.2 Convergence of Estimated Parameters Using 5.12 Seconds of Data

ITERATION	Z_α	M_α	M_θ	Z_{δ_e}	M_{δ_e}	$\sigma^2_{w_g}$
Initial start-up value	- 2.40	- 39.0	- 2.40	- .675	- 36.0	2.5
1	- 1.764	- 53.2	- 1.887	- .675	- 51.09	3.85
2	- 1.646	- 53.9	- 1.655	- .447	- 52.42	6.95
3	- 1.660	- 54.3	- 1.692	- .464	- 52.88	13.06
4	- 1.650	- 54.0	- 1.665	- .446	- 52.56	13.47
5	- 1.646	- 53.8	- 1.647	- .445	- 52.31	19.98
6	- 1.641	- 53.9	- 1.651	- .446	- 52.50	20.05
True value	- 1.65	- 54.0	- 1.65	- .45	- 52.5	25.0

Table 2.3. Statistics of Estimated Parameters

No. of independent runs = 10

No. of data point for each run = 256 (2.56 seconds)

			SIMULATION TEST	
PARAMETER	TRUE VALUE	C-R BOUND	MEAN	VARIANCE
Z_α	- 1.65		- 1.650	
		.00014		.00022
M_α	- 54.0		- 54.07	
		.057		.068
M_θ	- 1.65		- 1.636	
		.00079		.00072
Z_{δ_e}	- 0.45		- .4525	
		.00016		.00018
M_{δ_e}	- 52.5		- 52.55	
		.070		.067
$\sigma^2_{w_g}$	25.0		18.78	
		12.9		4.13

Table 2.4. Statistics of Estimated Parameters

No. of independent runs = 18

No. of data points for each run = 512 (5.12 seconds)

			SIMULATION TEST	
PARAMETERS	TRUE VALUE	C-R BOUND	MEAN	VARIANCE
Z_α	- 1.65		- 1.650	
		.000046		.000042
M_α	- 54.0		- 54.01	
		.019		.026
$M_{\dot{\theta}}$	- 1.65		- 1.641	
		.00027		.00031
Z_{δ_e}	- 0.45		- 0.4504	
		.000057		.000035
M_{δ_e}	- 52.5		- 52.51	
		.025		.025
$\sigma^2_{w_g}$	25.0		17.43	
		6.7		2.5

Table 2.5. Statistics of Estimated Parameters

No. of independent runs = 10

No. of data points for each run = 1024 (10.24 seconds)

			SIMULATION TEST	
PARAMETER	TRUE VALUE	C-R BOUND	MEAN	VARIANCE
Z_α	- 1.65		- 1.651	
		.000021		.000015
M_α	- 54.0		- 54.03	
		.0082		.0099
M_θ	- 1.65		- 1.650	
		.00012		.00014
Z_{δ_e}	- 0.45		- .4502	
		.000026		.000029
M_{δ_e}	- 52.5		- 52.55	
		.011		.011
$\sigma^2_{w_g}$	25.0		18.48	
		3.28		1.66

Table 2.6. Statistics of Estimated Parameters

No. of independent runs = 8

No. of data point for each run = 2048 (20.48 seconds)

			SIMULATION TEST	
PARAMETER	TRUE VALUE	C-R BOUND	MEAN	VARIANCE
Z_α	- 1.65		- 1.650	
		.0000082		.00001
M_α	- 54.0		- 54.03	
		.0032		.0029
M_θ	- 1.65		- 1.650	
		.000046		.000072
Z_{δ_e}	- .045		- 0.4499	
		.000011		.000015
M_{δ_e}	- 52.5		- 52.54	
		.0044		.0028
$\sigma^2_{w_g}$	25.0		18.42	
		1.29		2.94

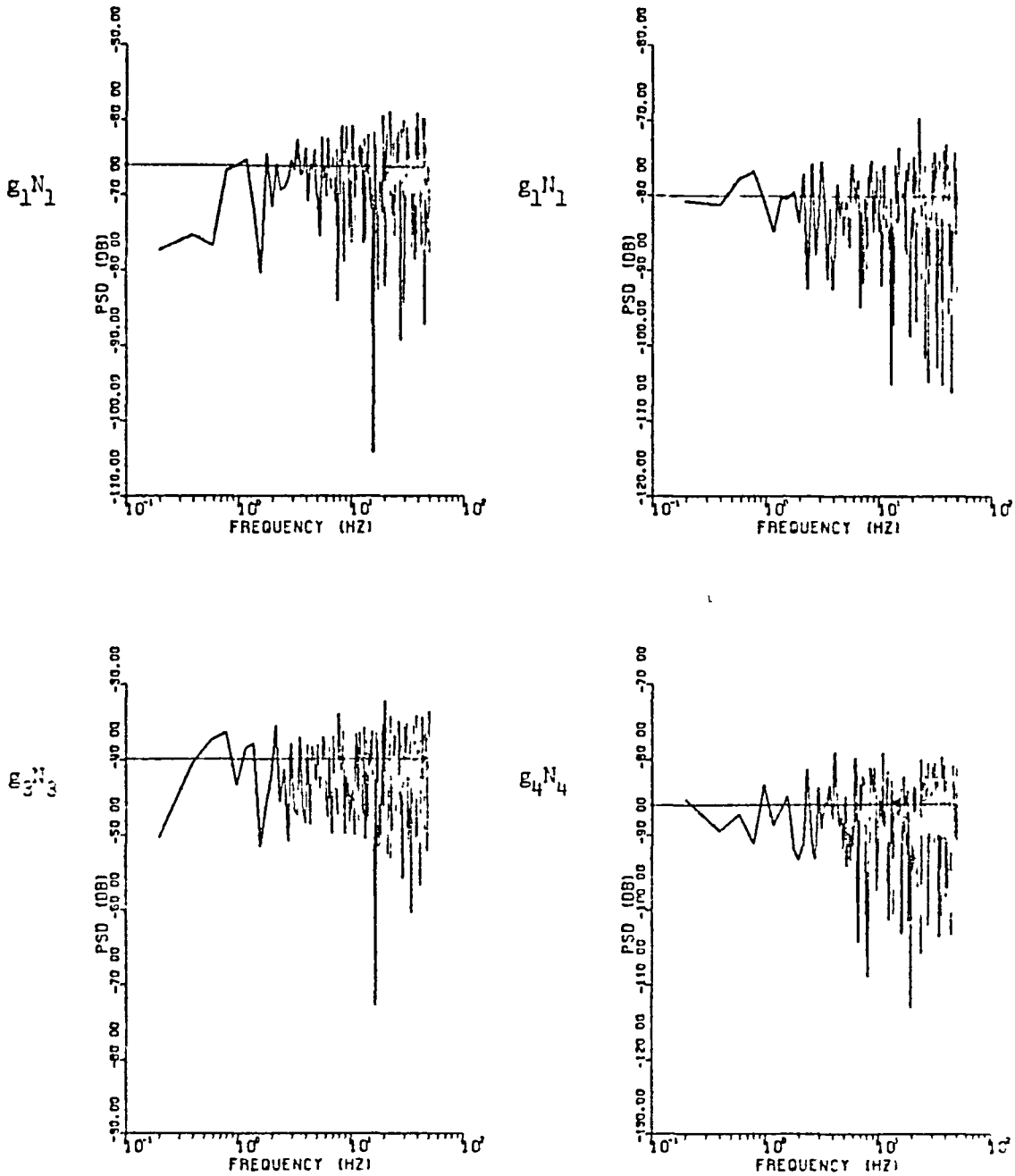

Power Spectral Densities of Simulated Measurement Noises for 512 points of data

Fig. 2.1

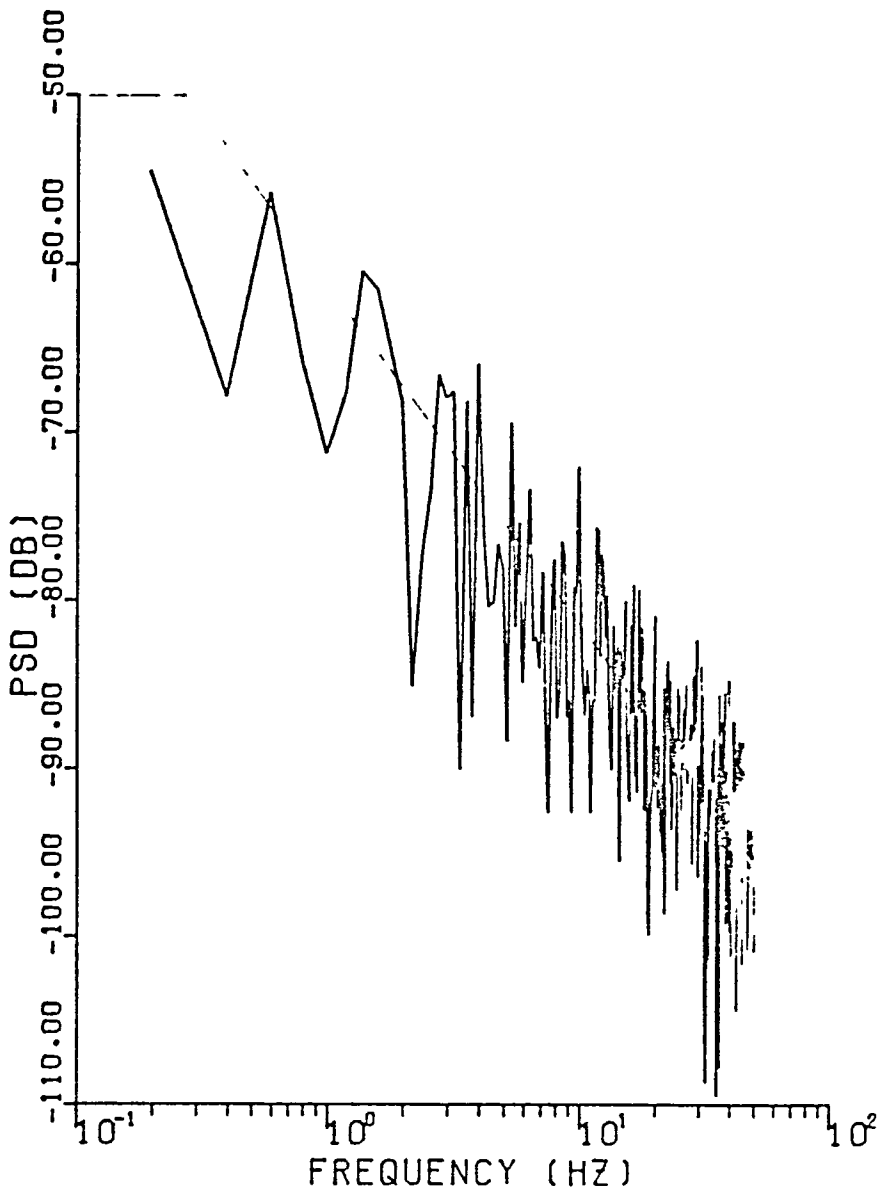

Power Spectral Density of Simulated Turbulence for 512 points of data

Fig. 2.1

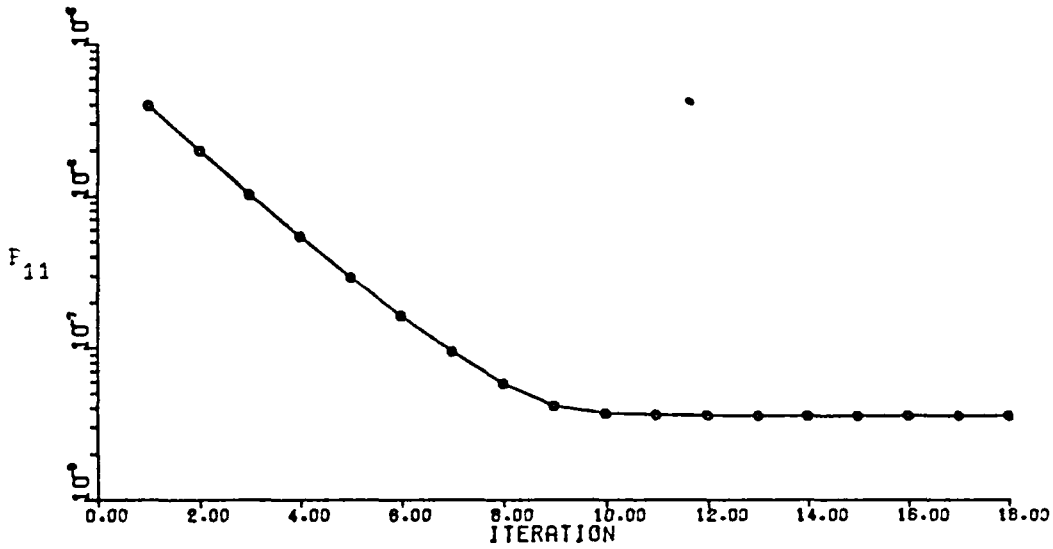

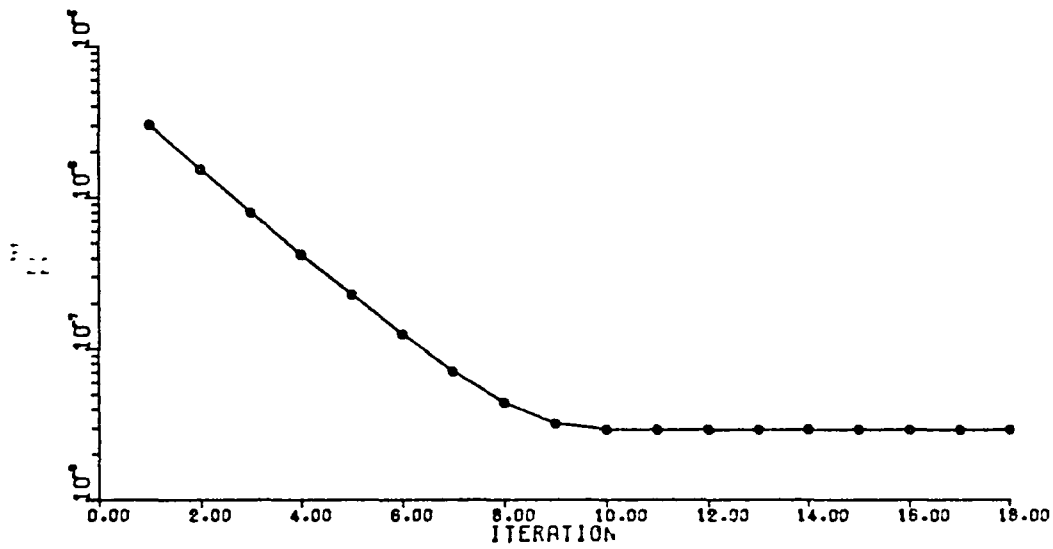

Convergence of Steady State Riccati Equation

Fig. 2.3

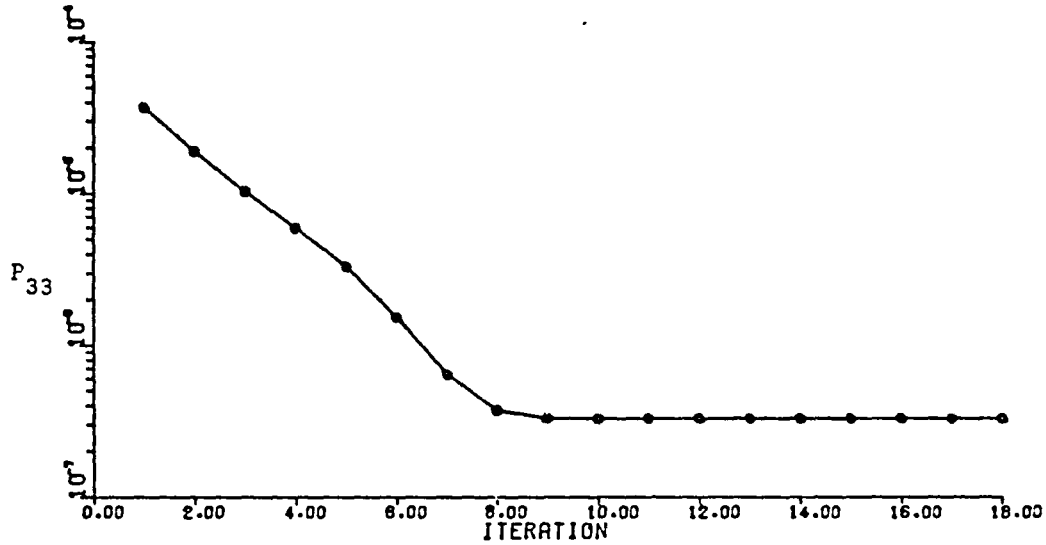

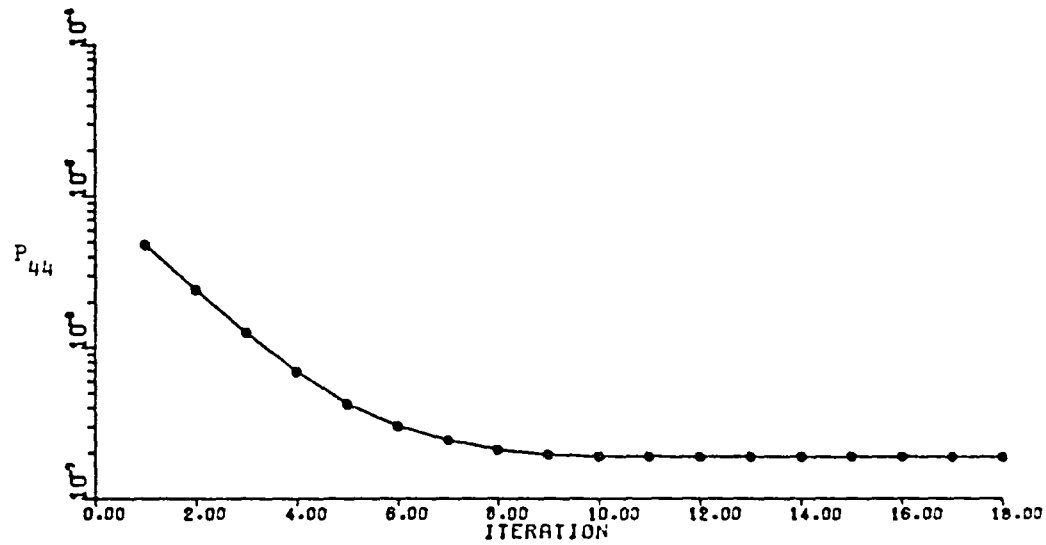

Convergence of Steady State Riccati Equation.

Fig. 2.4

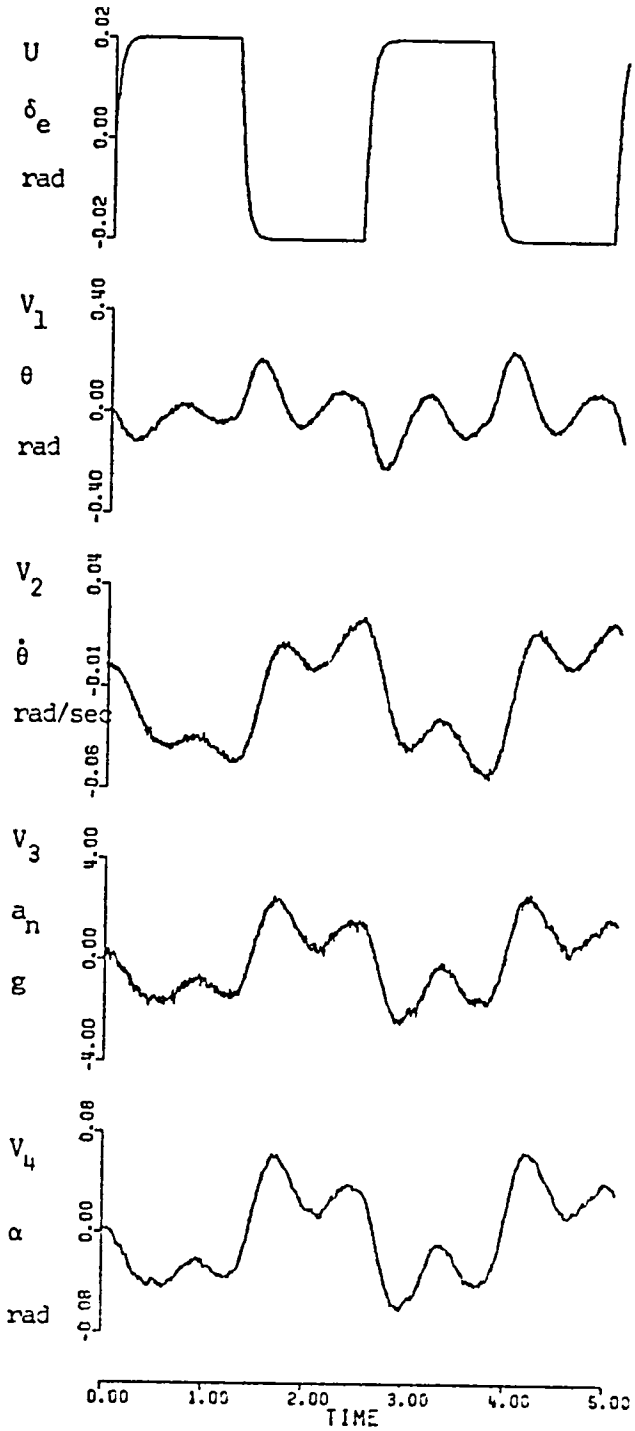

Comparison of Simulated and Estimated Data

Fig. 2.5

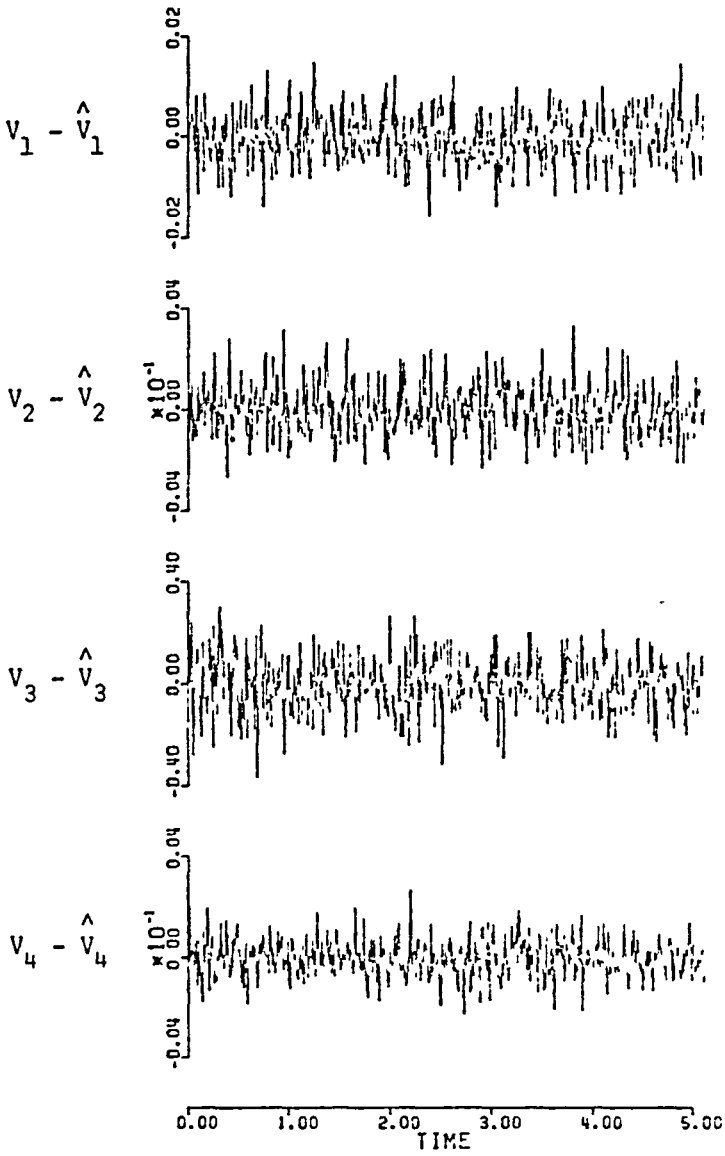

Residuals of Simulation Test Case

Fig. 2.3

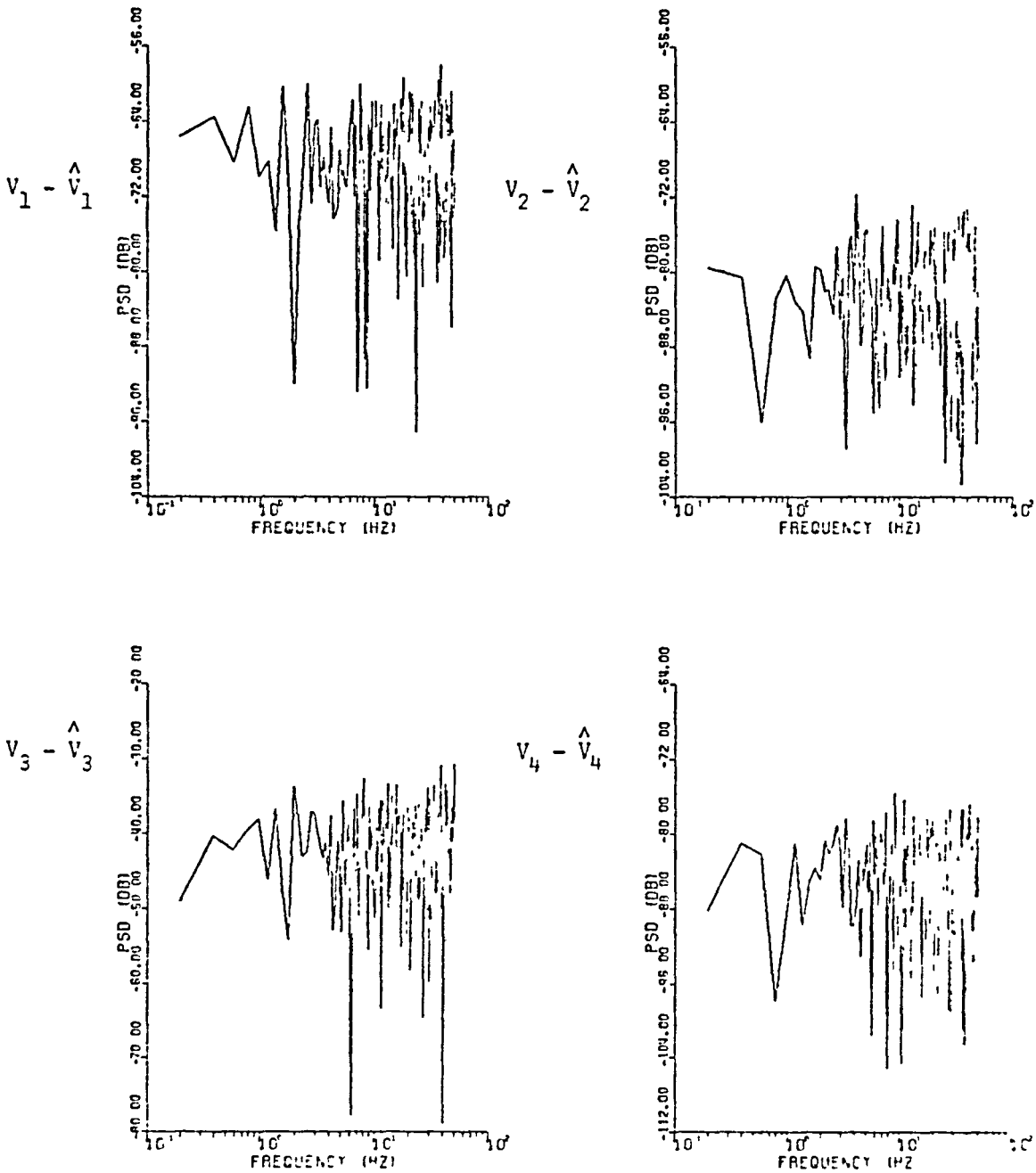

Power Spectral Densities of Residuals

Fig. 2.7

3. FLIGHT TEST DATA: LOCKHEED JET STAR

3. FLIGHT TEST DATA: LOCKHEED JET STAR

In this section we evaluate the performance of the identification algorithms on flight test data taken on a Lockheed Jet Star flying in turbulence (courtesy of K. Iliff, DFRC).

3.1. STATE SPACE MODEL DYNAMICS

The Flight data contained only the longitudinal short period mode. The turbulence was modelled by a Dryden spectrum, in which both the intensity and break frequency were allowed to be parameters to be estimated.

The sensor data vector $v(\cdot)$ consists of: pitch rate, pitch, normal acceleration, and angle of attack. The state equations can be written:

$$\dot{x}(t) = A\,x(t) + B\,u(t) + F\,n_s(t)$$

$$v(t) = C\,x(t) + D\,u(t) + G\,n(t)$$

where the state (enhanced to include the gust component) is the column vector:

angle of attack	α_s
pitch angle	θ
pitch rate	$\dot{\theta}$
gust	α_g

$$A = \begin{matrix} Z_\alpha & 0 & 1 & Z_\alpha \\ 0 & 0 & 1 & 0 \\ M_\alpha & 0 & M_{\dot{\theta}} & M_\alpha \\ 0 & 0 & 0 & -V/1000 \end{matrix}$$

$$B = \begin{matrix} Z_{\delta_e} & Z_0 \\ 0 & 0 \\ M_{\delta_e} & M_0 \\ 0 & 0 \end{matrix}$$

$$u = \begin{matrix} \delta_{e_1} \end{matrix}$$

The rest of the matrices are as in section 2, except for matrix G of error densities:

$$G = \text{Diag.} \ (0.0005, 0.0001, 0.01, 0.00005)$$

In the control derivative matrix B, it is optional whether Z_{δ_e} and M_{δ_e} are allowed to be independent parameters or not. It would appear that making them dependent (one a multiple of the other) yields better fit.

The time history data was subdivided into five segments of sub-maneuvers marke A, B, C, D, and E.

Each segment was processed independently of the others. The segments had to be combined to study the effect of changing the turbulence

spectrum break frequency. Table 3.1 lists the nominal Lockheed Jet Star data.

3.2. EXPLORATORY COMPUTER RUNS

Prior to actual processing, many exploratory computer runs were made to determine the relative role of the various parameters auxiliary to the main derivatives.

3.2.1 ITERATIONS REQUIRED TO MINIMISE COST FUNCTIONAL: TYPICAL CASE.

In addition to the parameters already listed, additional bias parameters as well as initial states were included. Figure 3.1 shows the behavior of the cost functional as a function of the number of iterations. As may be expected it drops steeply in the beginning and flattens out after five or six iterations. The maneuver chosen is maneuver A; the wind tunnel values of the derivatives were chosen for the starting values, and the initial states all set to zero. Table 3.2 shows the actual values of the cost functional for each iteration. The initial sharp drop occurs as a result of adjusting the 'lineary dependent' parameters: the biases and the control derivatives. A plot of the behavior of the derivatives in shown in Figure 3.2. The gust scale-length was taken to be $L_{w_\xi} = 1000$, the intensity being allowed to be unknown. The starting value for

$$\sigma^2_{w_\xi}$$

was taken to be zero.

3.2.2. EFFECT OF CHANGING STARTING DERIVATIVE VALUES.

It is of interest to determine the effect of choice of starting values of the derivatives on convergence of iteration and the final values of the derivatives estimated. This is illustrated using maneuver A. Table 3 shows the values of the derivatives for various choices of the starting values, as well as the corresponding final (minimal) values of the cost functional. The starting values of the biases and states were set to be zero in all cases. Note that the final values of derivatives are relatively insensitive to the starting values. The number of iterations to attain the minimising cost functional value were always four or five, and not sensitive enough for inclusion in the table.

3.2.3. EFFECT OF DELAYING ANGLE OF ATTACK (MEASURED).

Because of the physical displacement of the vane measuring angle of attack, an attempt was made to see whether delaying the angle of attack time history with respect to the rest of the data would have any effect on derivative extraction. This is shown (Run 6) in Table 3.3. It is concluded that no significant improvement results from doing this. In the rest of the work reported the angle of attack data was not delayed.

3.2.4. EFFECT OF CHANGING BREAK FREQUENCY IN DRYDEN SPECTRUM.

To determine the effect of changing the (3-db) break frequency in the gust (Dryden) spectrum, maneuver A was run (with starting values set at the wind-tunnel values), changing the break frequency to values an octave above and an octave below. As can be seen there is virtually no effect on

T A B L E 3.1

LOCKHEED JET-STAR DATA (NOMINAL)

V = 600 ft/sec

Weight = 3500 lbs.

Sampling interval: .02 sec.

ℓ_Z = 0

ℓ_α = 26 ft

K_α = 1.6

Z_α = -1.5 rad/sec

M_α = -8.82 rad/sec^2

M_θ = -1.4 rad/sec

Z_{δ_e} = -0.11 rad/sec

M_{δ_e} = -10.9 rad/sec^2

maneuver A, as is to be expected because the time history duration is not large enough. To remedy this, maneuvers A, B, C, and D were combined, and same changes made in the break frequency. Figures 3.3 and 3.4 show the estimated gust spectrum. The effect even here does not appear to be significant, because the time-history is still not long enough.

3.2.5. EFFECT OF MAKING Z_{δ_e} DEPENDENT ON M_{δ_e}

As mentioned earlier, the control derivatives Z_{δ_e} and M_{δ_e} may be allowed to be independently determined, or one allowed to be a multiple of the other, and the coefficient of multiplication estimated. Table 3.3, run 9 shows the effect of making them dependent. As compared to the standard run, run 1, in the same table, there does not appear to be any significant change, except perhaps in the value of Z_{δ_e} itself.

3.3 MAIN RESULTS

In this section we present the main results of derivative extraction. The results on each maneuver are grouped and identified by the segment of time-history: A, B, C, D, E, CD, and ABCD. In all the cases, the starting values of the derivatives were the wind-tunnel values, with the initial states all set to be zero, and L_{w_g} taken to be 1000.

For each maneuver a set of five figures, each clearly identified by the segment used are given the time history plot superimposed on the estimated time history for visual comparison, the time history plot of the errors.

Δq

$\Delta\theta$

Δa_n

$\Delta\alpha$;

and the corresponding P.S.D's and estimated states:

$\hat{\theta}$

$\hat{q}$

$\hat{\alpha}_s$

$\hat{\alpha}_g$,

Note that $\hat{\alpha}_g$ yields (an estimate of) the actual gust incident waveform. The p.s.d. derived from this, the estimated gust p.s.d., is also shown. The figures have been numbered consecutively, from Fig. 3.5 thru fig. 3.39. The parameter values for all these maneuvers and the C.R. bounds (in parenthesis) are tabulated in Table 3.4. Finally figure 3.40 shows the means and variances over these maneuvers, along with the wind-tunnel values.

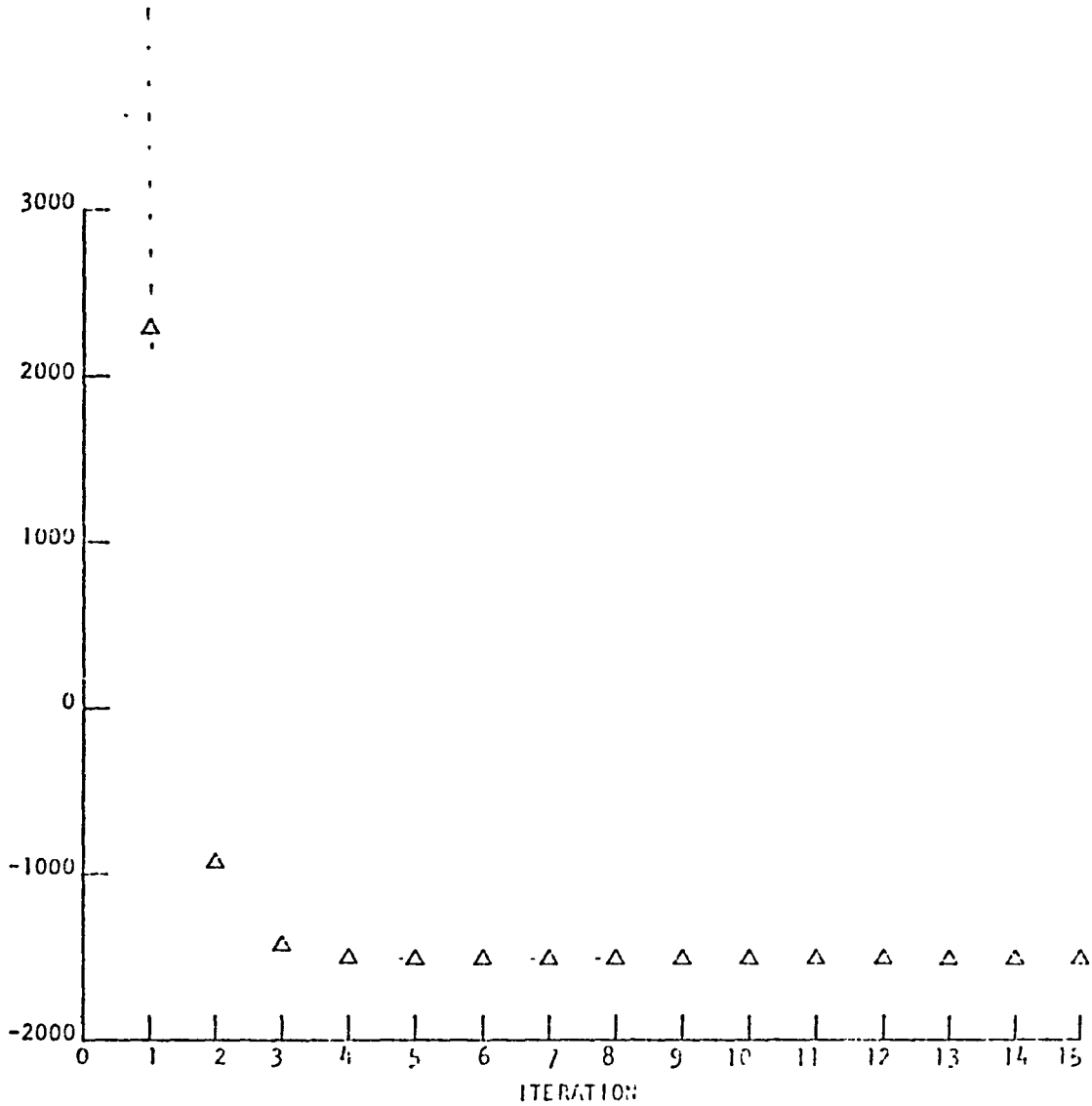

Fig. 3.1 Cost Functional Vs. Iteration

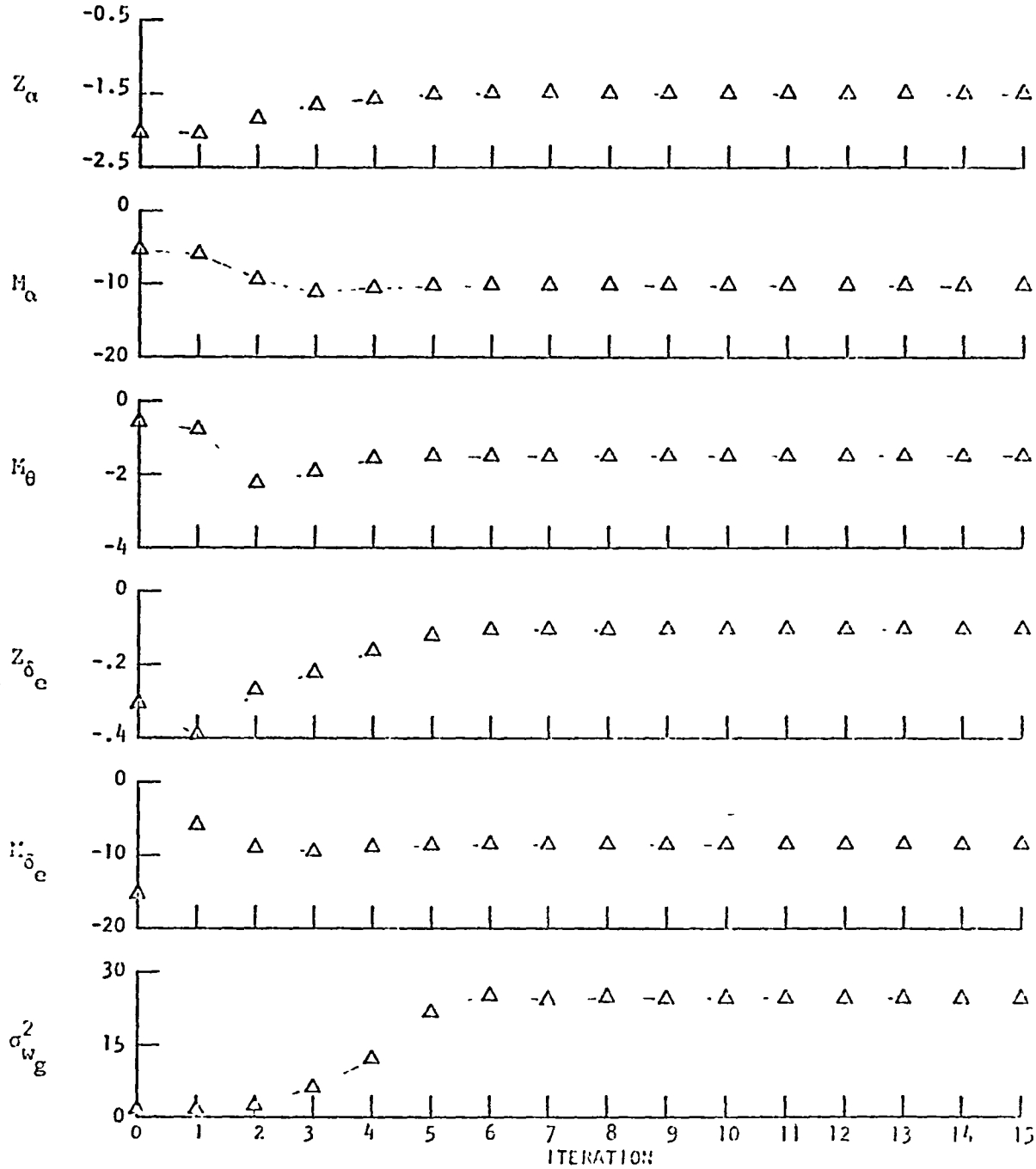

Fig. 3.2: Plot of Derivative Values vs. Iteration

TABLE : 3.2

Iteration	Cost Functional
0	324568.27
1	2303.46
2	-918.270
3	-1417.5673
4	-1493.9562
5	-1497.4350
6	-1497.5041
7	-1497.5119
8	-1497.5084
9	-1497.5103
10	-1497.5094
11	-1497.5099
12	-1497.5097
13	-1497.5099
14	-1497.5098
15	-1497.5099

TABLE : 3.3

RUN	Z_α	M_α	M_θ	Z_{δ_e}	M_{δ_e}	$\sigma^2_{w_g}$	Z_0	M_0	$\alpha_s(0)$	$q(0)$	$\alpha_g(0)$	Cost Funct.
1	-1.45	-9.79	-1.43	-.098	-8.15	25.20	.011	-.276	-.015	-.0022	.015	-1497.1992
2	-1.45	-9.79	-1.43	-.098	-8.15	25.18	.011	-.276	-.015	-.0022	.016	-1497.2302
3	-1.45	-9.79	-1.43	-.098	-8.15	25.17	.011	-.276	-.015	-.0022	.016	-1497.2401
4	-1.45	-9.79	-1.43	-.098	-8.15	25.19	.011	-.276	-.015	-.0022	.016	-1497.5099
5	-1.45	-9.76	-1.44	-.096	-8.17	25.78	.009	-.277	0.0	0.0	0.0	-1497.2622
6	-1.46	-9.86	-1.57	-.066	-8.15	26.95	.012	-.276	-.014	-.0006	.013	-1498.8137
7	-1.46	-9.89	-1.43	-.110	-8.24	11.95	.010	-.279	-.010	-.0021	.011	-1497.4225
8	-1.45	-9.79	-1.43	-.098	-8.16	50.13	.012	-.276	-.027	-.0022	.028	-1497.2538
9	-1.44	-9.73	-1.44	-.075	-8.04	25.90	.012	-.272	-.015	-.0021	.016	-1496.9238

RUN 1 : Start at Wind Tunnel Value.
RUN 2 : Start at -1.3, -10.84, -1.83, -.001, -7.16,10.0, 0, 0, 0, 0, 0, 0, 0
RUN 3 : Start at -1.0, -15.0, -2.0, 0., -5.0, 2.0, 0, 0, 0, 0, 0, 0, 0
RUN 4 : Start at -2.0, -5.0, -.5, -.3, -15.0, 2.0, 0, 0, 0, 0, 0, 0, 0
RUN 5 : Start at Wind Tunnel Value, x(0) = 0.
RUN 6 : Start at Wind Tunnel Value, α measurement delayed .04 second (2 data points)
RUN 7 : Start at Wind Tunnel Value, L_{w_g}=500
RUN 8 : Start at Wind Tunnel Value, L_{w_g} = 2000
RUN 9 : Start at Wind Tunnel Value, Set $Z_{\delta_e} = F_c M_{\delta_e}$, F_c=0.00932

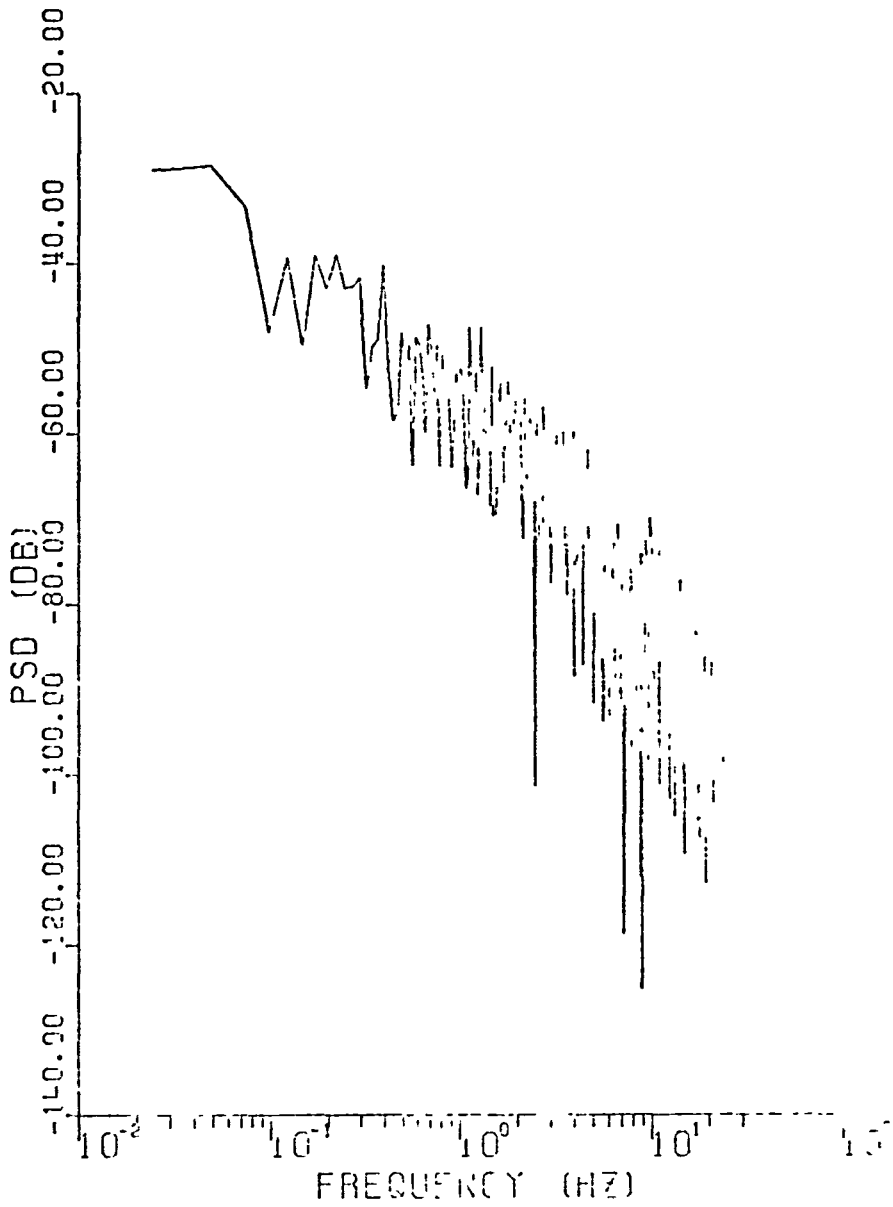

α_g

PSD OF EST. TURB. E CE :JET ST. & MANEUVER FTC

Fig. 3.3: Maneuver ABC with L_{w_ε} =800.

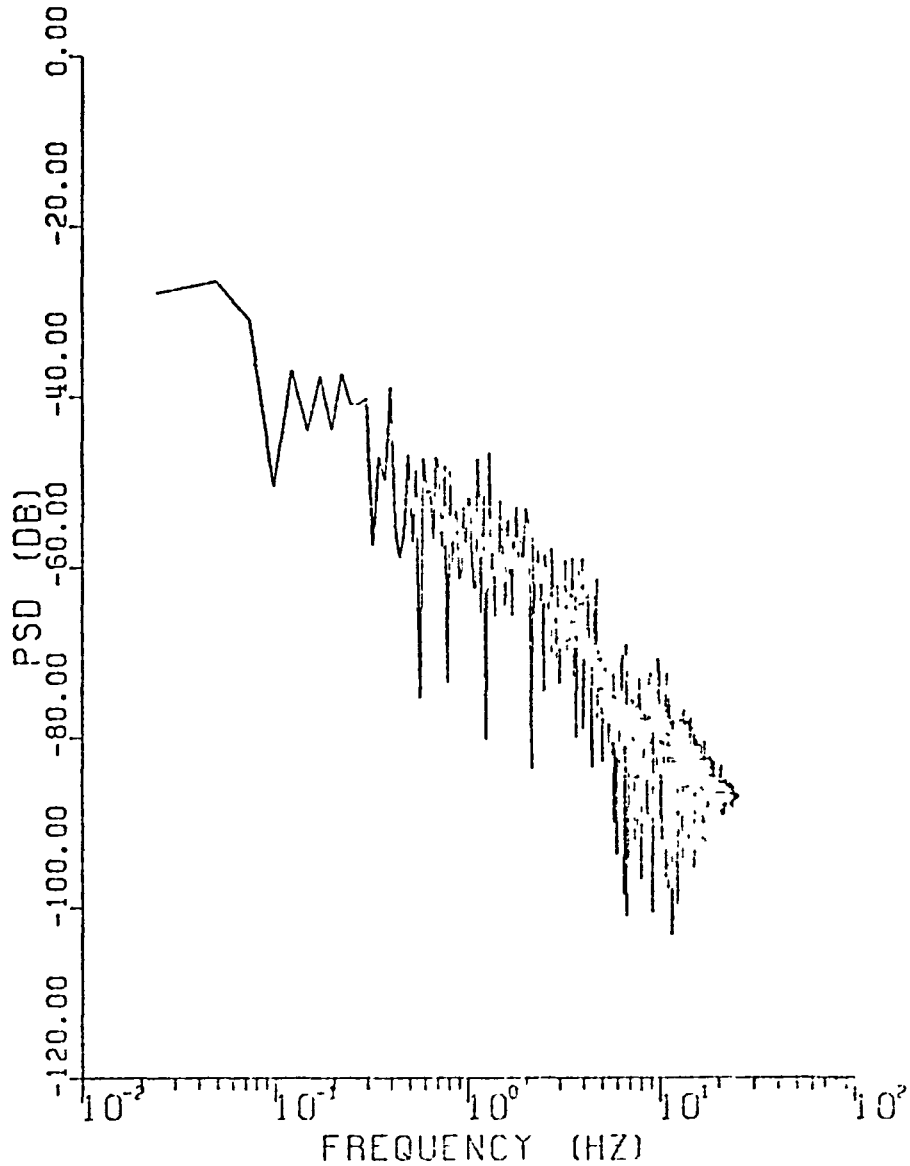

α_g

PSD OF EST. TURBULENCE -JET STAR MANOUVER PSCD

Fig. 2.4: Maneuver AEC with L_t =200.

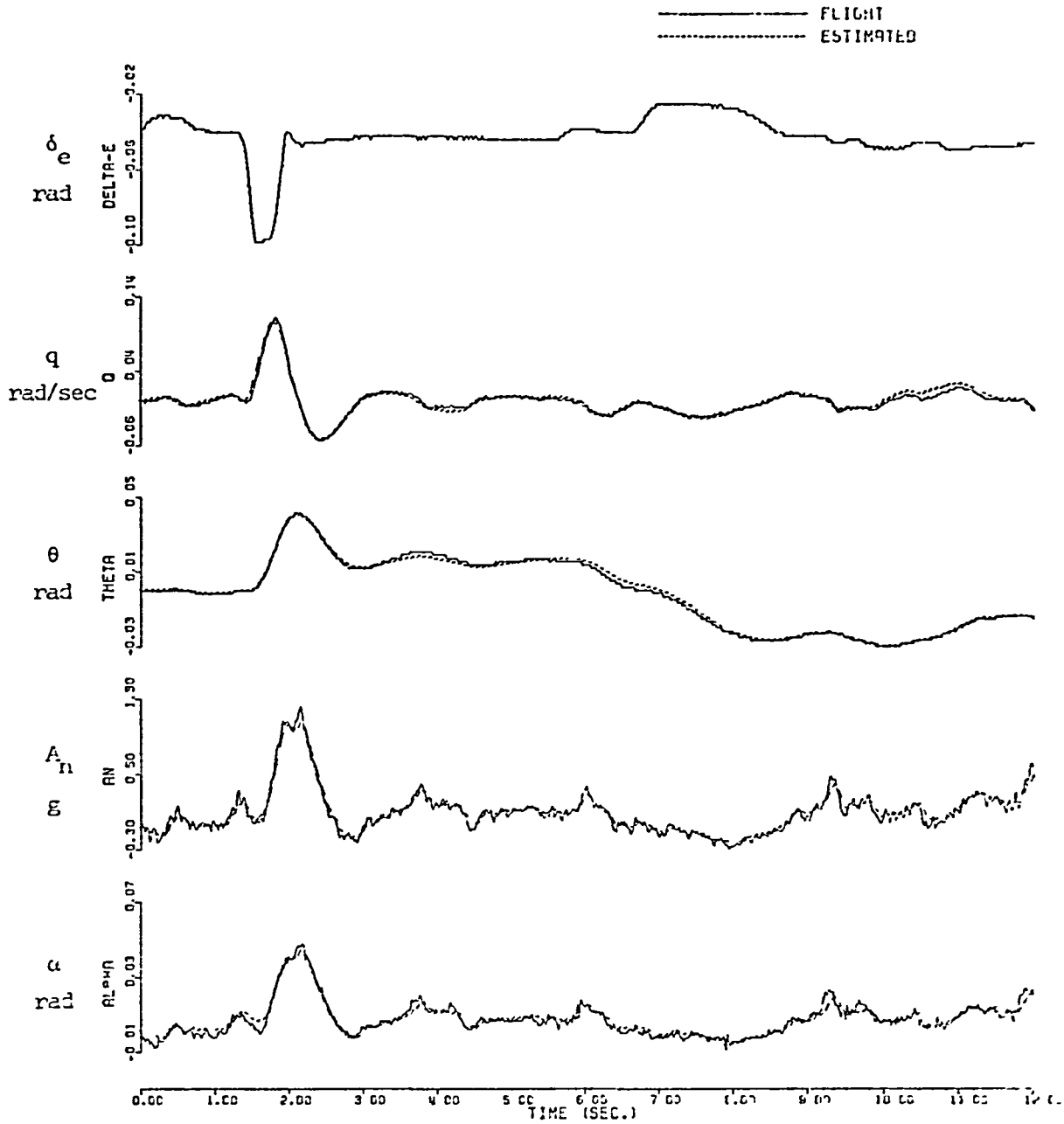

Fig. 3.5 TIME HISTORY PLOT : JET STAR MANEUVER A

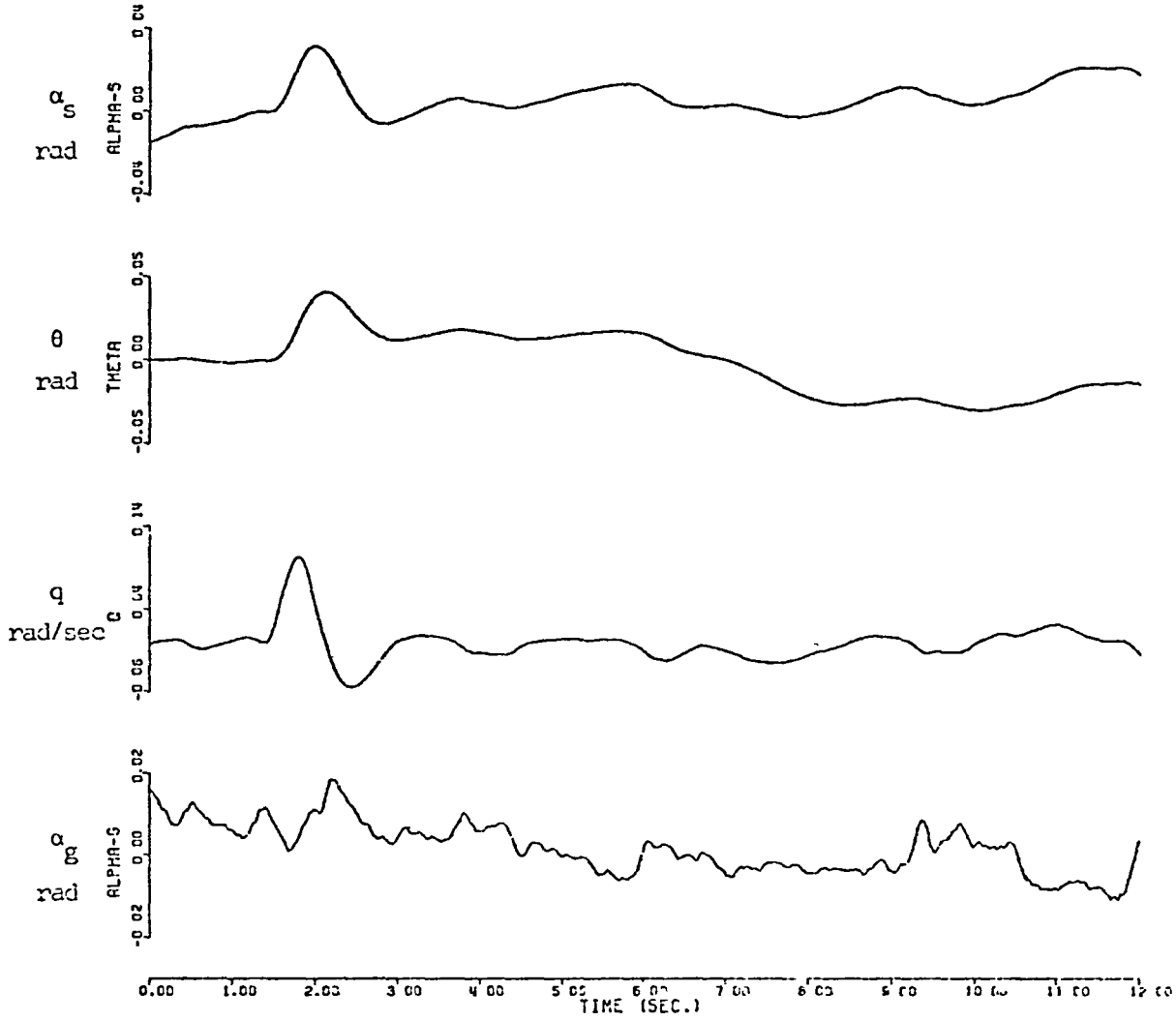

Fig. 3.6 ESTIMATED STATE : JET STAR MANEUVER A

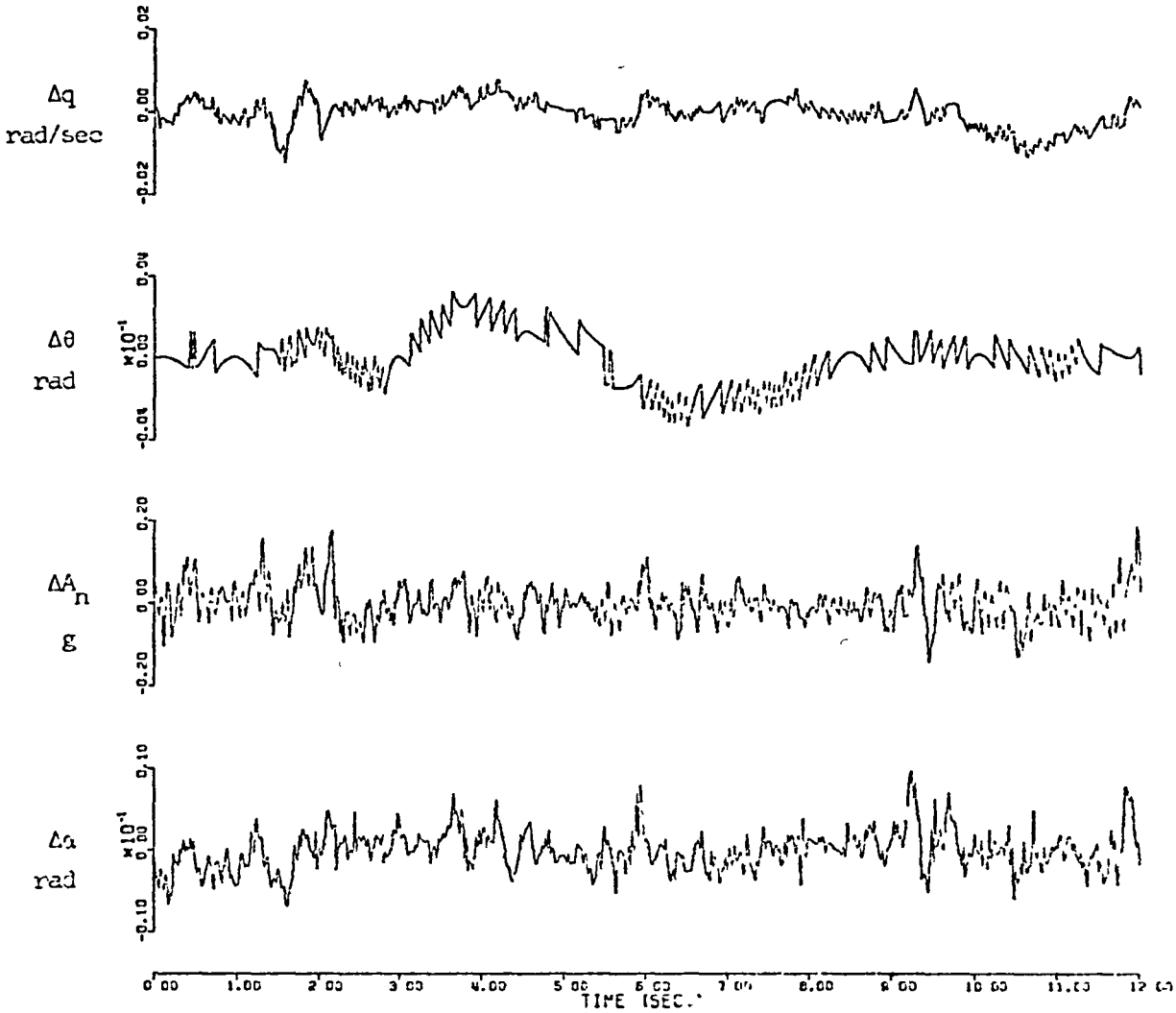

Fig. 3.7 FIT ERROR : JET STAR MANEUVER A

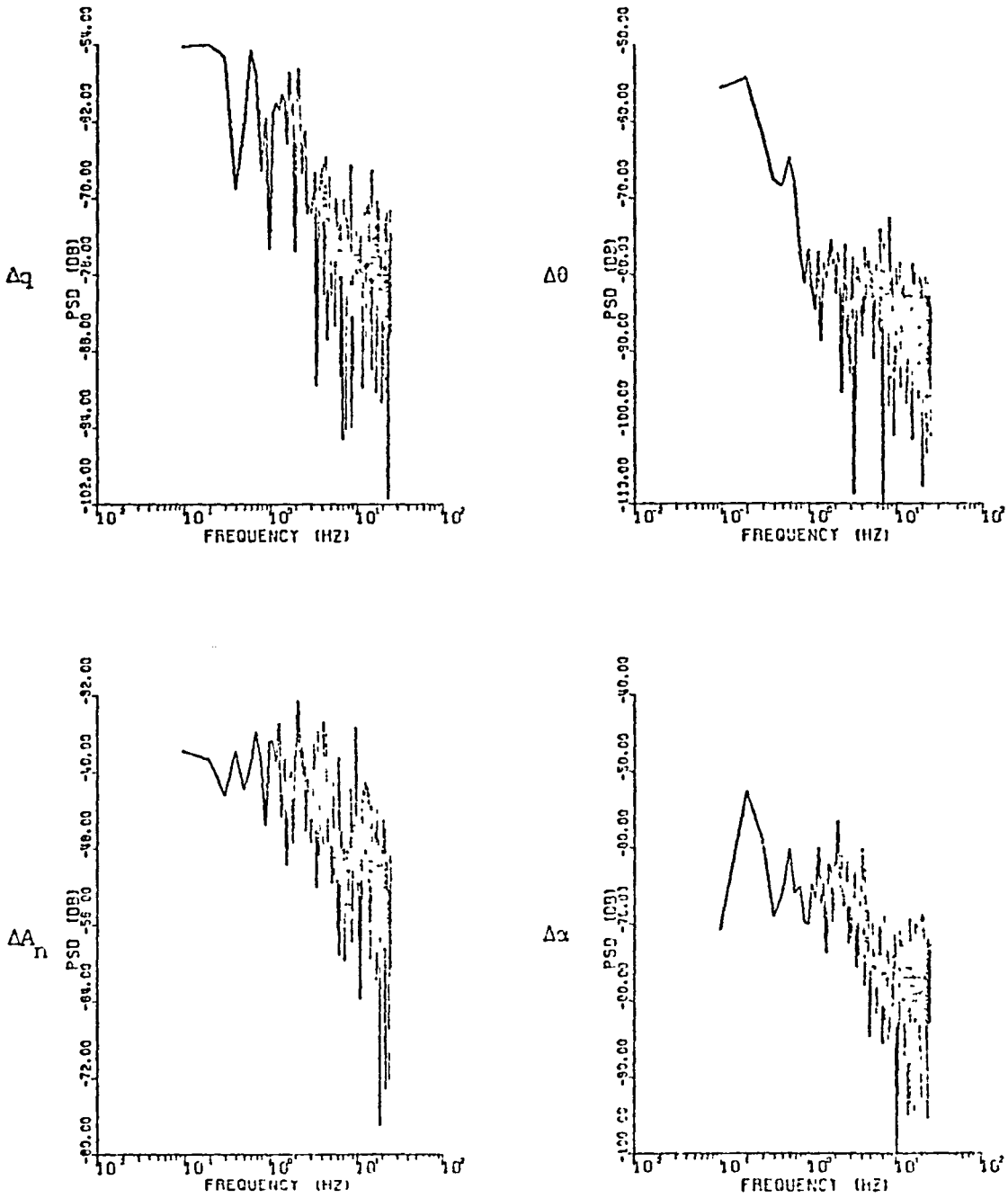

Fig. 3.8 PSD Of FIT ER-3 JET STAR MANEUVER 8

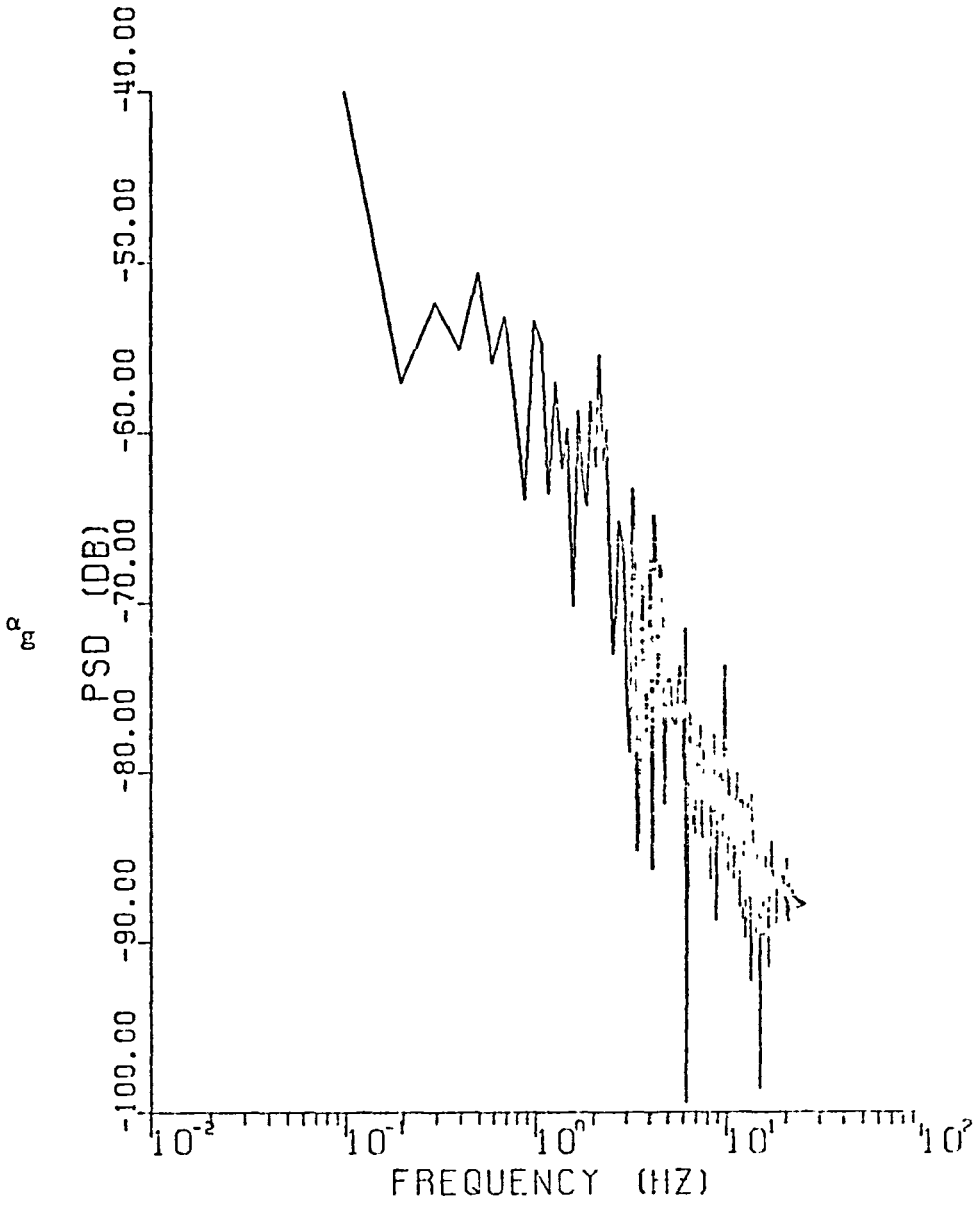

Fig. 3.9 PSD OF EST. TURBULENCE : JET STAR MANEUVER A

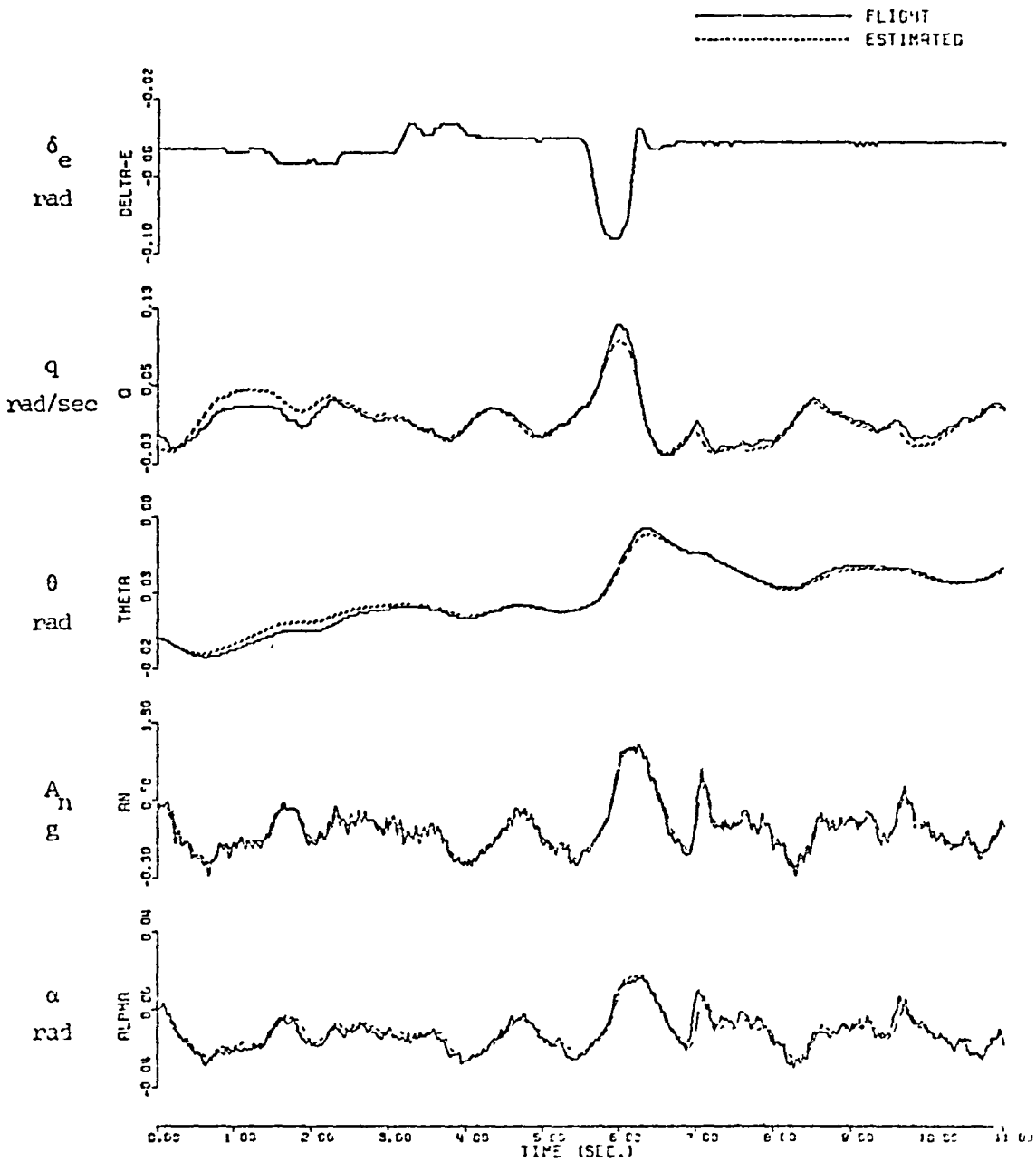

Fig. 3.10 TIME HISTORY PLOT JET STAR MANEUVER B

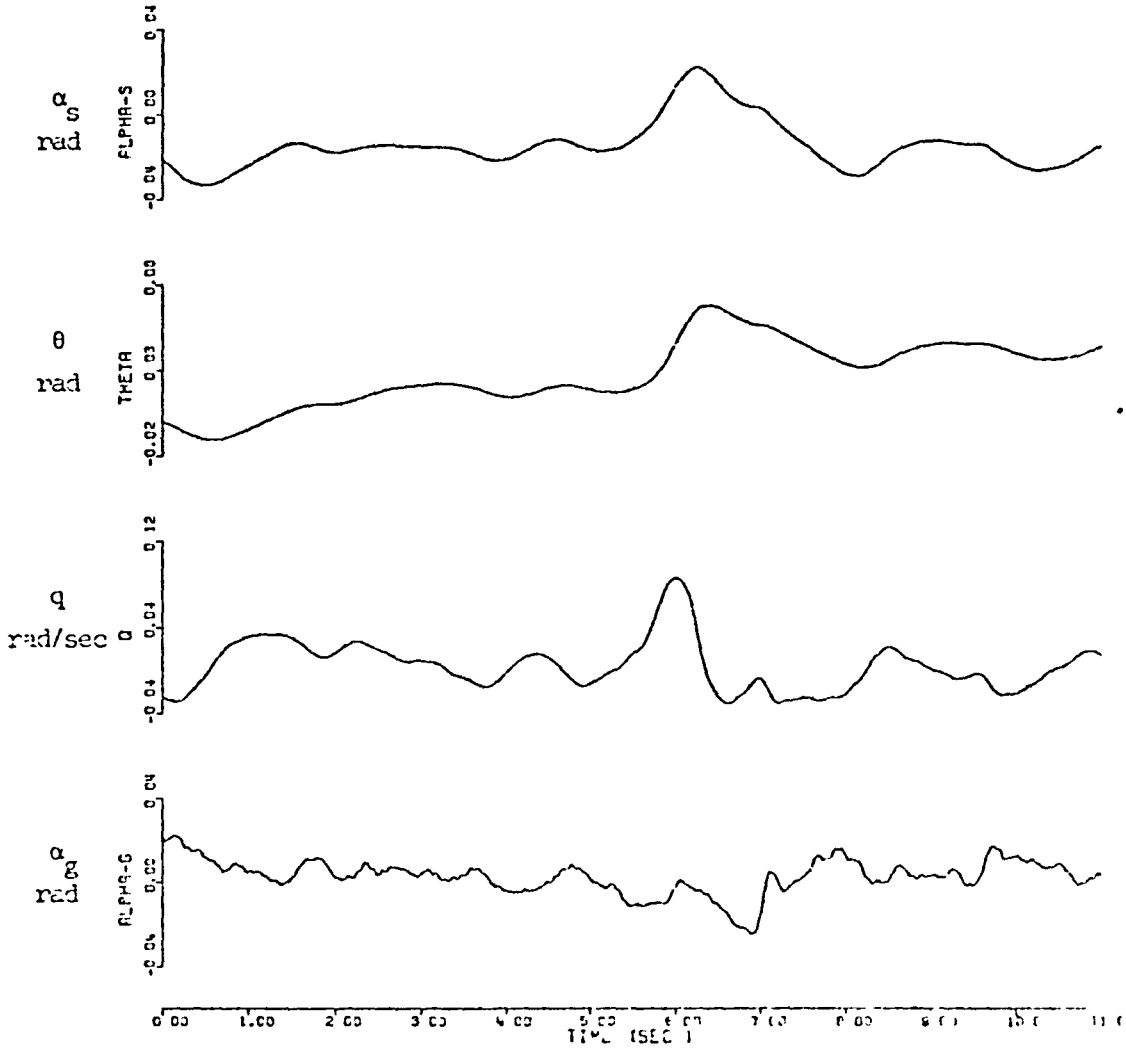

Fig. 3.11 ESTIMATED STATE . JET STAR MANEUVER B

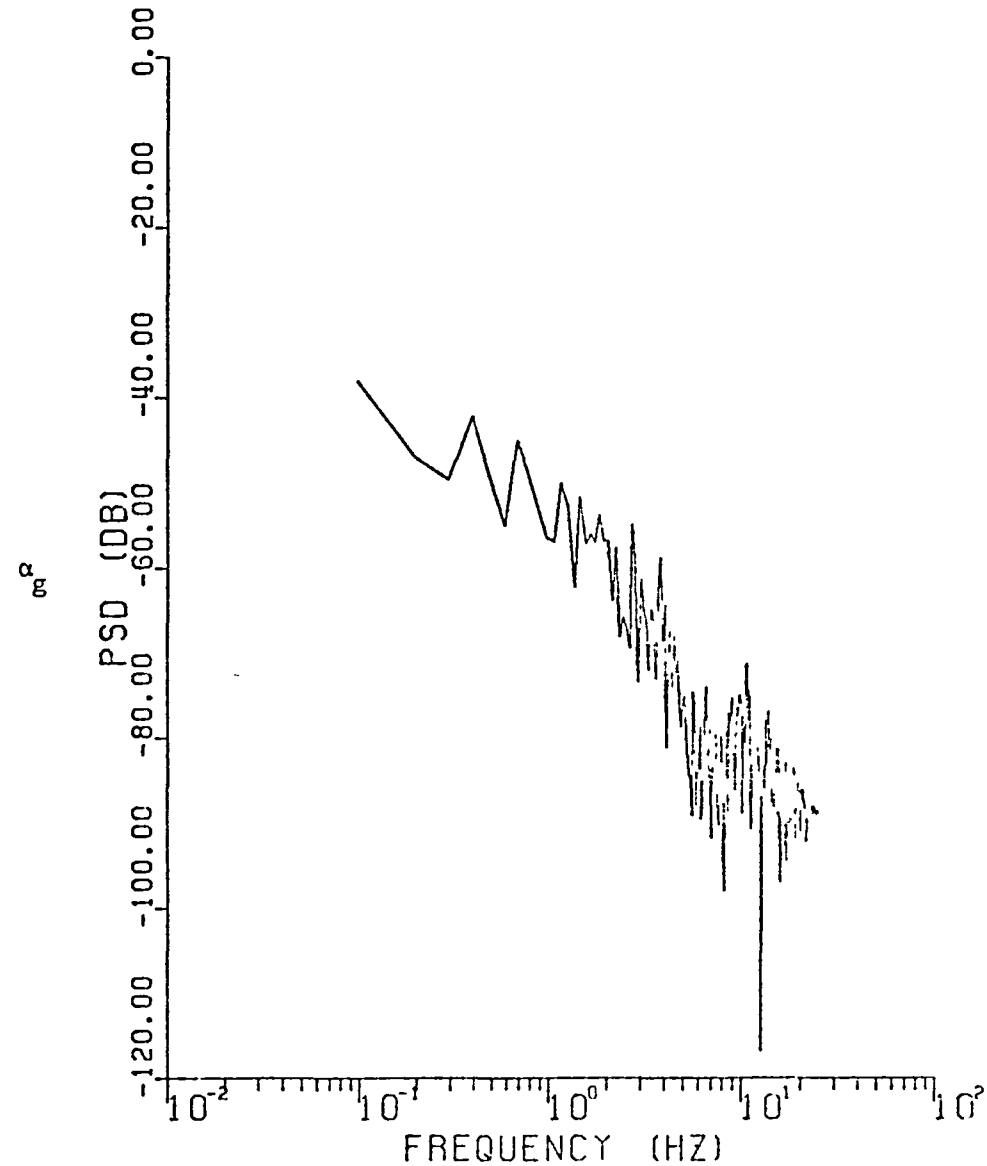

Fig. 3.12 PSD OF EST. TURBULENCE :JET STAR MANEUVER B

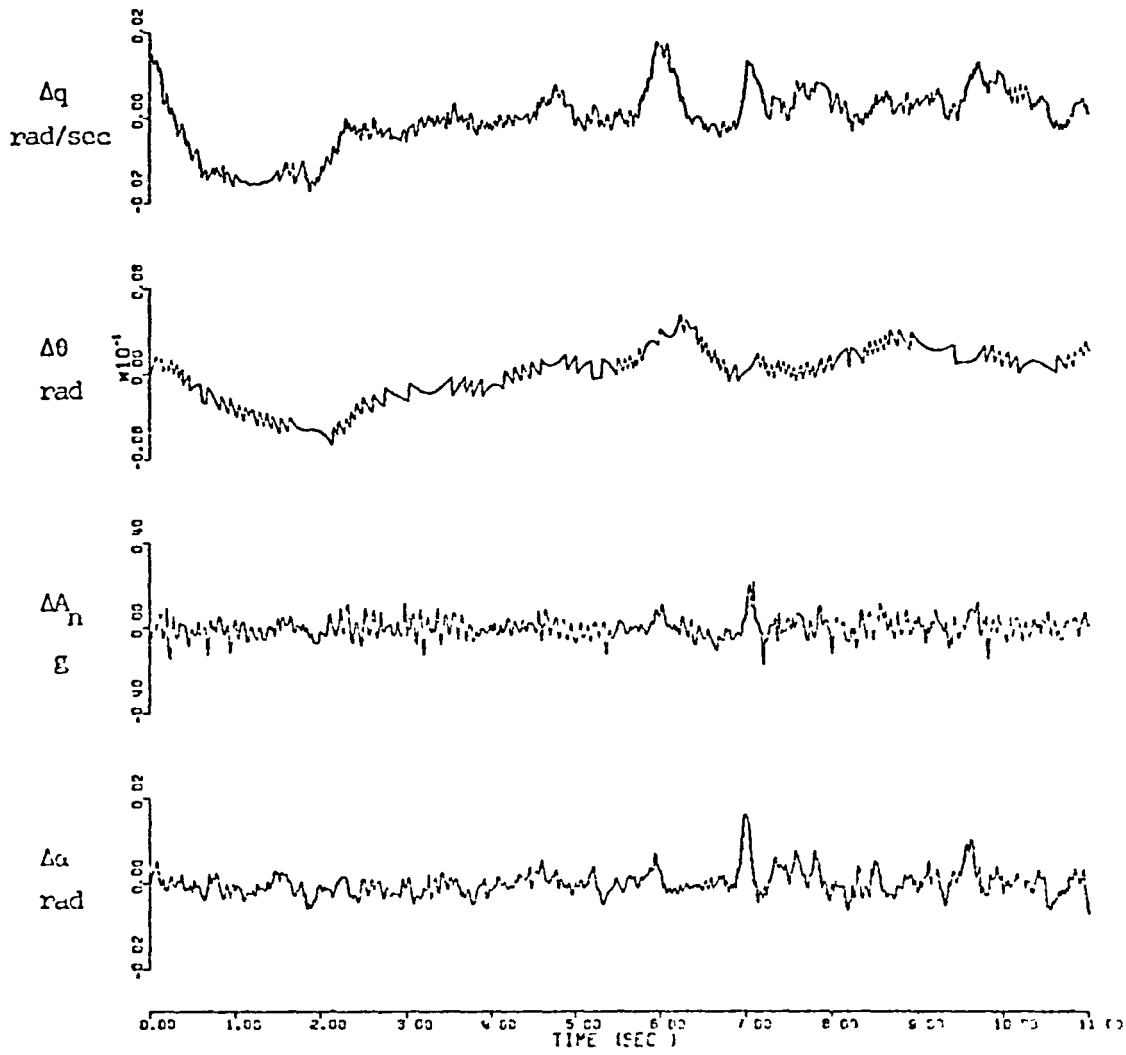

Fig. 3.13 FIT ERROR : JET STAR MANEUVER 8

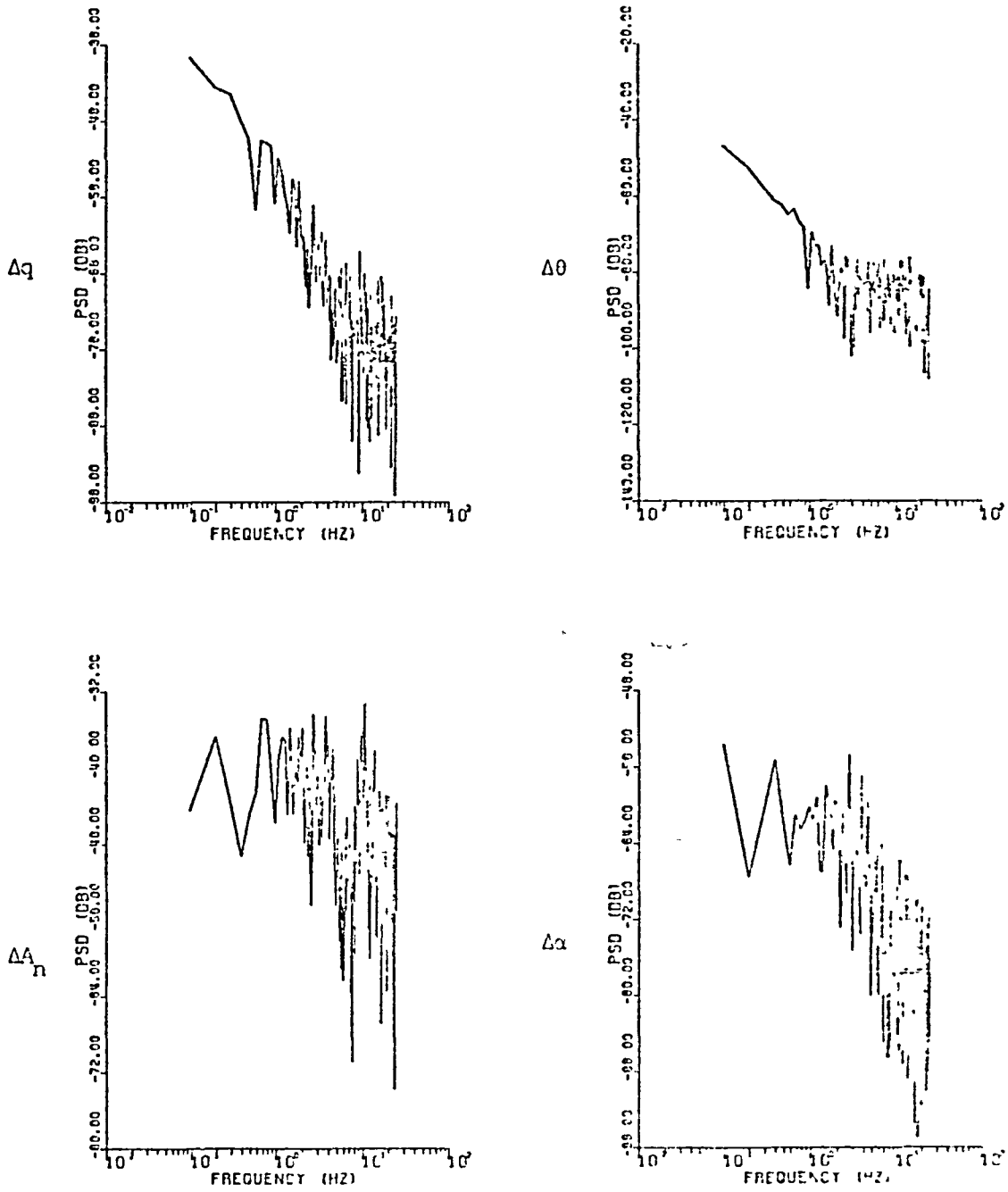

Fig. 3.14 PSD OF FIT ERROR . JET STR MANEUVER 5

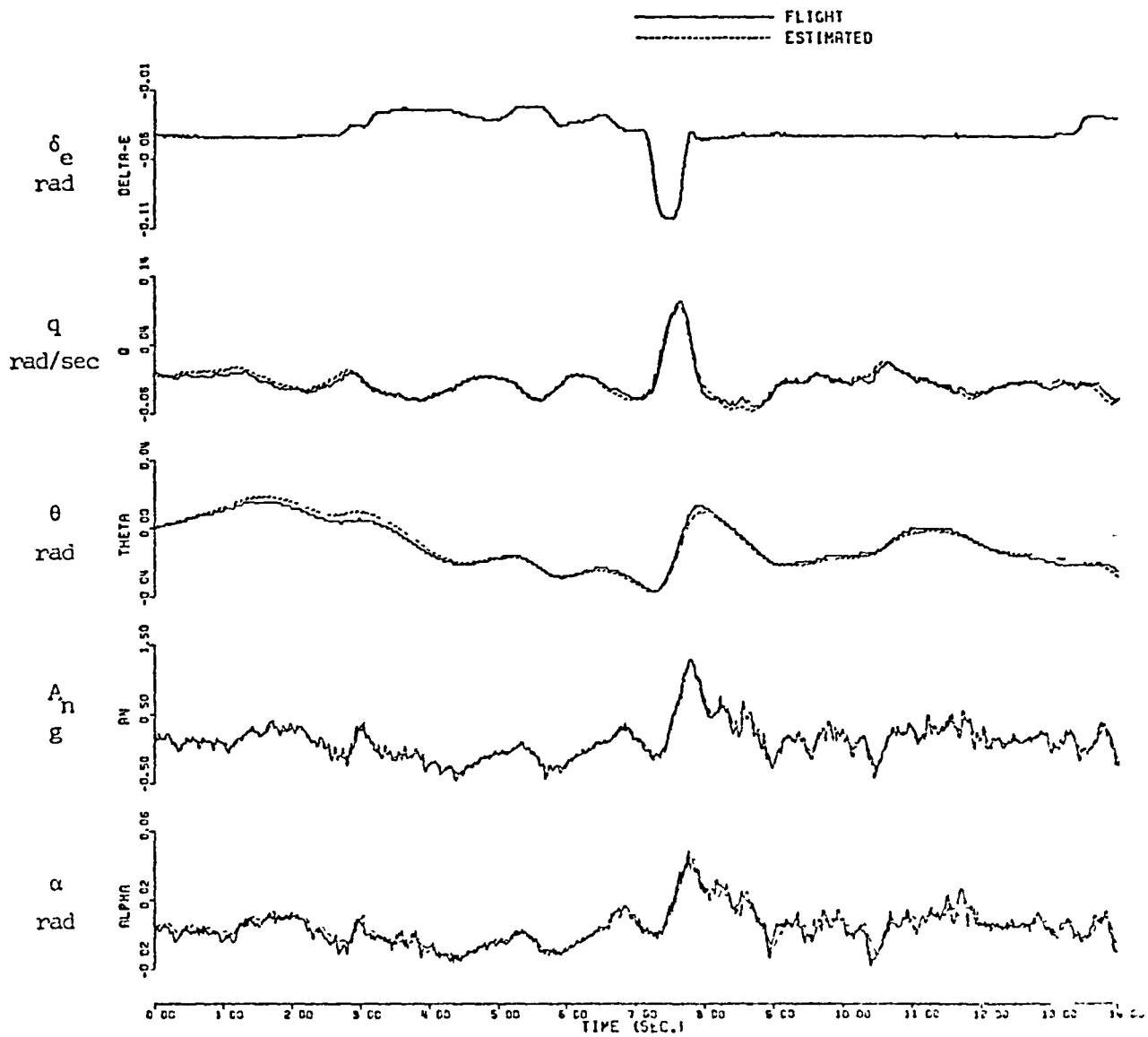

Fig. 3.15 TIME HISTORY PLOT : JET STAR MANEUVER C

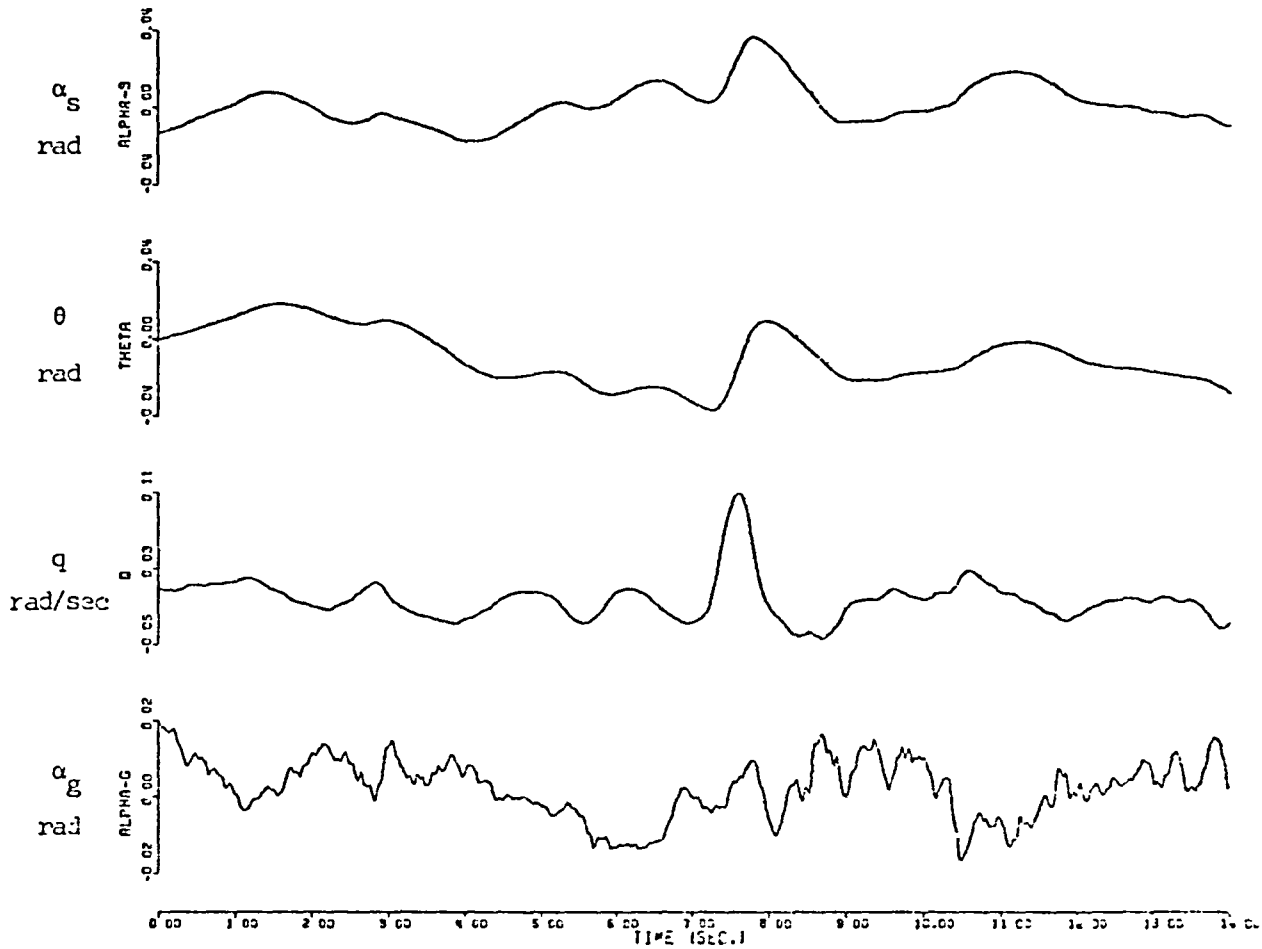

Fig. 3.16 ESTIMATED STATE : JET STAR MANEUVER C

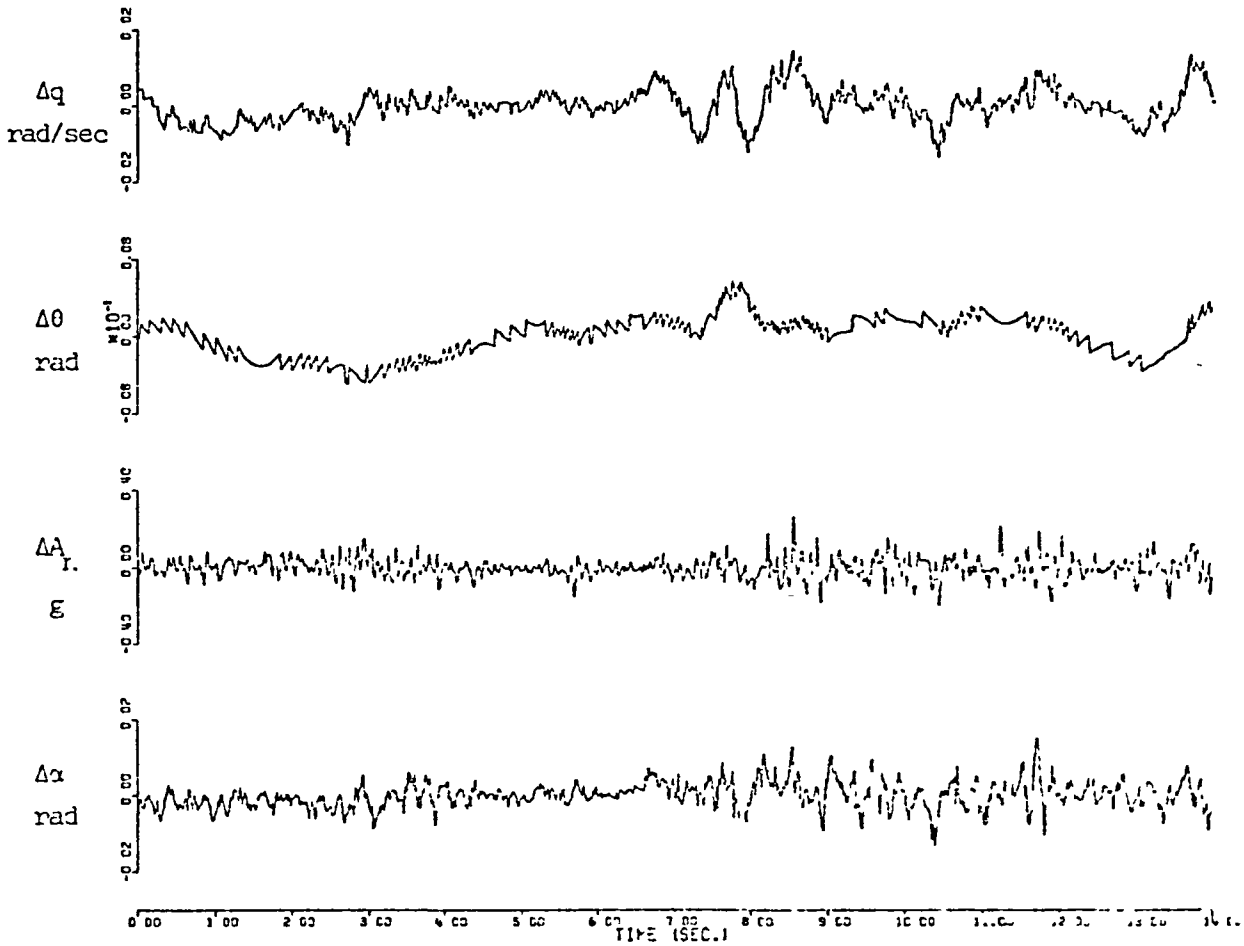

Fig. 3.17 FIT ERROR : JET STAR MANEUVER C

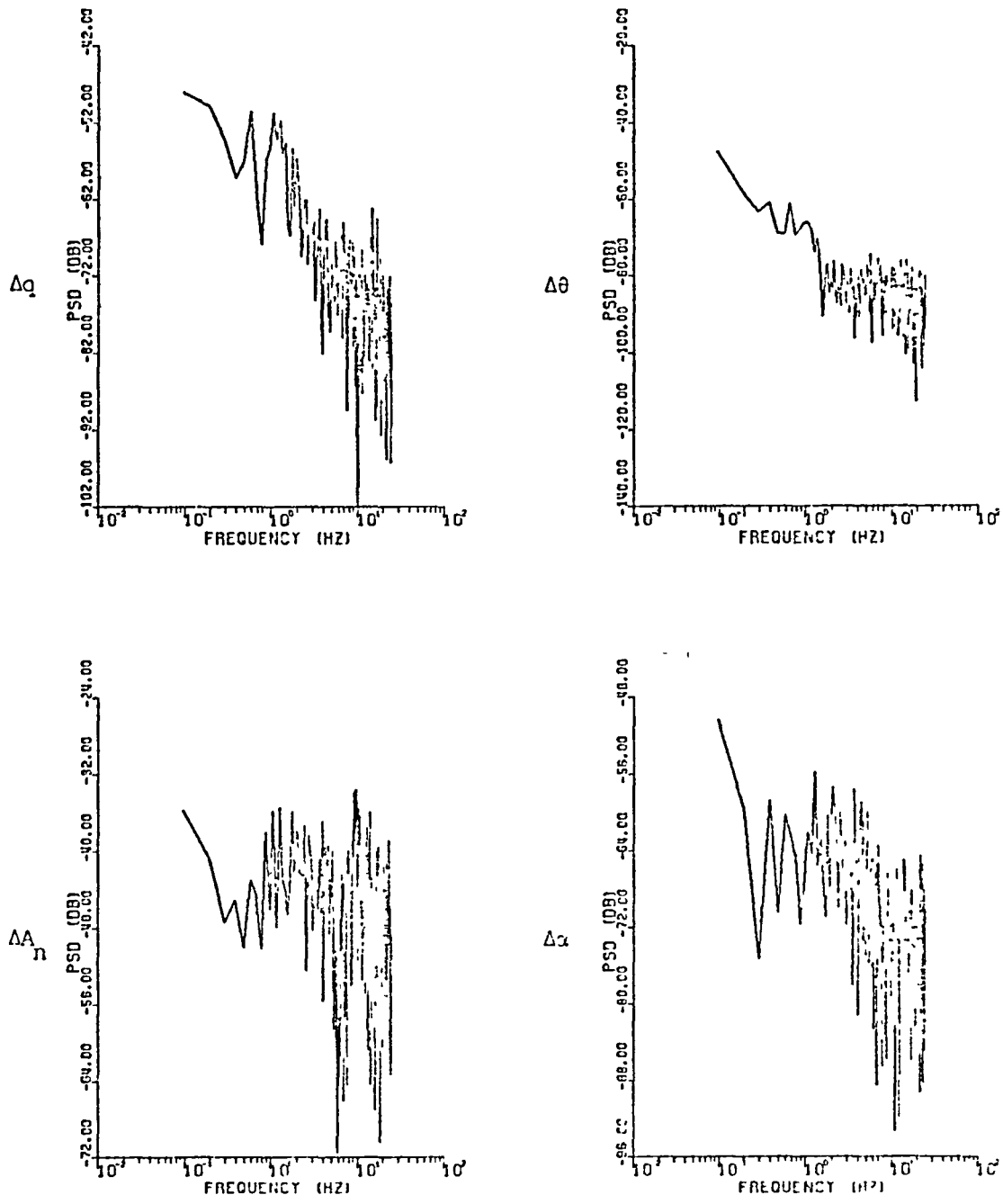

Fig. 3.18 PSD OF FIT ERROR . JET STAR POWER C

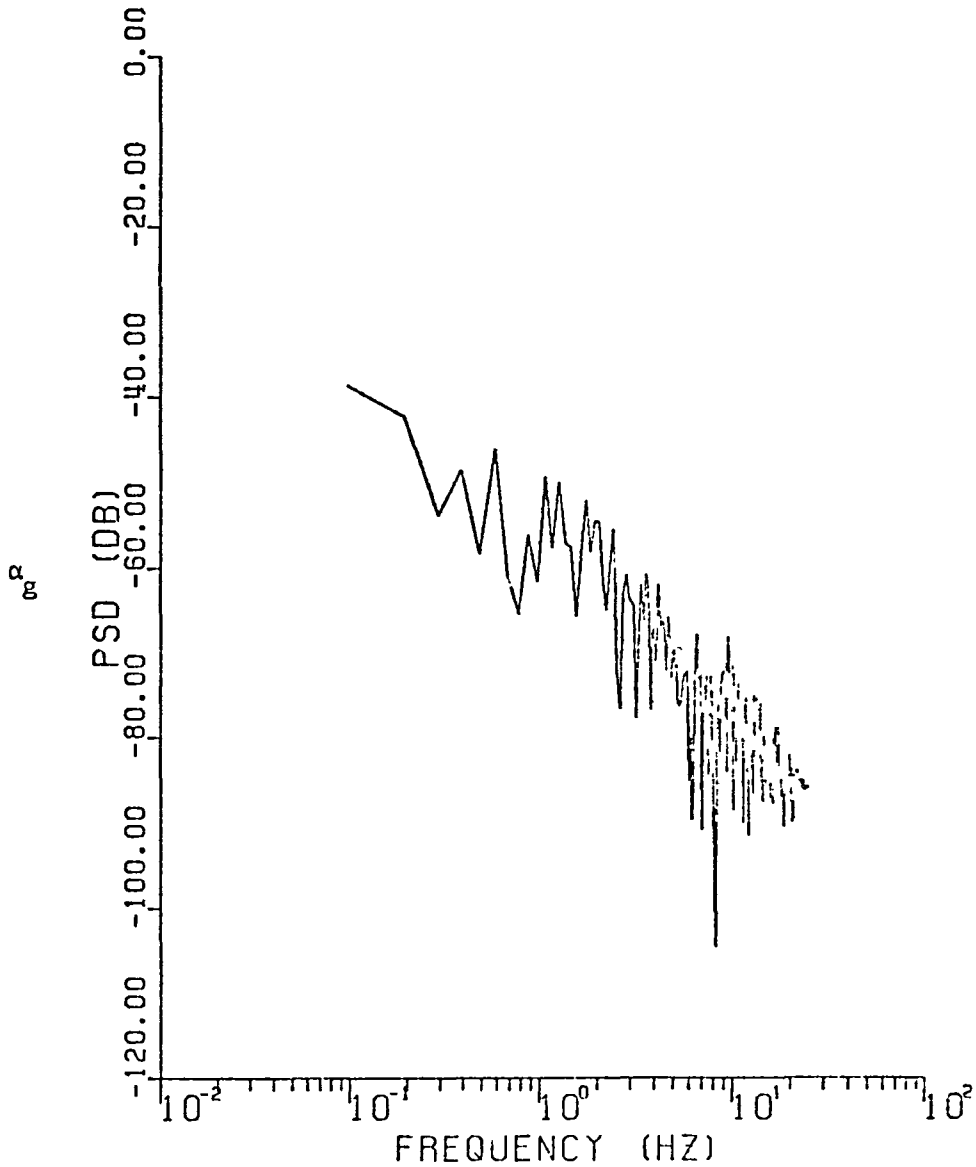

Fig. 3.19 PSD OF EST. TURBULENCE - JET STAR MANEUVER C

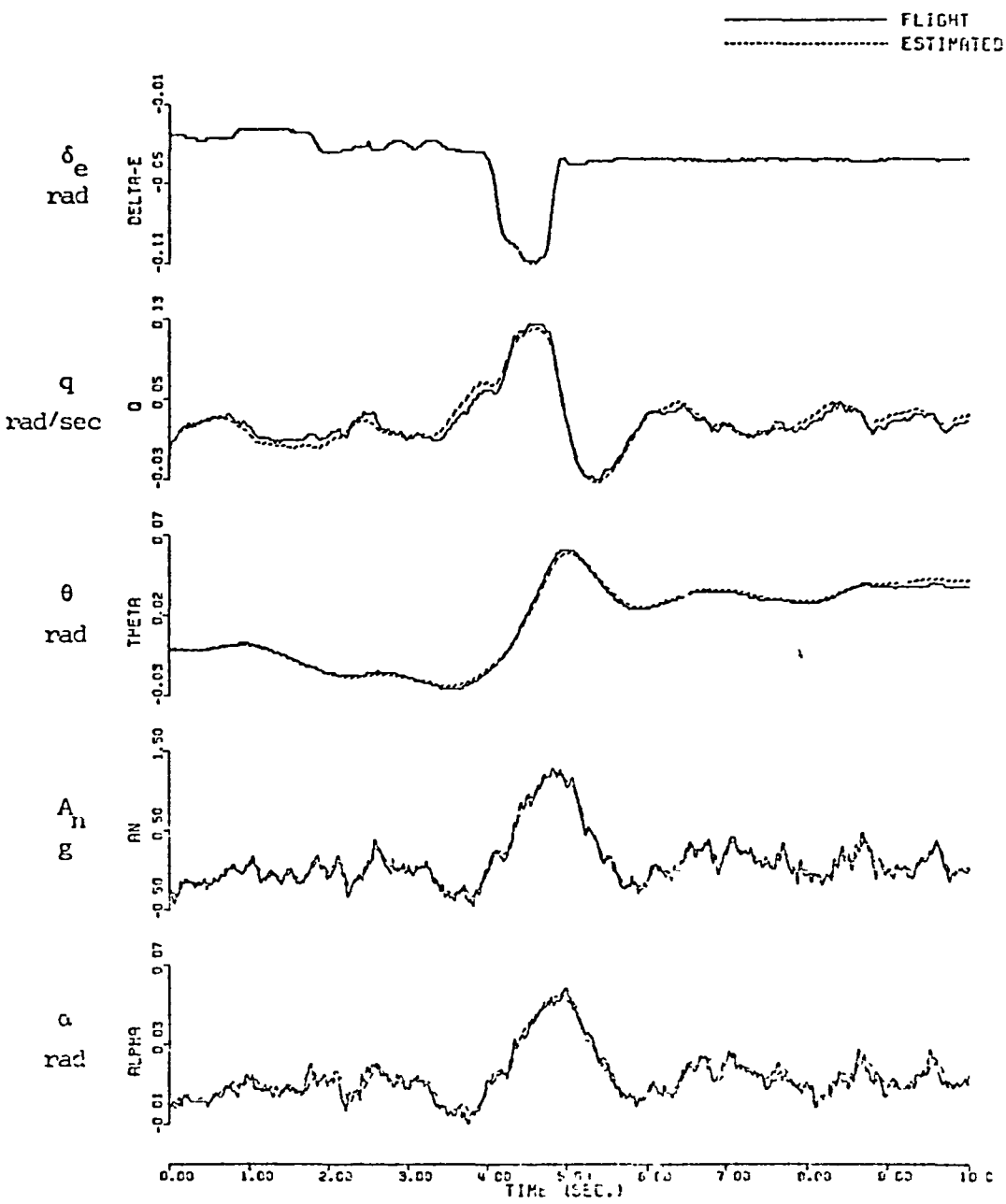

Fig. 3.20 TIME HISTORY PLOT : JET STAR MANEUVER D

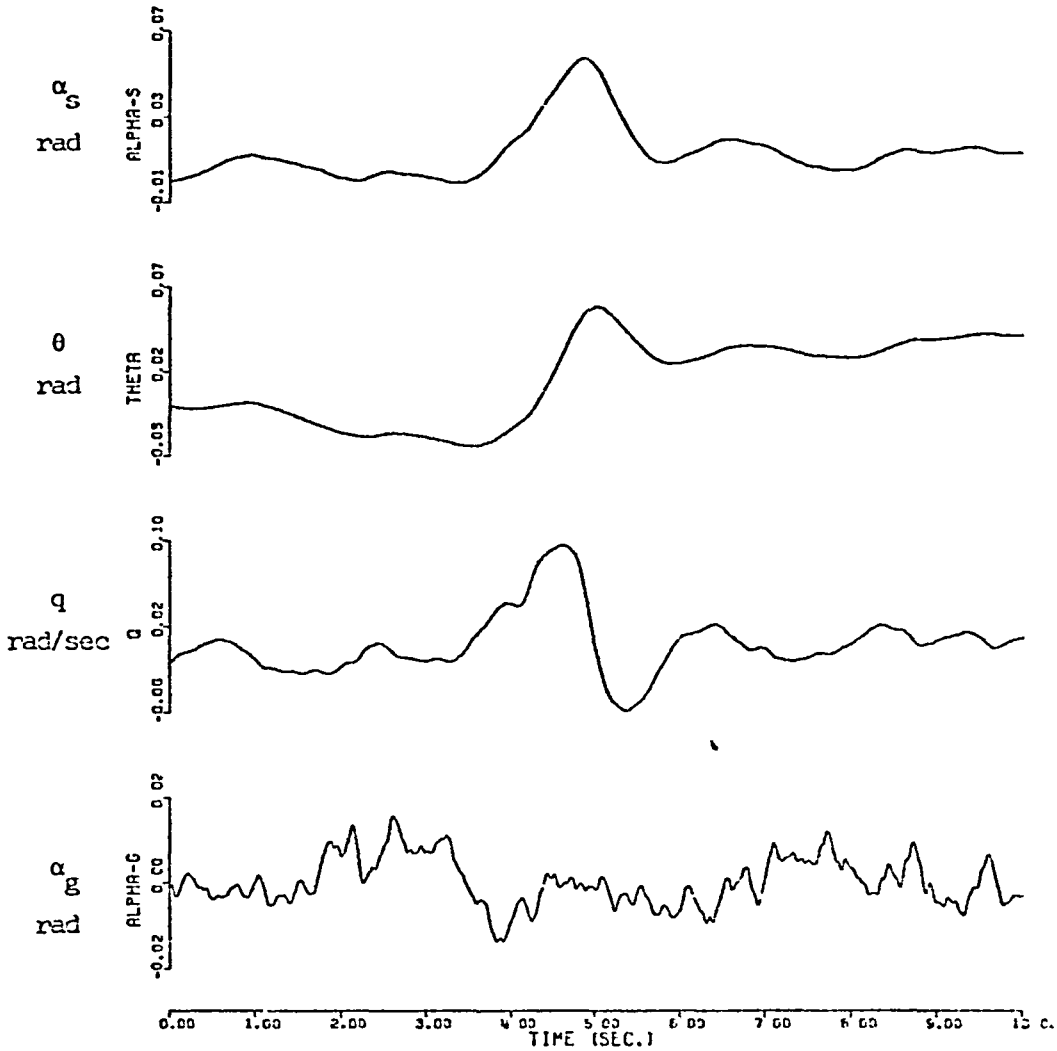

Fig. 3.21 ESTIMATED STATE : JET STAR MANEUVER D

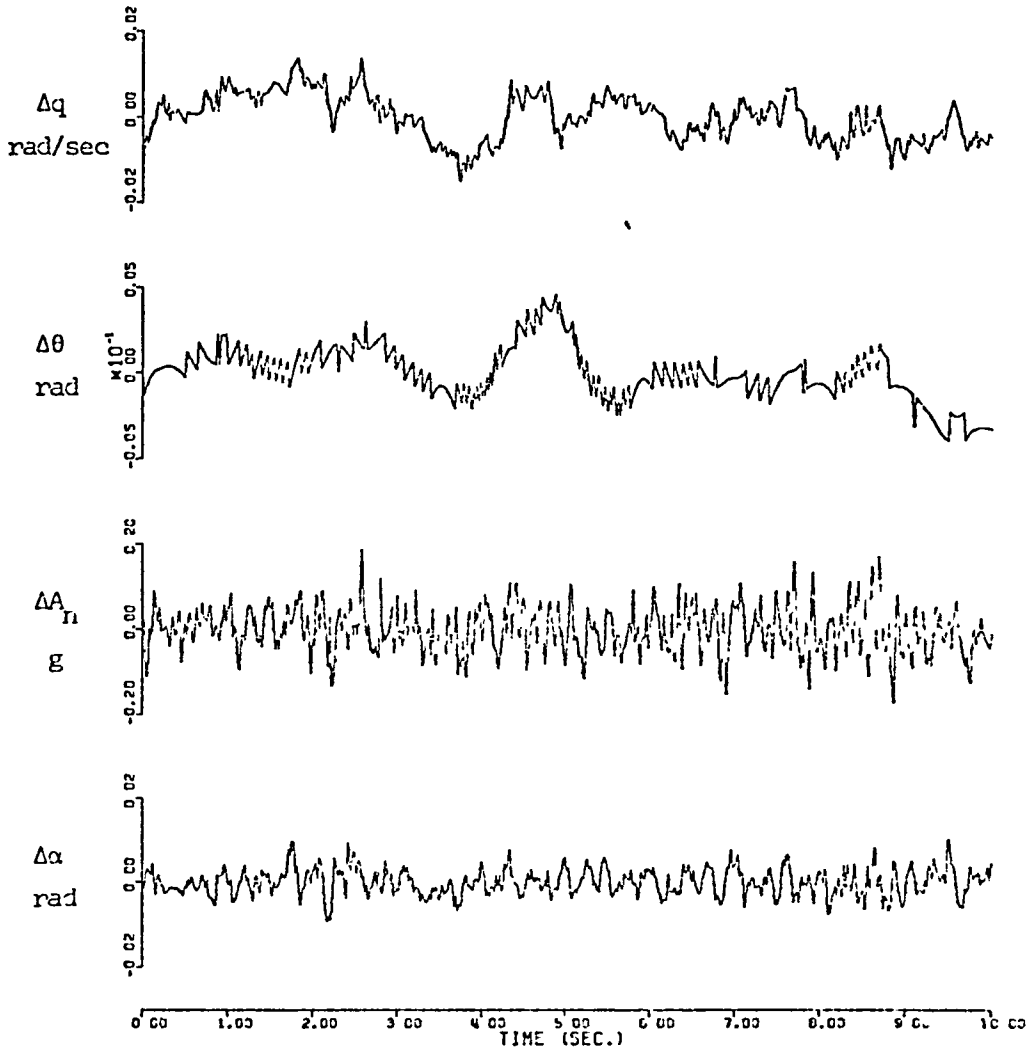

Fig. 3.22 FIT ERROR : JET STAR MANEUVER D

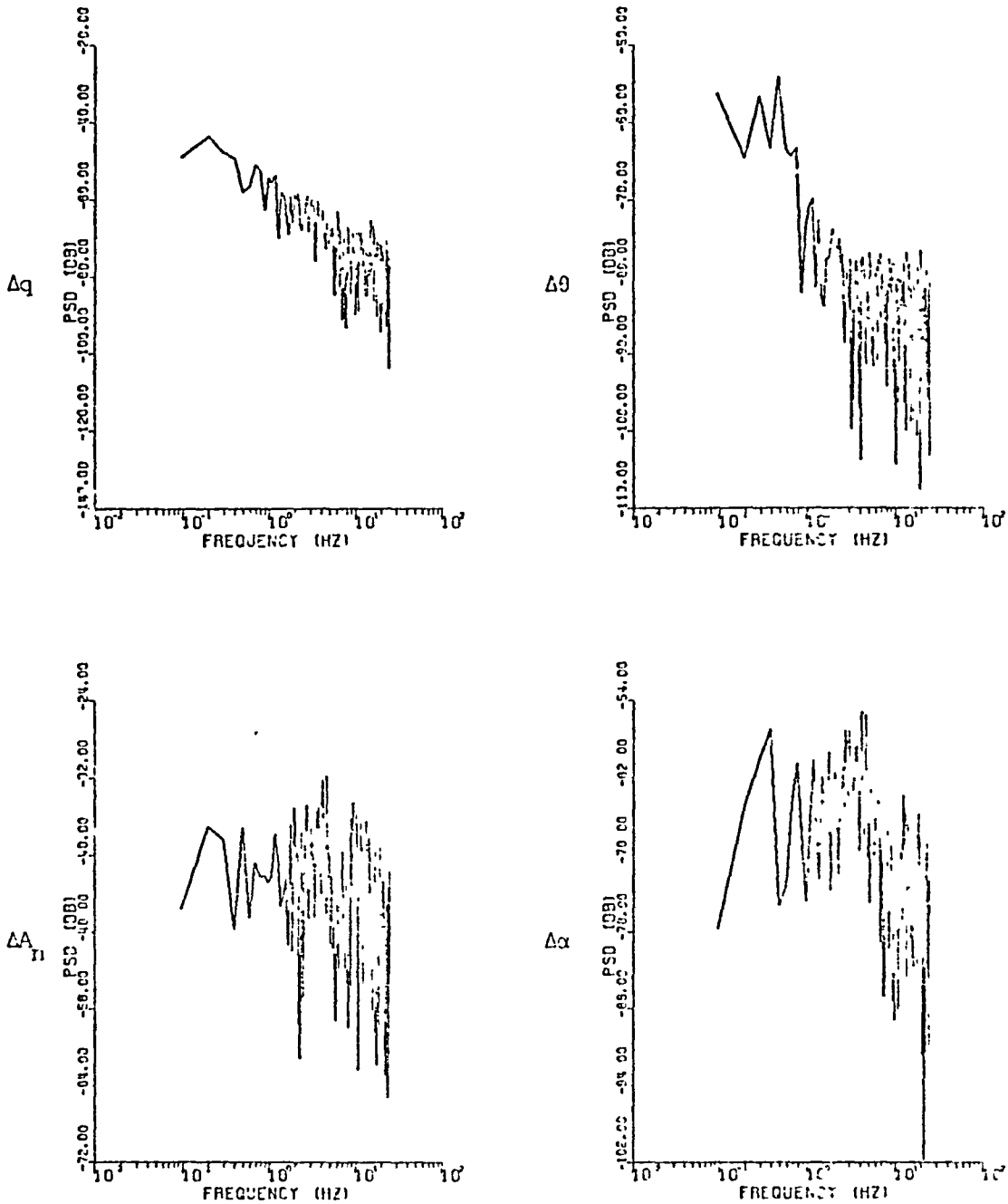

Fig. 3.23 PSD OF FIT ERROR : JET STAR MANEUVER D

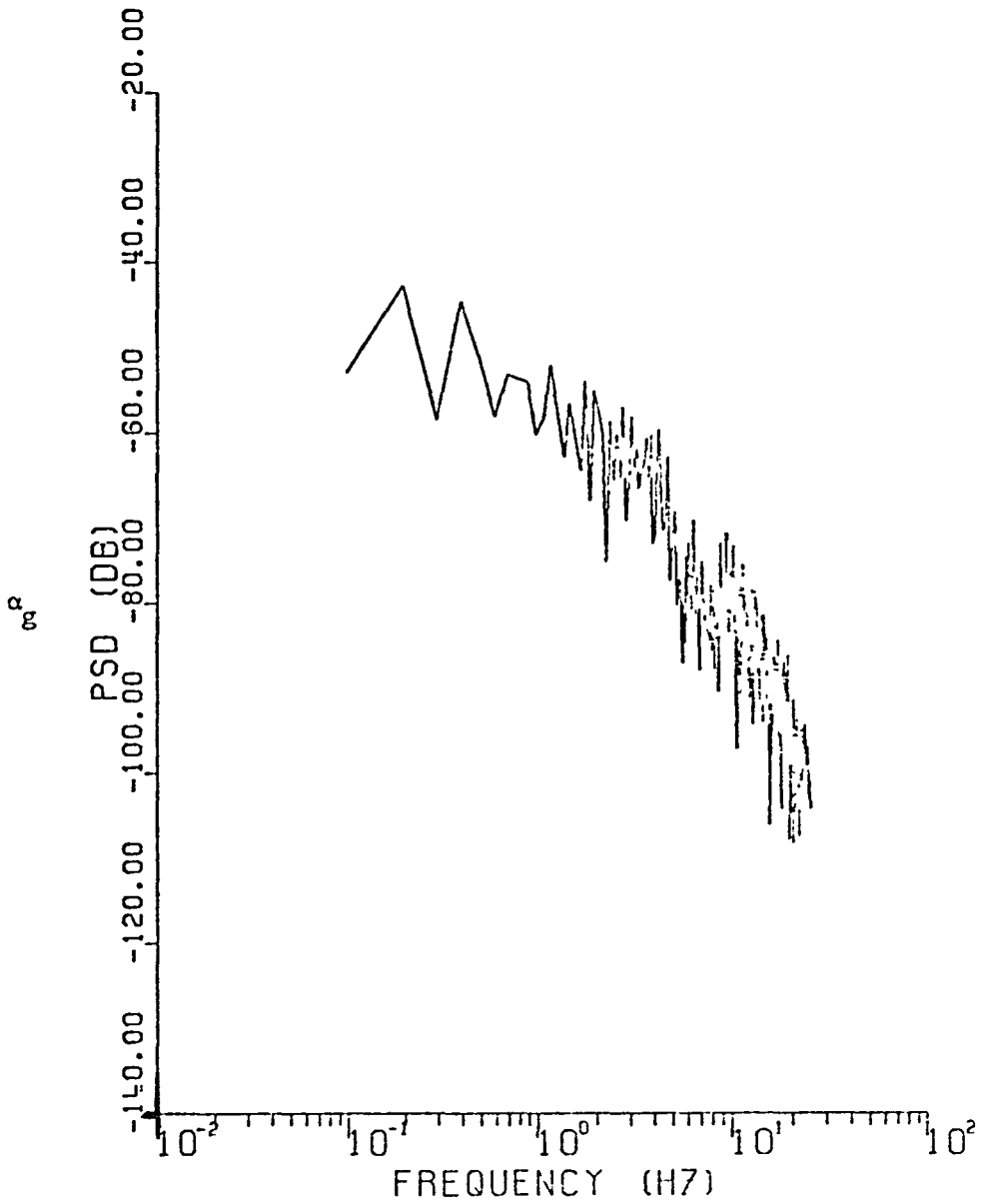

Fig. 3.24 PSD OF EST. TURBULENCE : JET STAR MANEUVER D

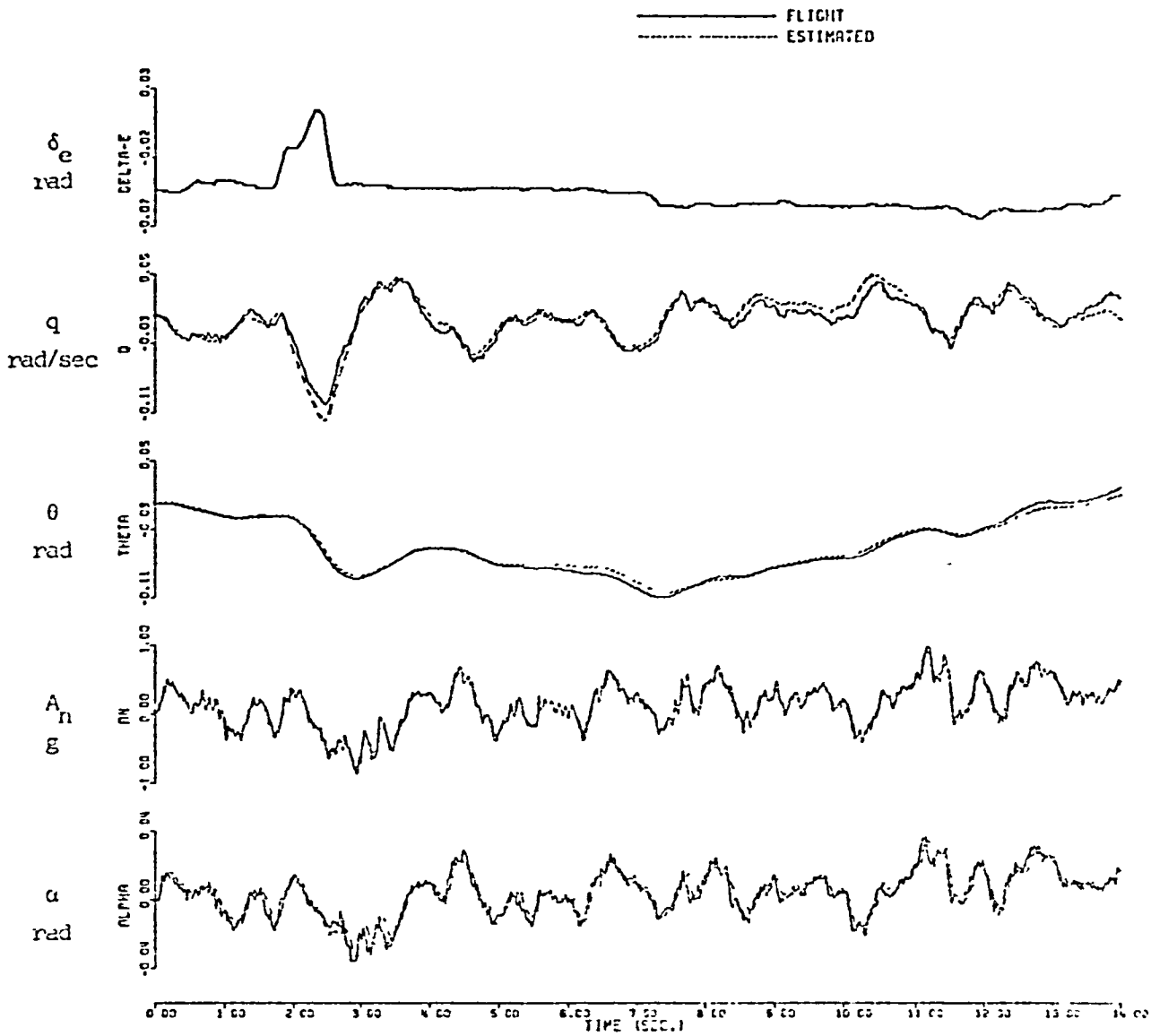

Fig. 3.25 TIME HISTORY PLOT : JET STAR MANEUVER E

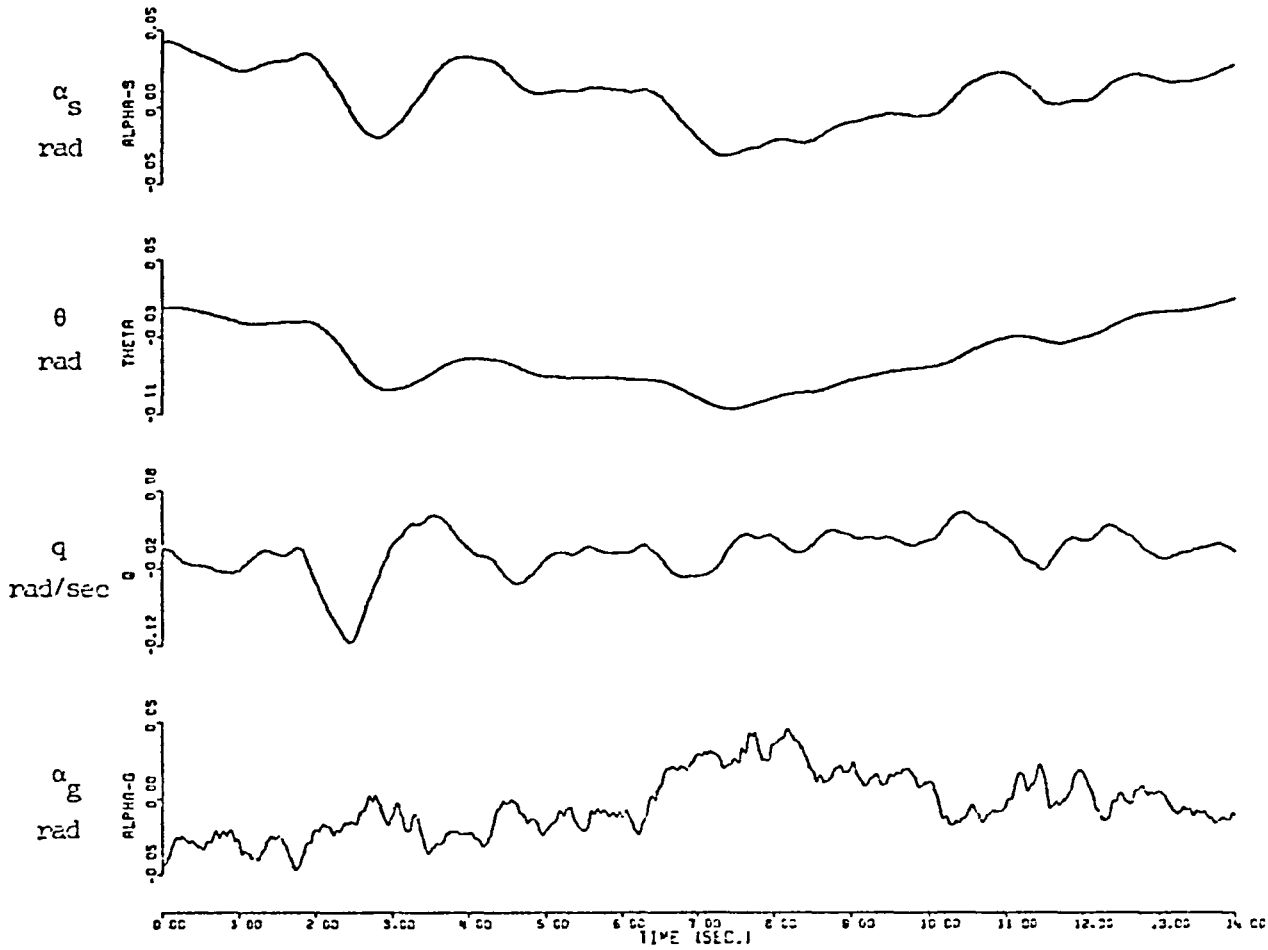

Fig. 3.26 ESTIMATED STATE : JET STAR MANEUVER E

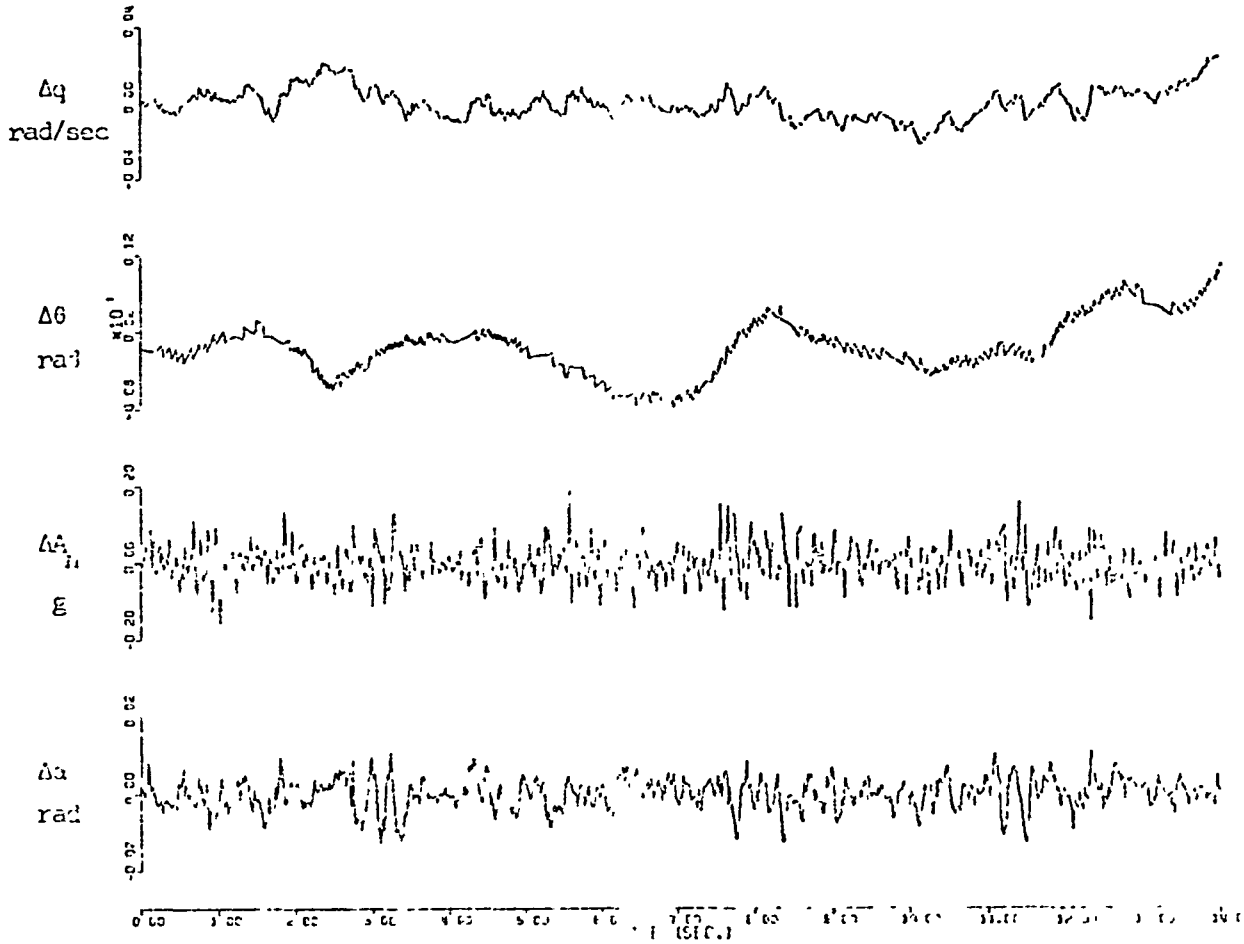

Fig. 3.27 FIT ERROR . JET STEP RESPONSE

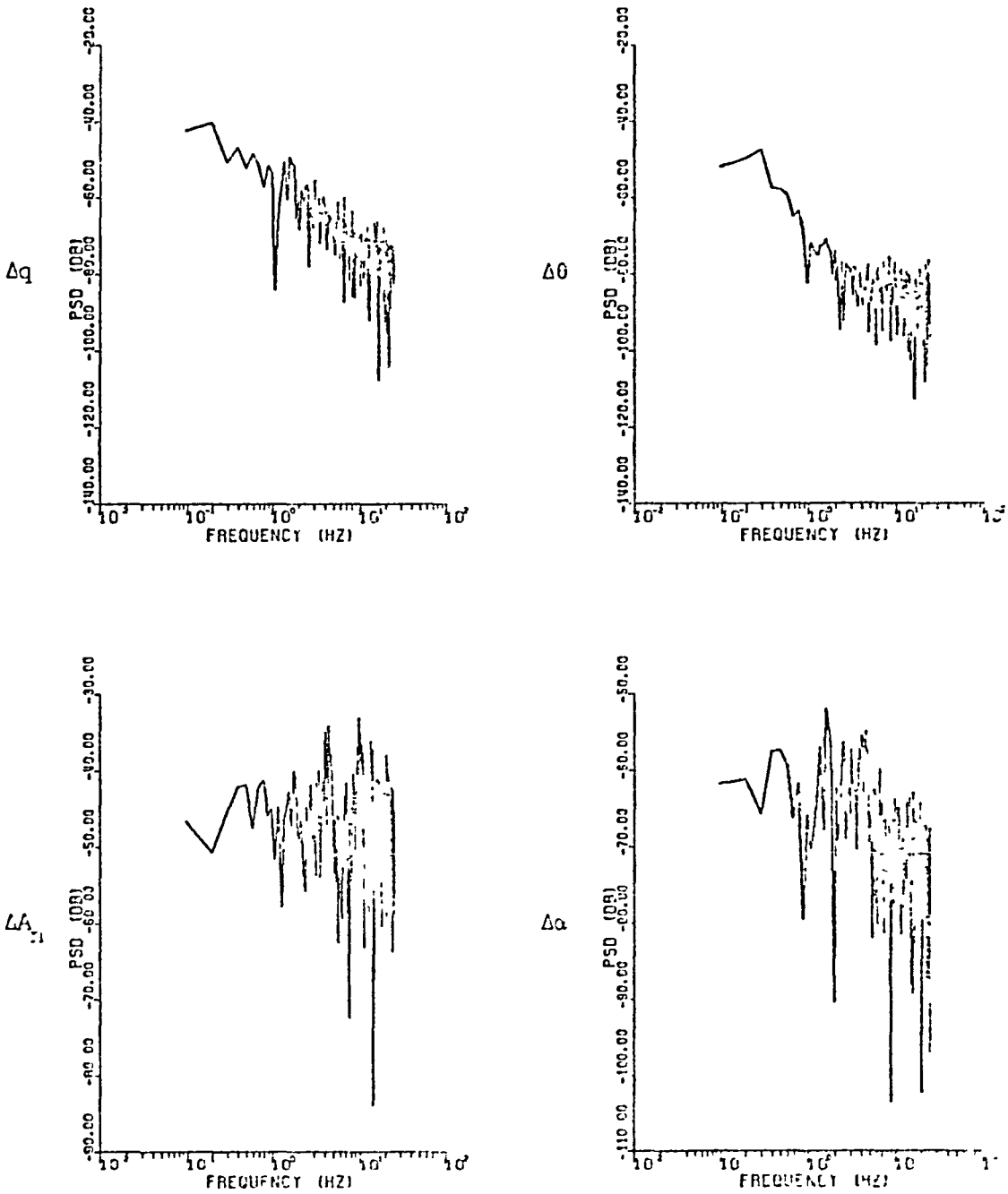

Fig. 3.28 PSD OF FIT ERROR . JET STAR MANEUVER E

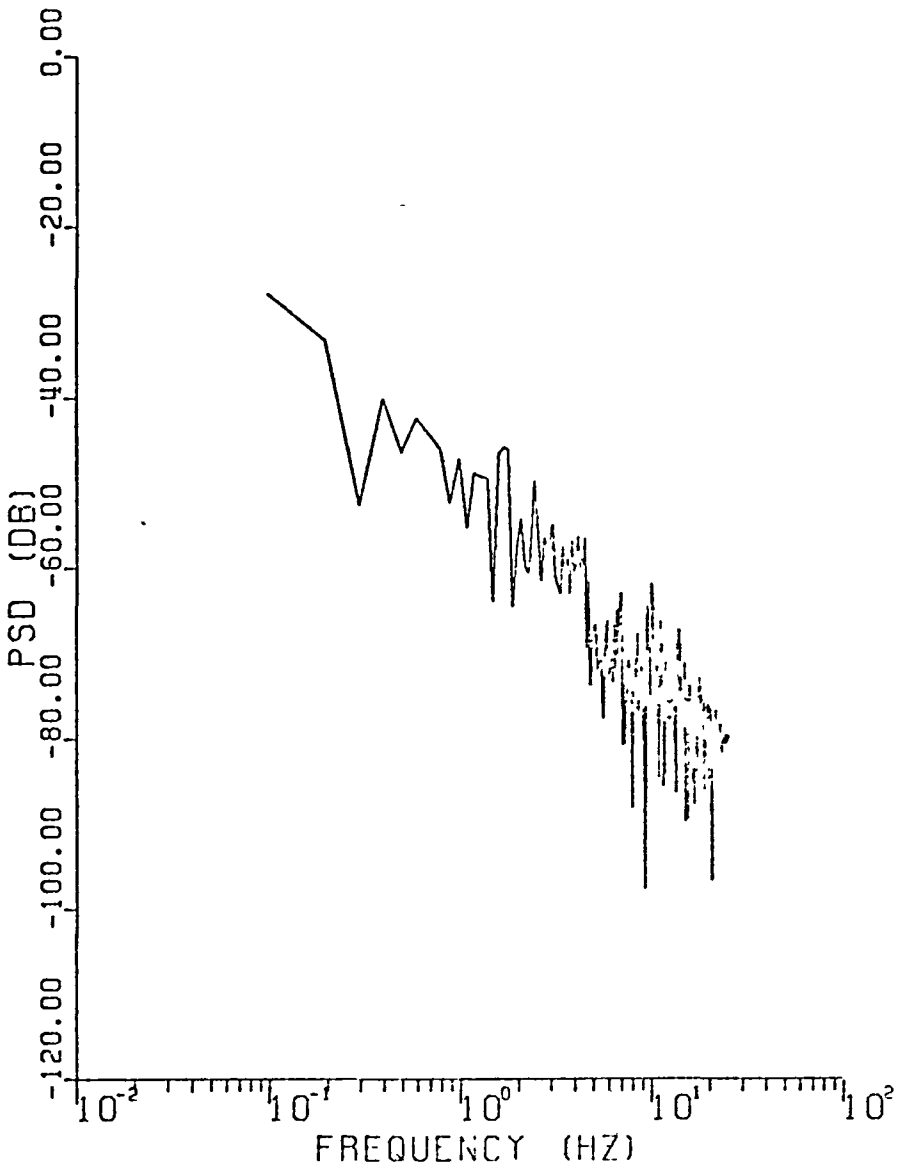

Fig. 3.29 PSD OF EST. TURBULENCE -JET STAR MANEUVER E

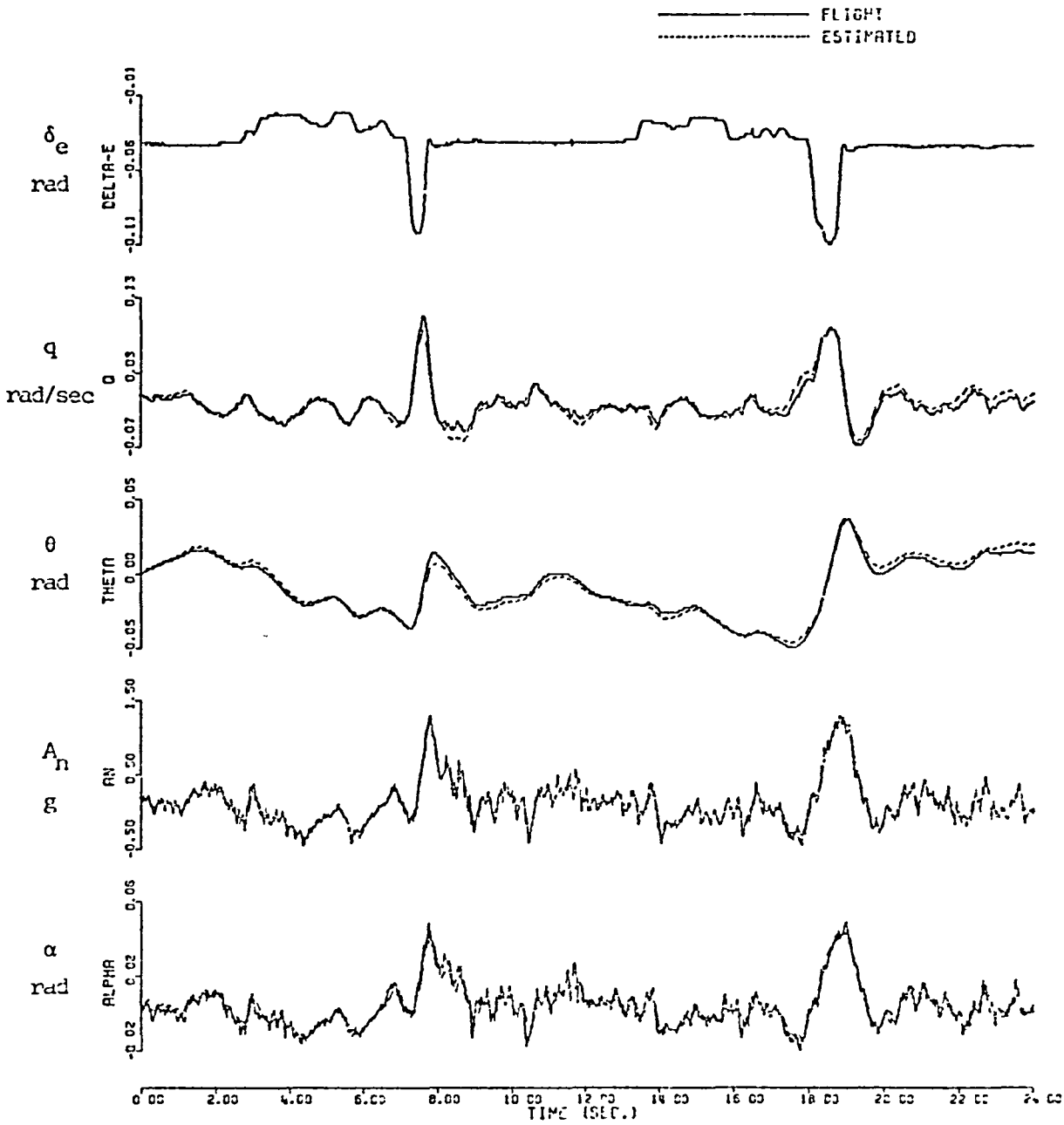

Fig. 3.30 TIME HISTORY PLOT : JET STAR MANEUVER CO

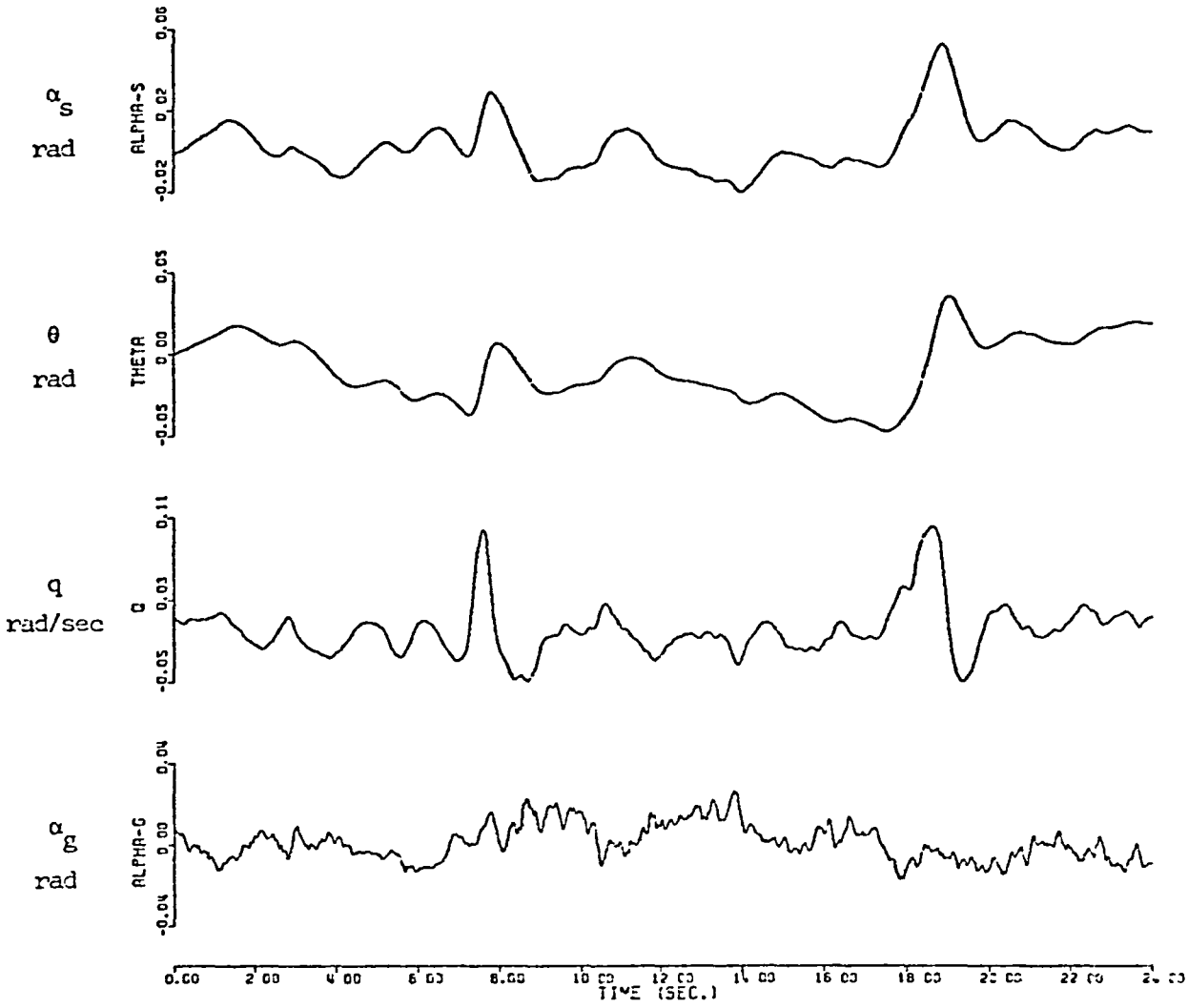

Fig. 3.33 ESTIMATED STATE . JET STAR MANEUVER CD

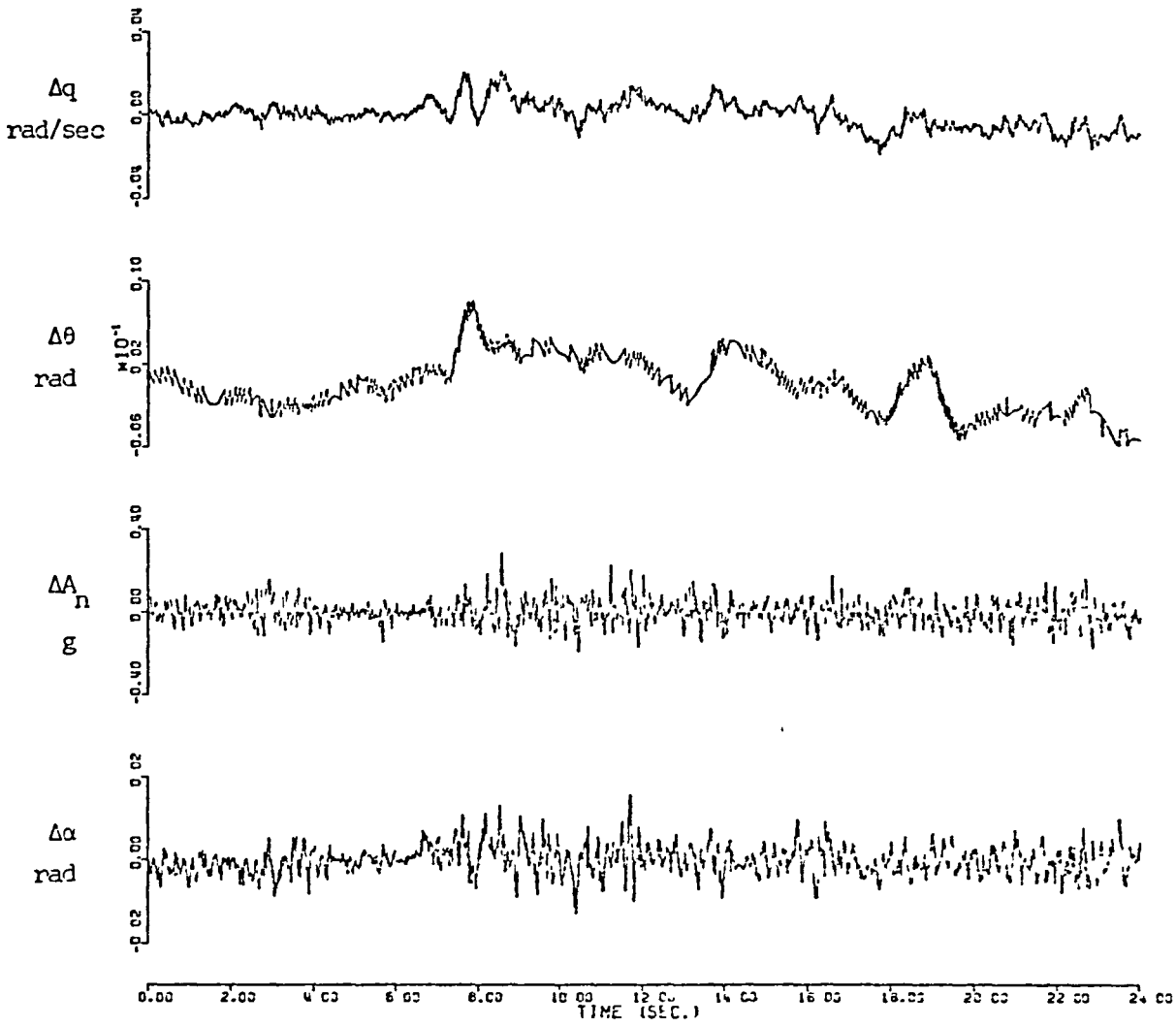

Fig. 3.32 FIT ERROR . JET STAR MANEUVER CO

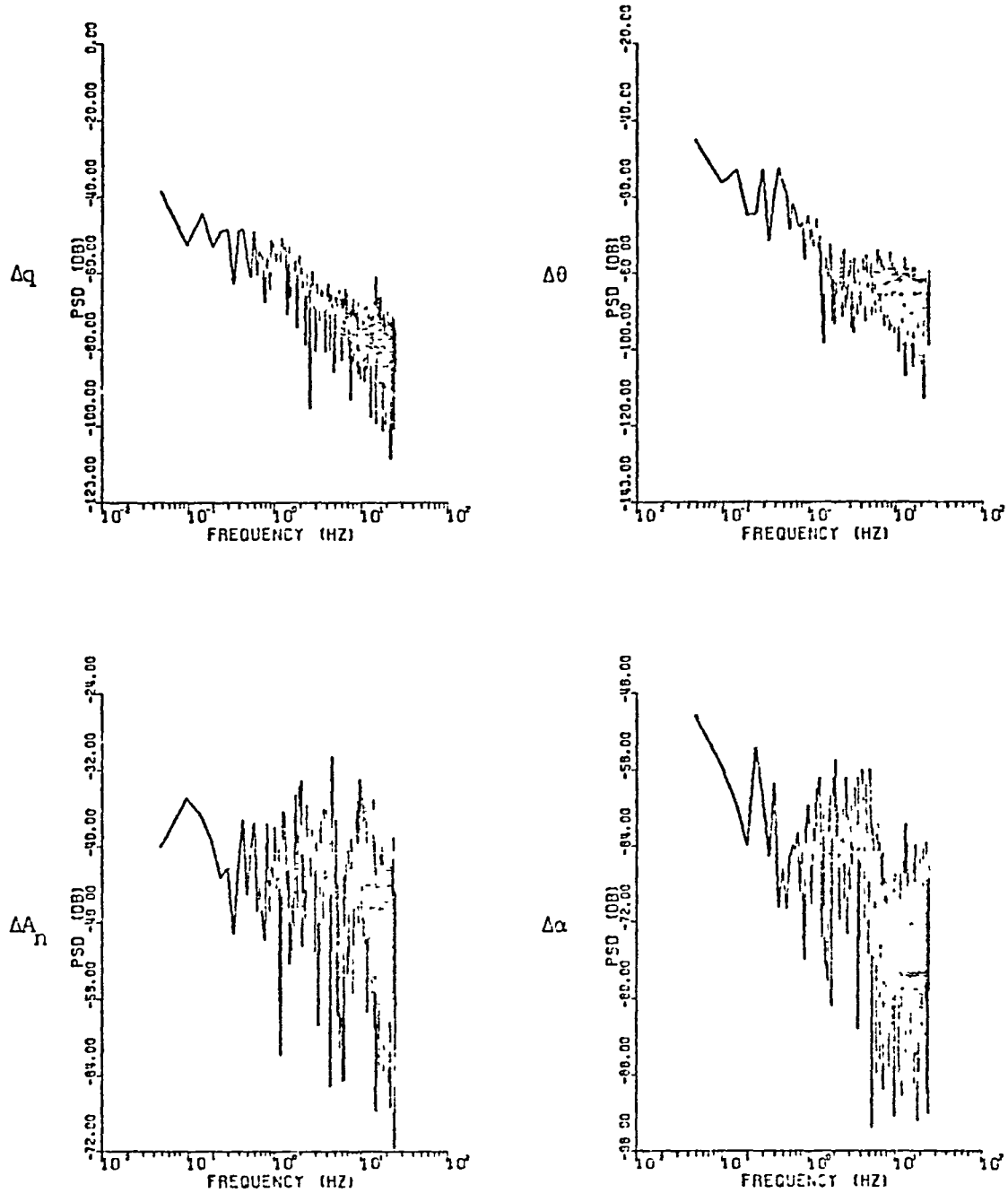

Fig. 3.33 PSD OF FIT ERROR : JET STAR MANEUVER CD

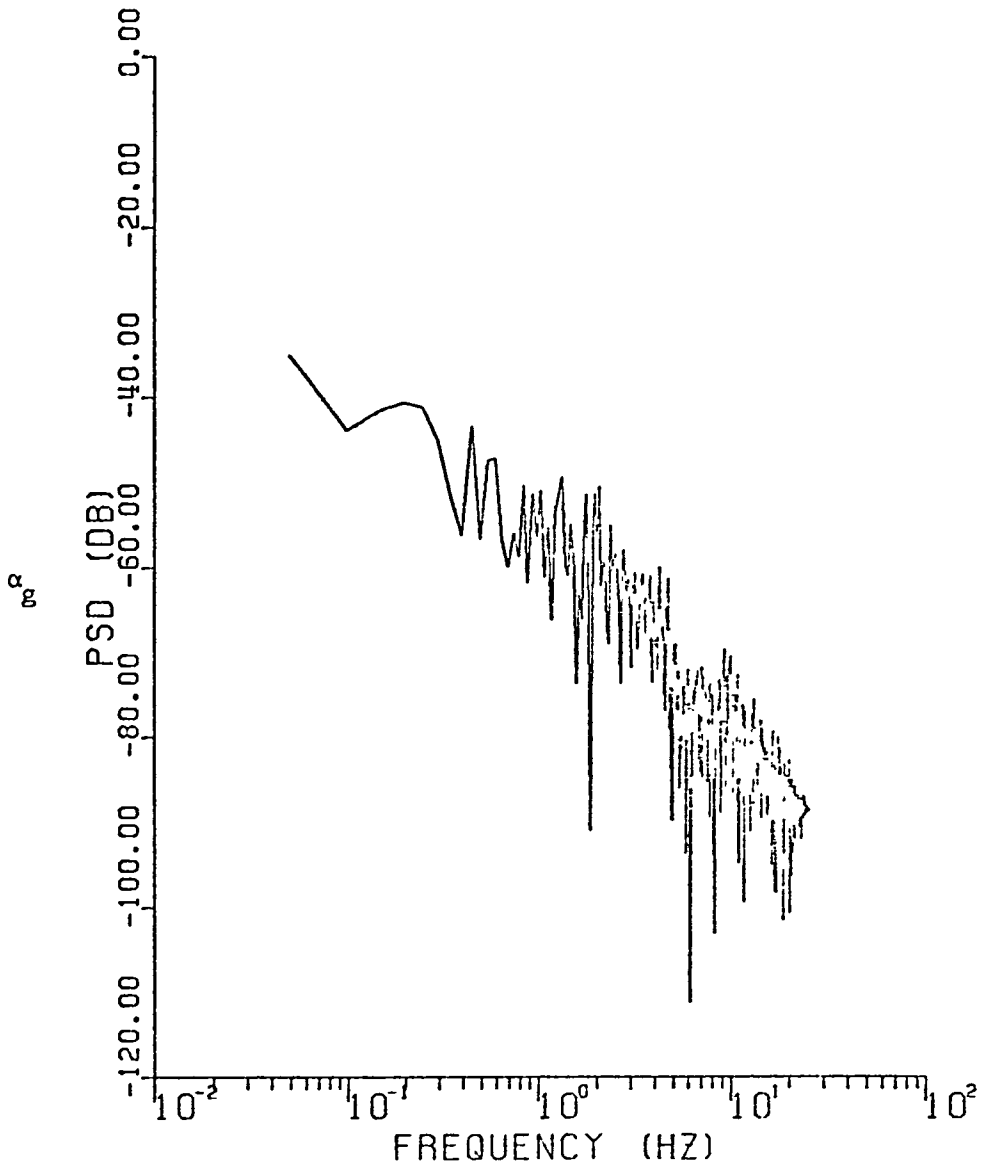

Fig. 3.34 PSD OF EST. TURBULENCE - JET STAR MANEUVER CD

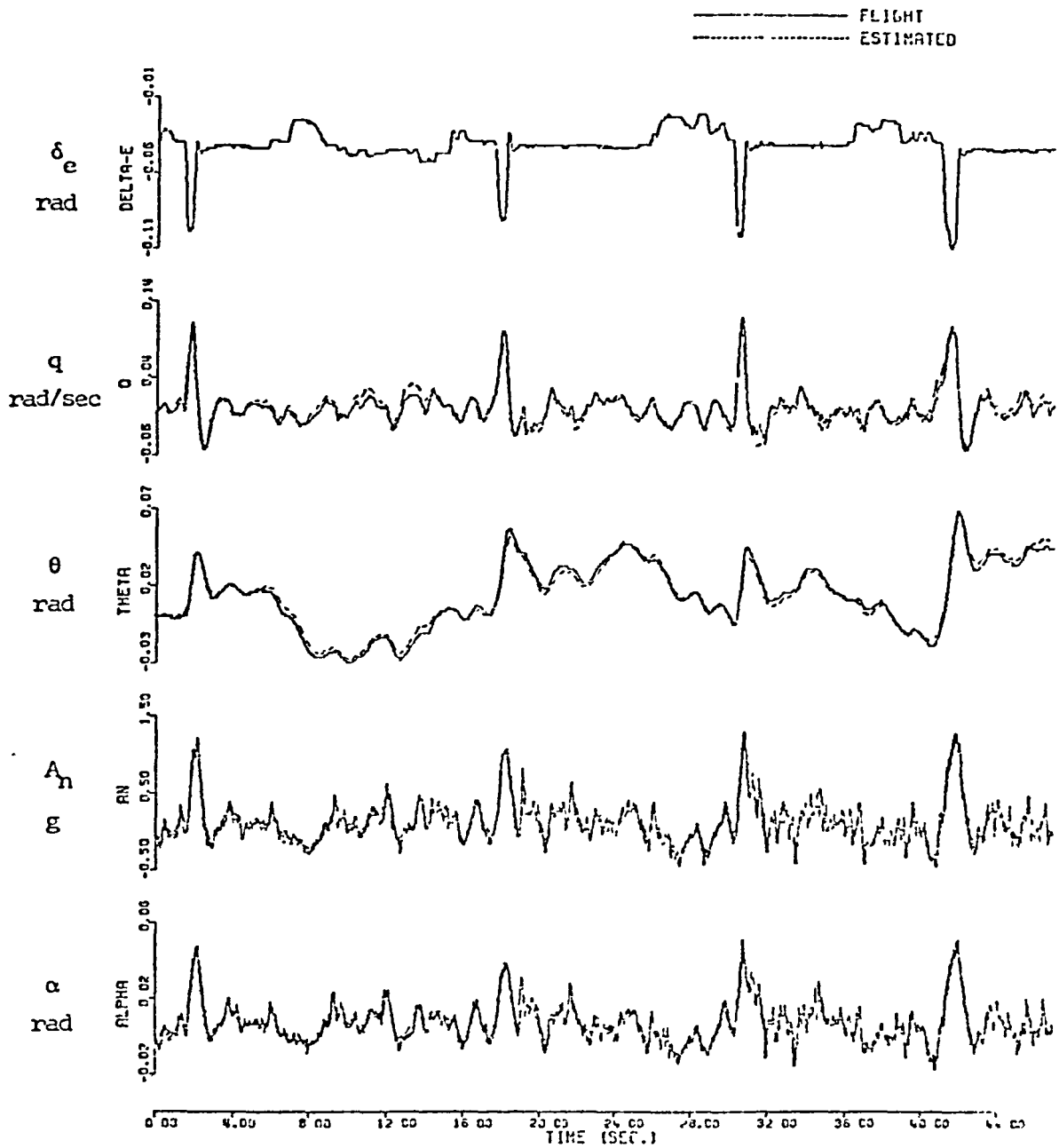

Fig. 3.35 TIME HISTORY PLOT : JET STAR MANEUVER A3CO

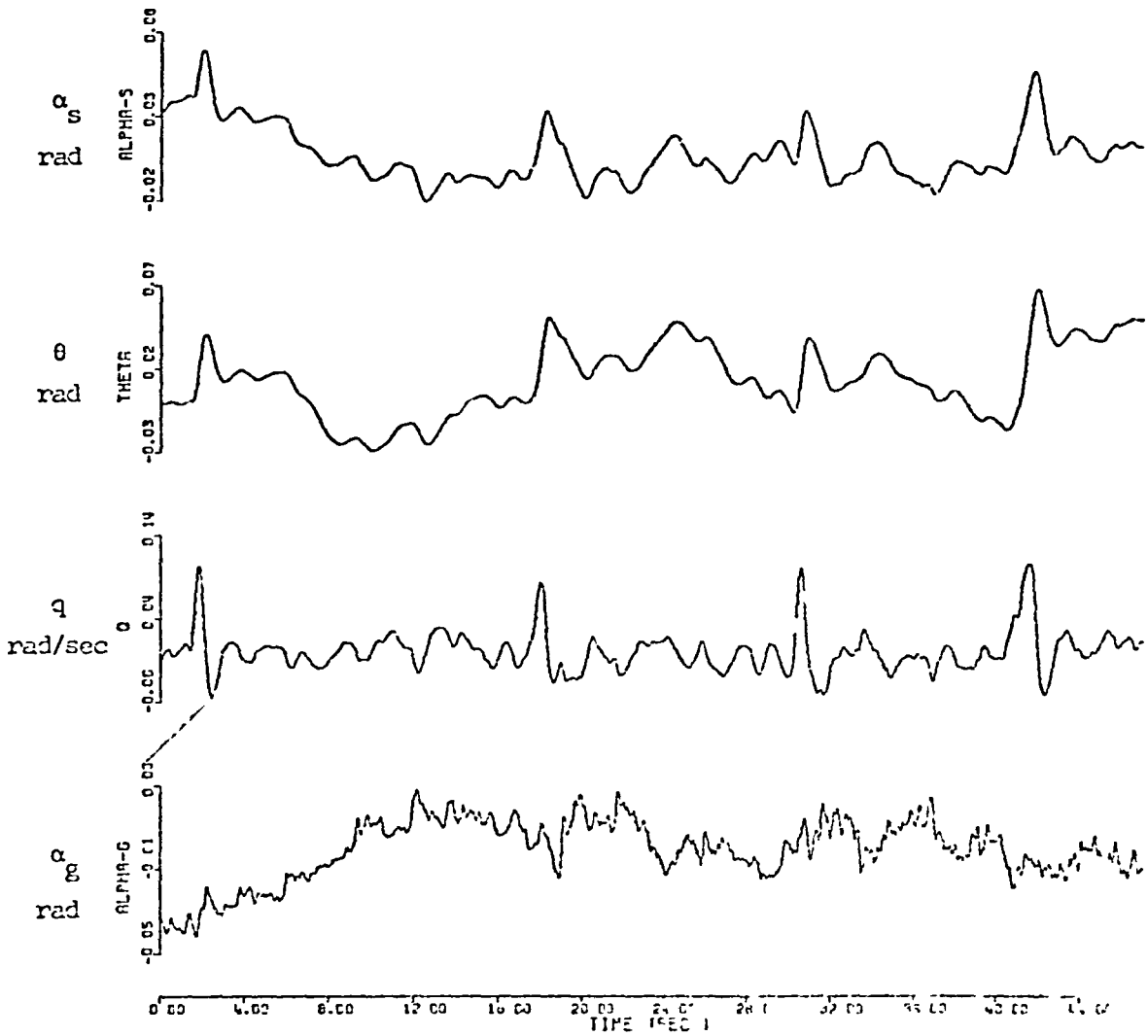

Fig. 3.38 ESTIMATED STATE . JET STAR MANEUVER ACCD

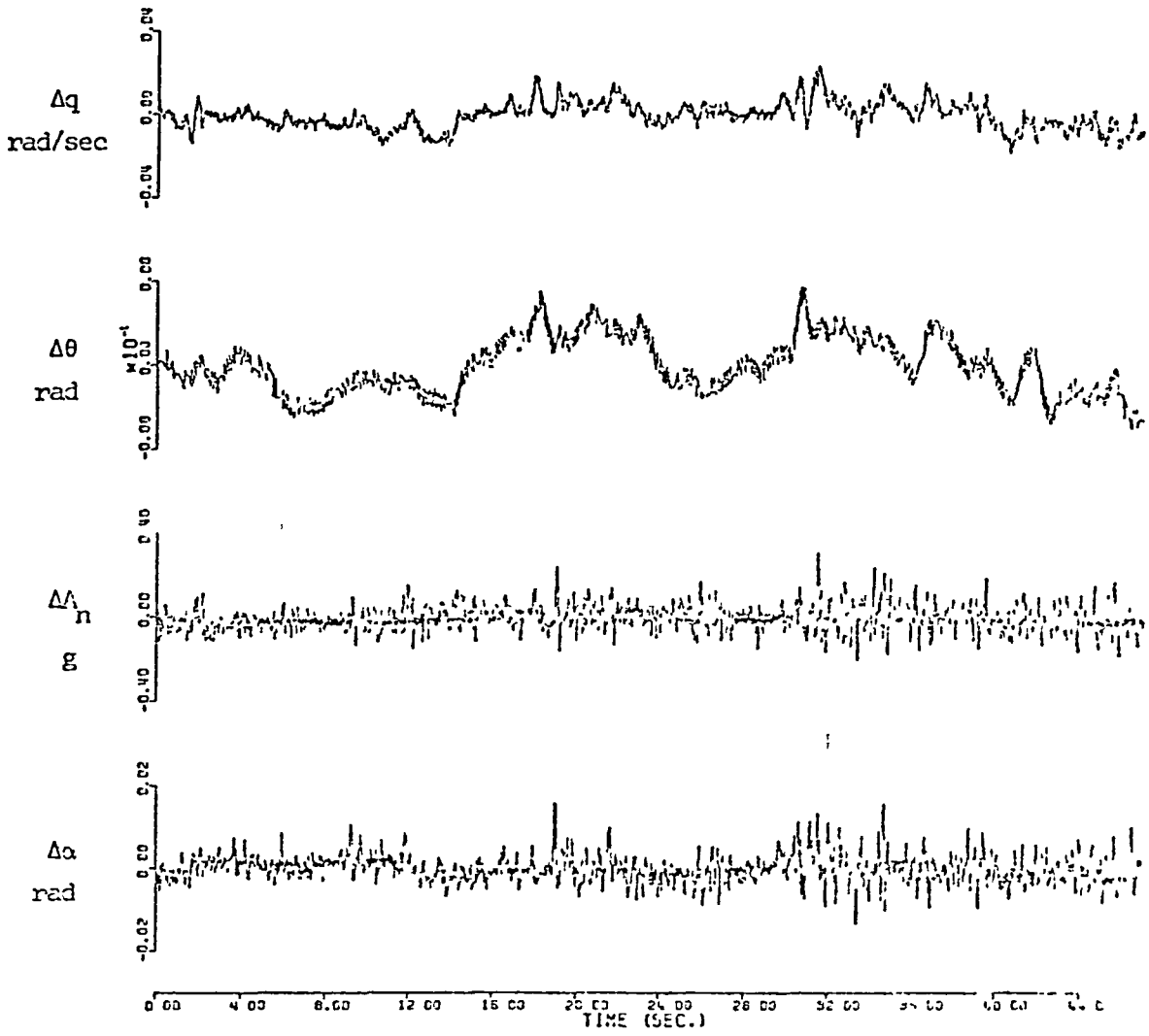

Fig. 3.37 FIT ERROR : JET STAR MANEUVER ABCD

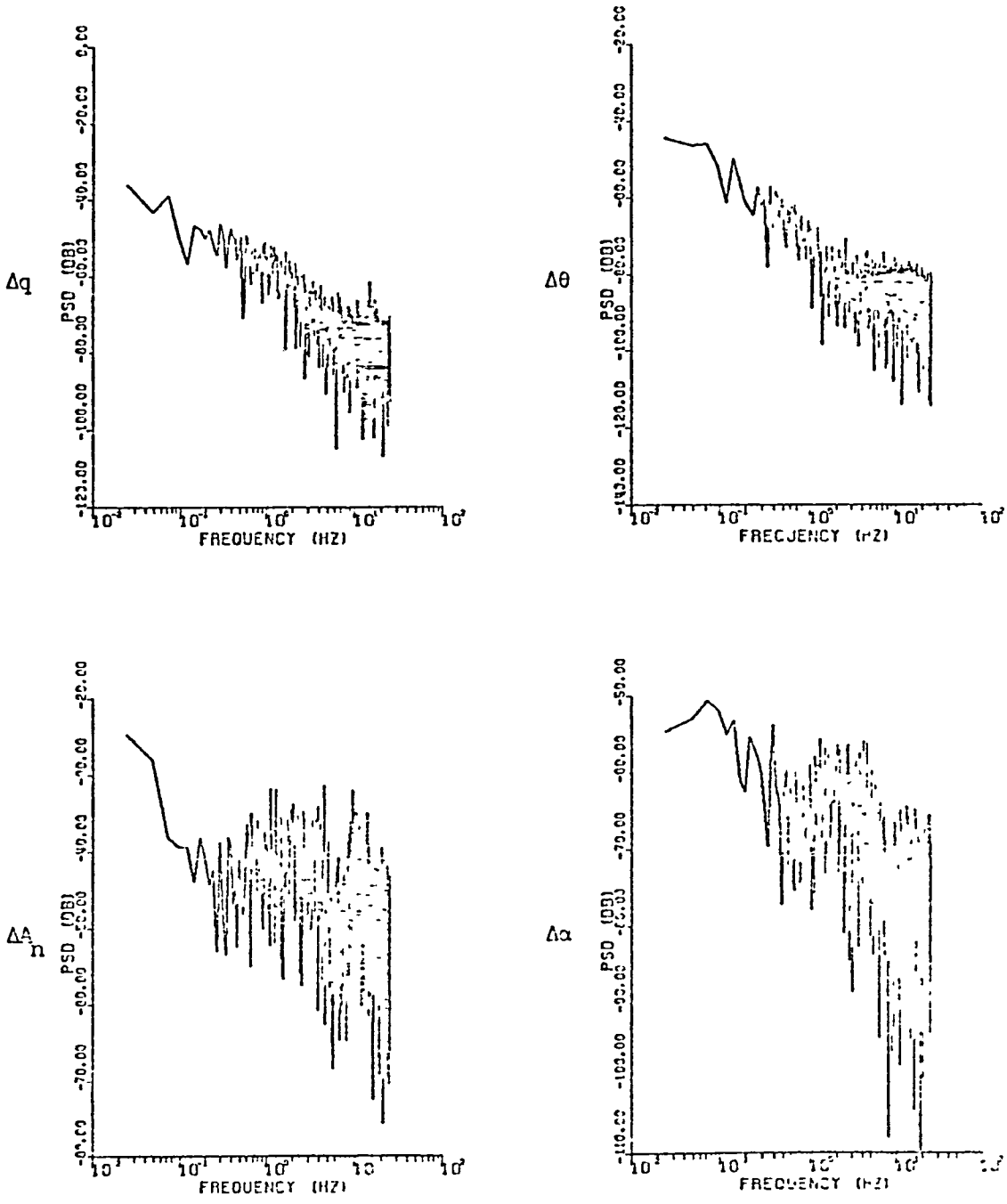

Fig. 3.38 PSD OF FIT ERROR . JET STAR MANEUVER ABCD

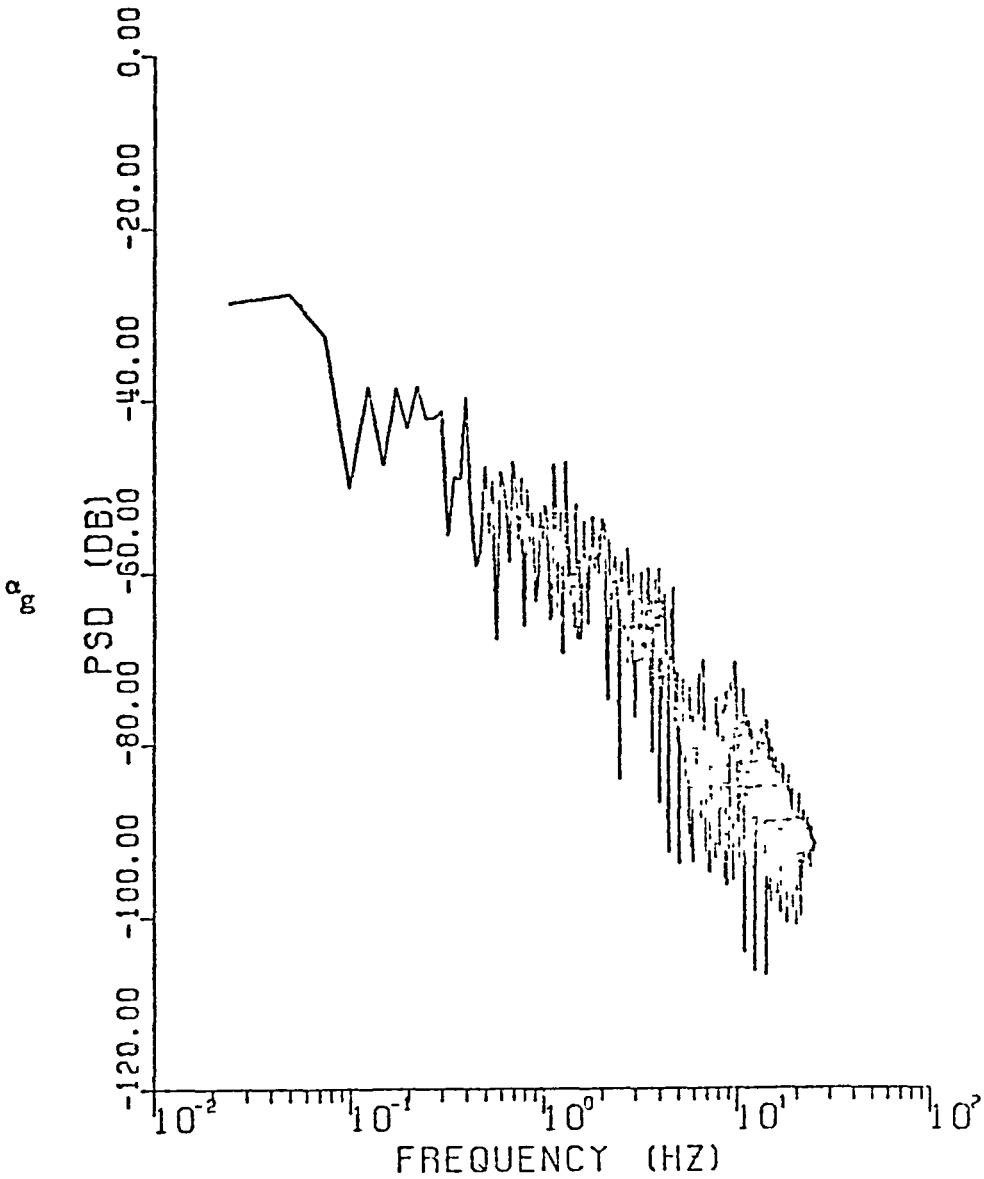

Fig. 3.39 PSD OF EST. TURBULENCE :JET STAR MANEUVER A5CD

TABLE 3.4 Composite Derivative Values

NUMBER	Z_α	M_α	M_θ	Z_{δ_e}	M_{δ_e}	$\sigma^2_{w_g}$
A	-1.45 (.0472)	-9.79 (.349)	-1.43 (.1297)	-.098 (.0355)	-8.15 (.329)	25.20 (5.3)
B	-1.46 (.0505)	-9.79 (.380)	-1.48 (.1233)	-.0077 (.0437)	-7.35 (.404)	63.51 (12.6)
C	-1.47 (.0429)	-9.66 (.321)	-1.86 (.1039)	-.150 (.0335)	-9.00 (.294)	75.00 (13.2)
D	-1.43 (.0449)	-9.76 (.330)	-1.18 (.1086)	-.011 (.0331)	-6.68 (.302)	65.04 (13.5)
E	-1.33 (.0315)	-8.03 (.220)	-1.83 (.0788)	-.044 (.0310)	-8.03 (.244)	305.98 (158.7)
AB	-1.44 (.0337)	-9.89 (.255)	-1.31 (.0826)	-.031 (.0275)	-7.80 (.251)	45.22 (6.4)
CD	-1.47 (.0312)	-10.01 (.239)	-1.62 (.0747)	-.078 (.0230)	-7.76 (.208)	71.76 (9.3)
ABCD	-1.45 (.0226)	-9.94 (.174)	-1.43 (.0537)	-.062 (.0175)	-7.65 (.159)	57.70 (5.3)
[illegible]	-1.[illegible]	-7.79	-1.31	-.123	-9.75	-----

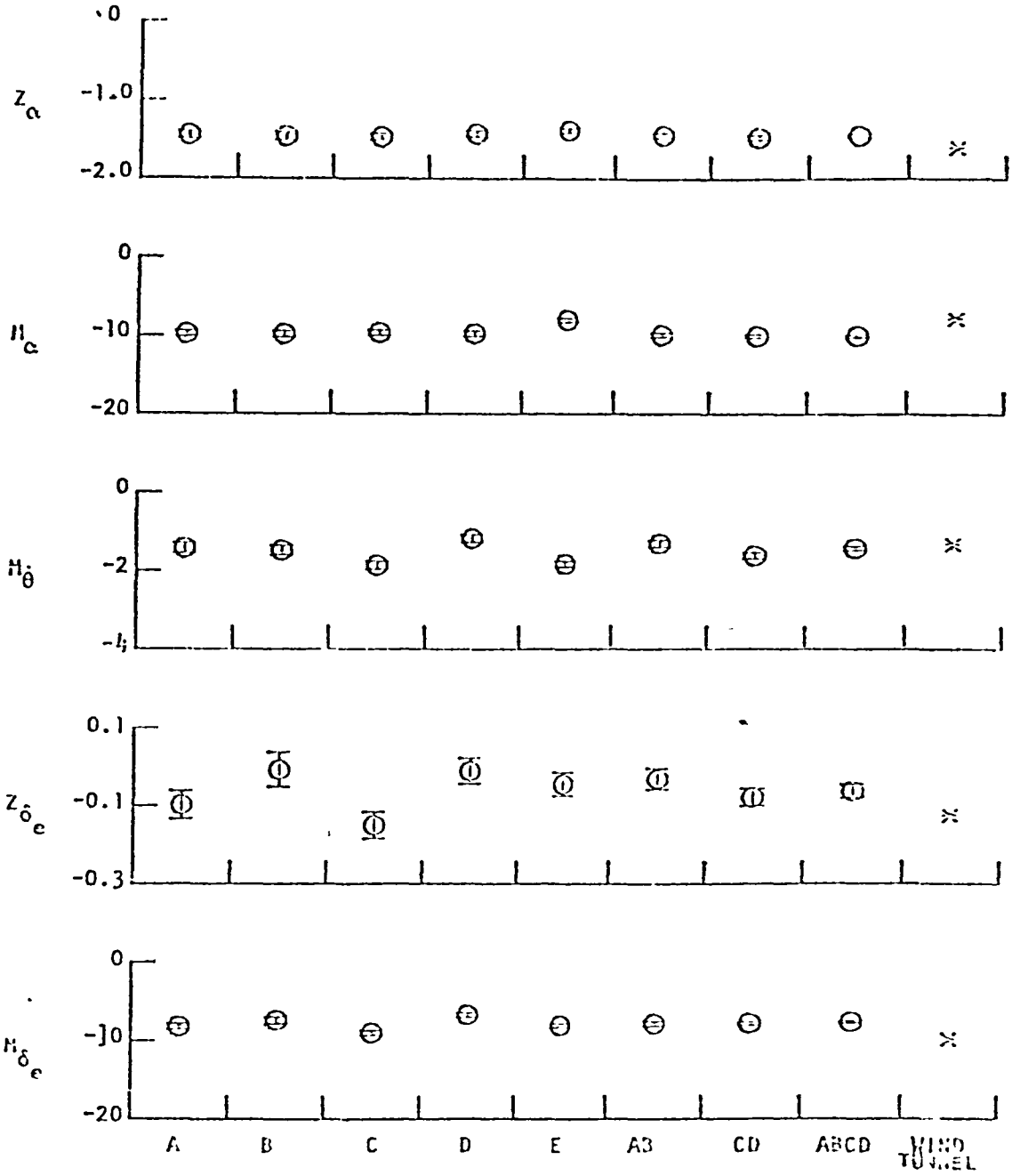

Fig. 3.40. Plot of Derivative Spreads

4. FLIGHT TEST DATA: EVALUATION OF DITHER-INPUT

4. FLIGHT TEST DATA: EVALUATION OF DITHER-INPUT.

One of the unresolves questions in parameter identification is the need for a conscious manual input by the pilot. In all the identification cases studies and reported, time histories were chosen which contained an impulse-like pilot input (cases A, B, C, D, E). In order to study the possibility of using a dither-like input instead, we took portions of the data where there was no sustained pilot input. Instead of the segments A, B, C, D, E as before, we used the segments marked "X" and "Y" on Figure 4.0 which shows the total Jet Star time-history available. The section X and Y are well beyond the pilot impulses, the pilot input excursion being now almost "dither-like".

The parameter extraction program was applied to the segments X and Y, and the results obtained are shown in a series of figures. Figure 4.1 shows the time-histories of the sensor data as well as the (dither) inputs corresponding to the segment X. The estimated values for θ, ω, n_z, and α are shown in broken lines in the same figure for comparison. Since the scale chosen may tend to obscure the discrepancy, Figure 4.2 shows the actual error time-histories, now to a different scale. Figure 4.3 shows the (Kalman) estimates of the states. The p.s.d. of the estimated turbulence is given in Figure 4.4, and the p.s.d.'s of the fit errors are shown in Figure 4.5. The corresponding quantities for maneuver Y are given in Figures 4.6 thru 4.10.

The estimated parameter values for both dither segments, as well as the contiguous pilot maneuvers X and Y, are shown in Table 4.1, where

have also shown the wind-tunnel values for purposes of comparison. The large error in M_{ζ_e} is expected, being a control derivative. The discrepancy in $M_{\dot{\theta}}$, a stability derivative, is a surprise. The values of Z_α and M_α obtained are close to those obtained in maneuvers A and E, as expected. The corresponding degradation in control performance has been calculated in section 1.

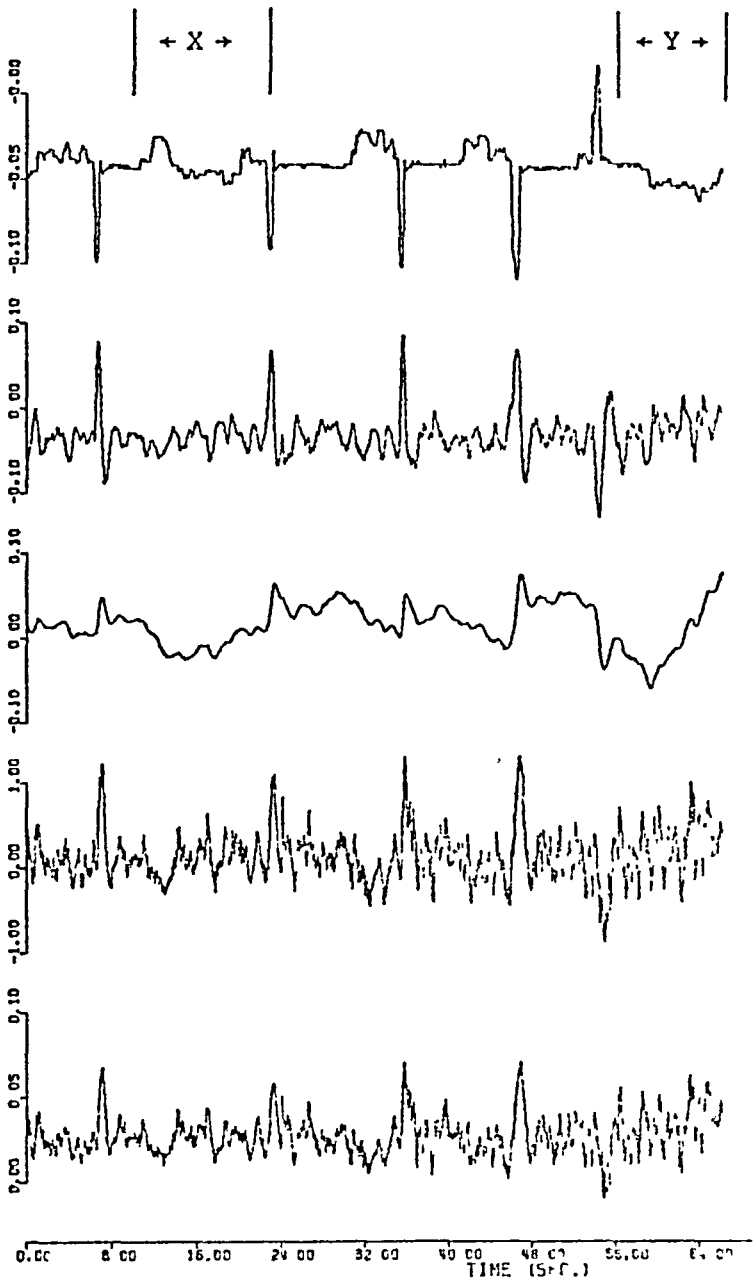
← X →
← Y →
-0.00
-0.05
-0.10
0.10
0.00
-0.10
0.10
0.00
-0.10
1.00
0.00
-1.00
0.10
0.05
0.00
0.00
8.00
16.00
24.00
32.00
40.00
48.00
56.00
TIME (Sec.)

Figure 4.0

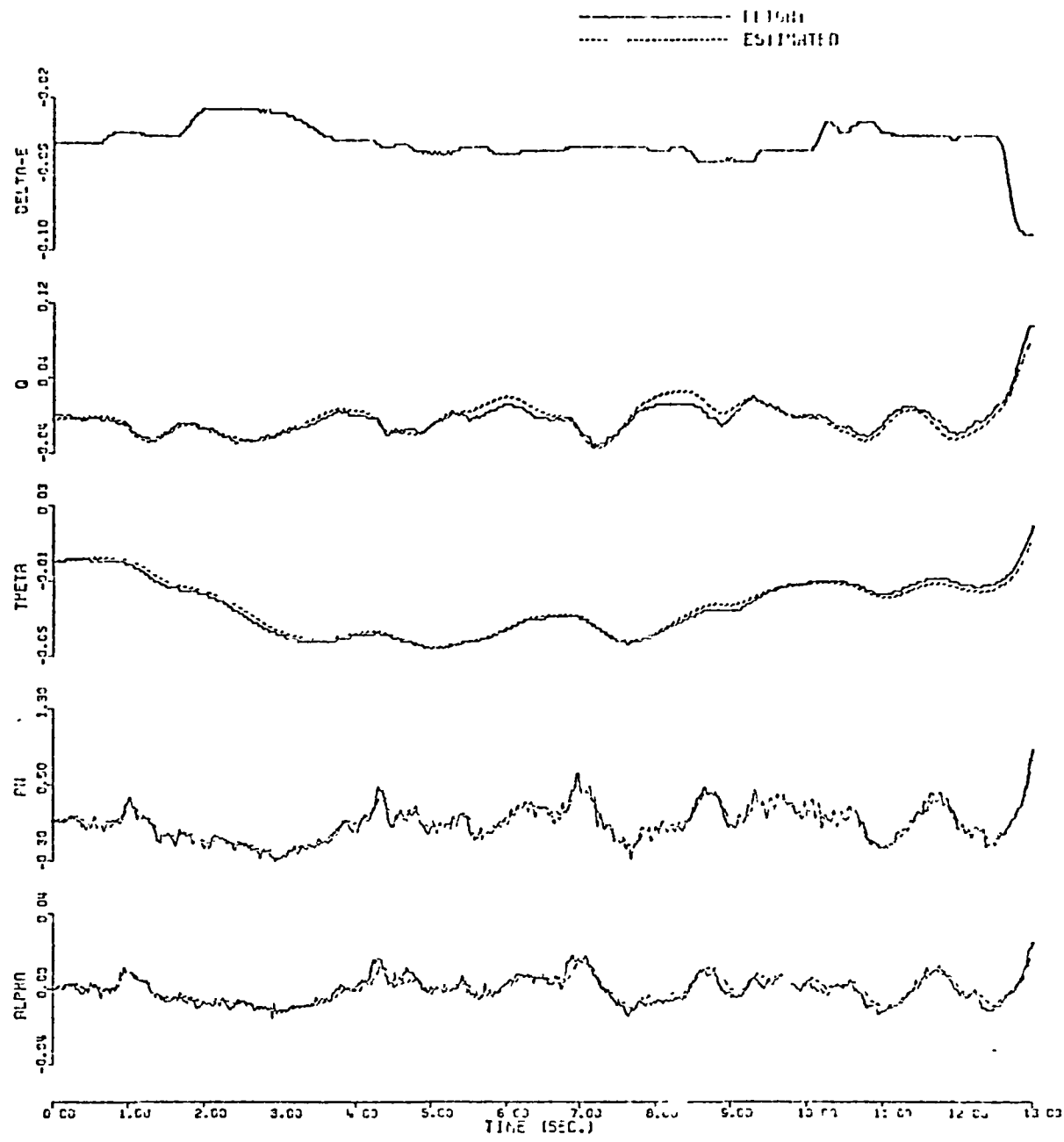

TIME HISTORY PLOT : JETSTAR MANEUVER X

Figure 4.2

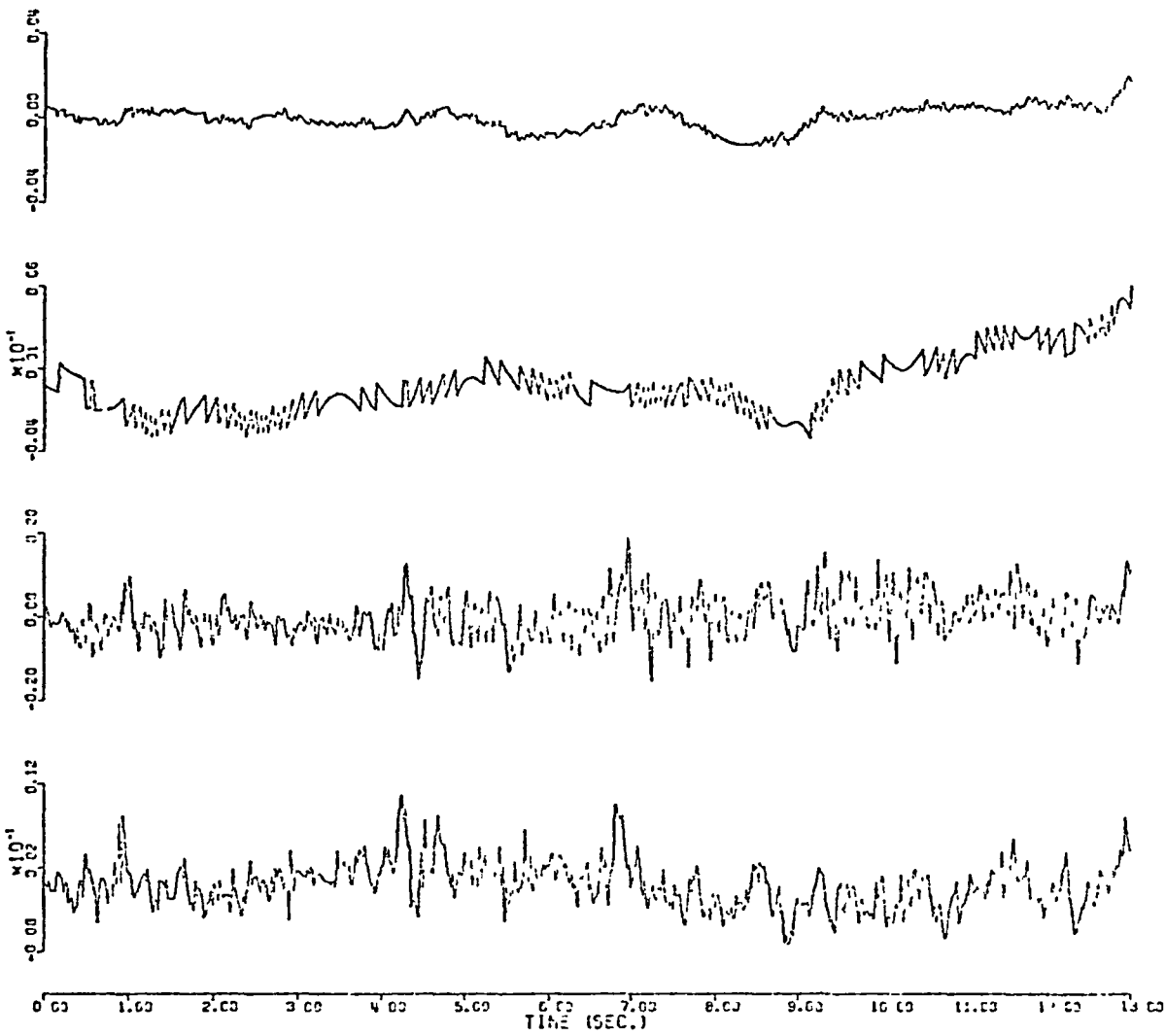

FIT ERROR : JETSTAR MANEUVER X

Figure 4.2

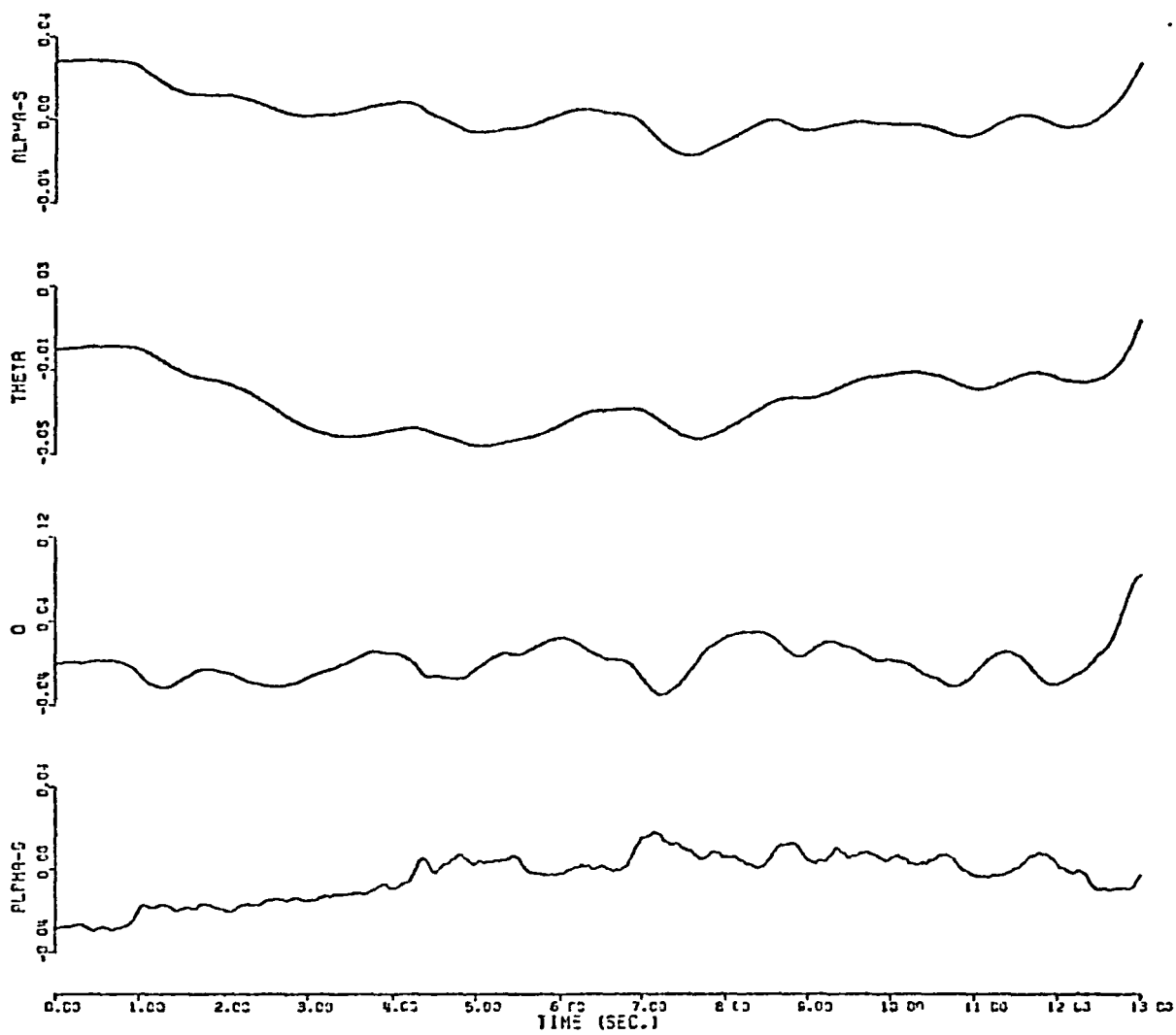

ESTIMATED STATE : JETSTAR MANEUVER X

Figure 4.3

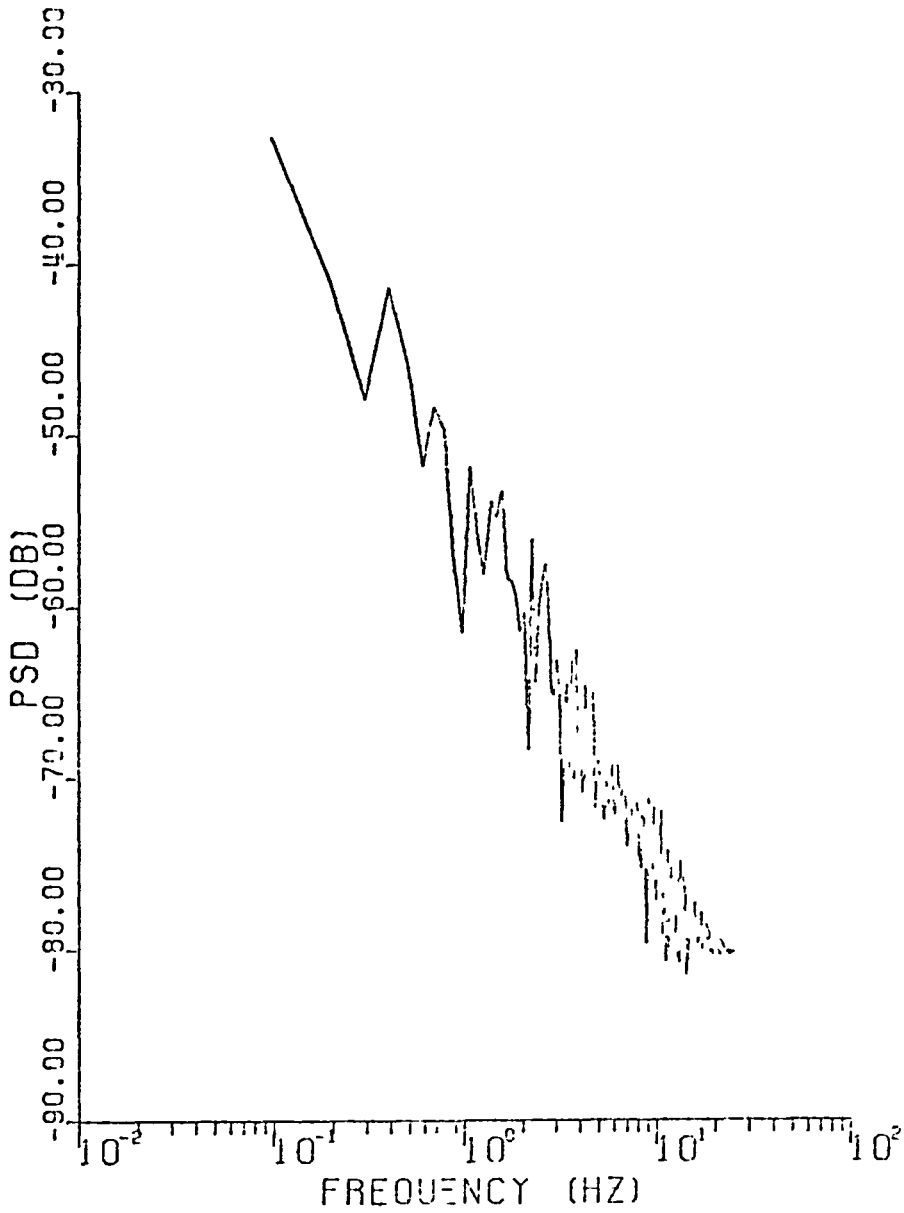

PSD OF EST. TURBULENCE JETSTAR MANEUVER X

Figure 4.4

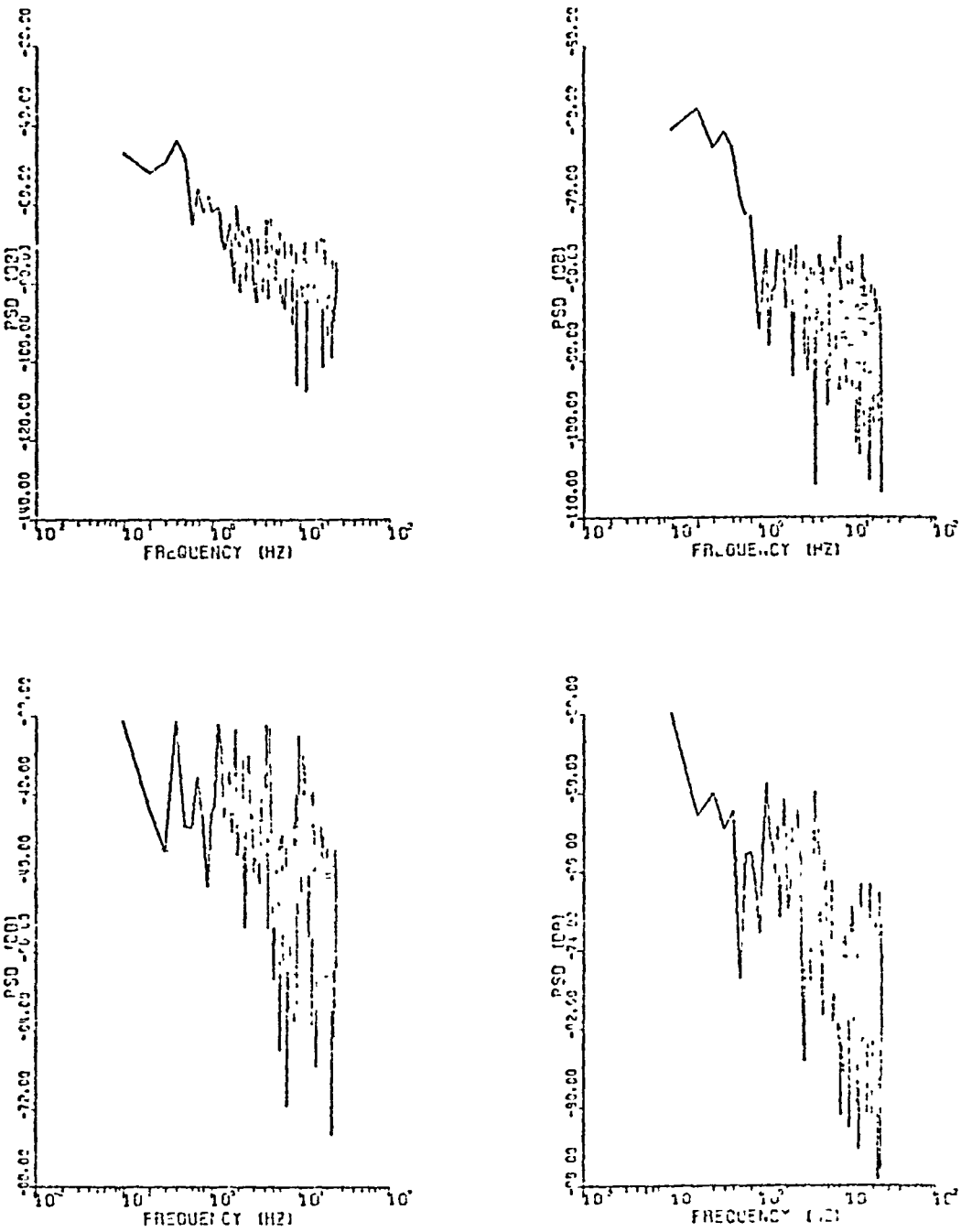

PSD OF FIT ERROR - TEST 1 MANEUVER X

Figure 4.1

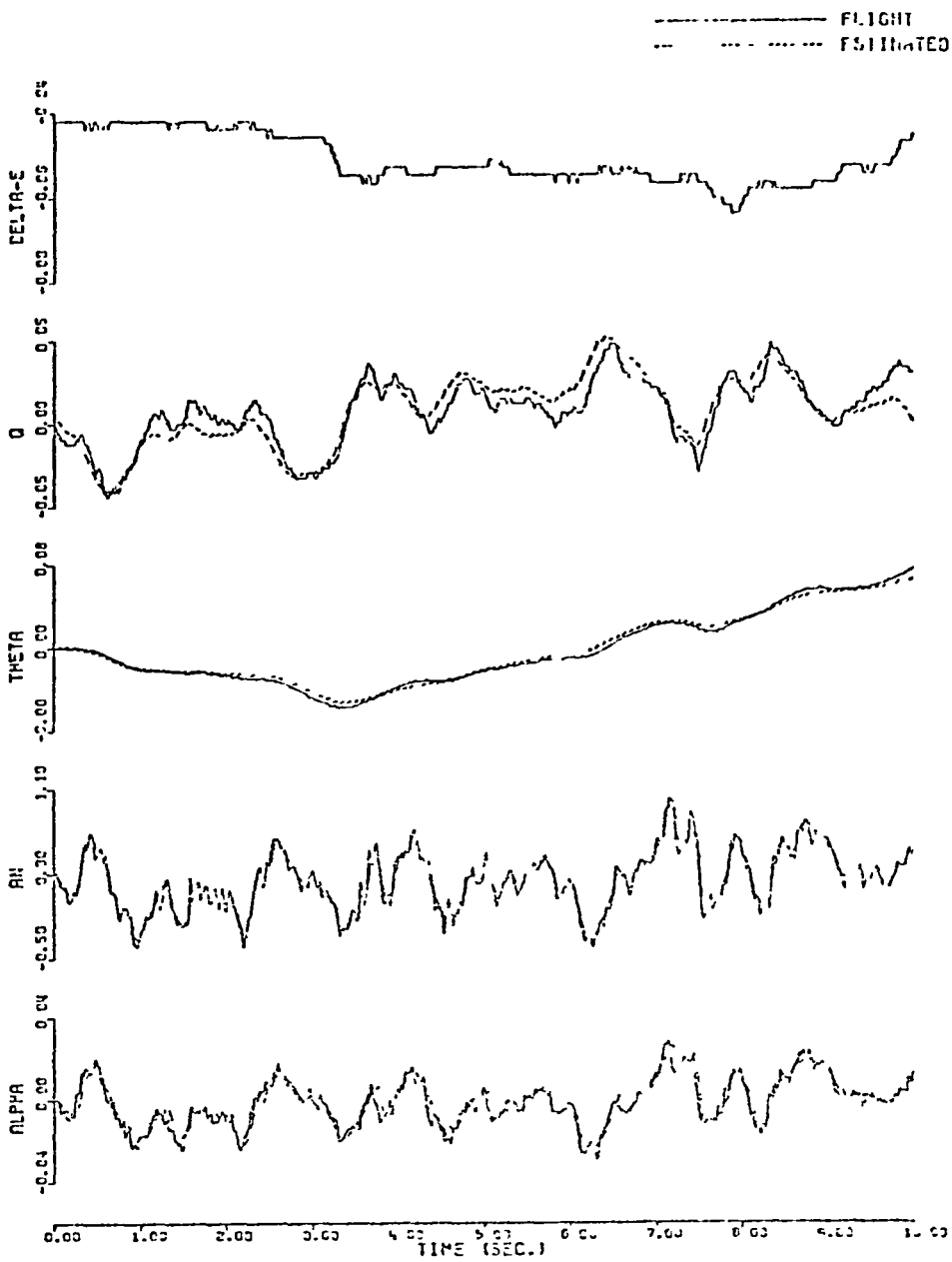

TIME HISTORY PLOT : JETSTAR MANEUVER Y

Figure 4.7

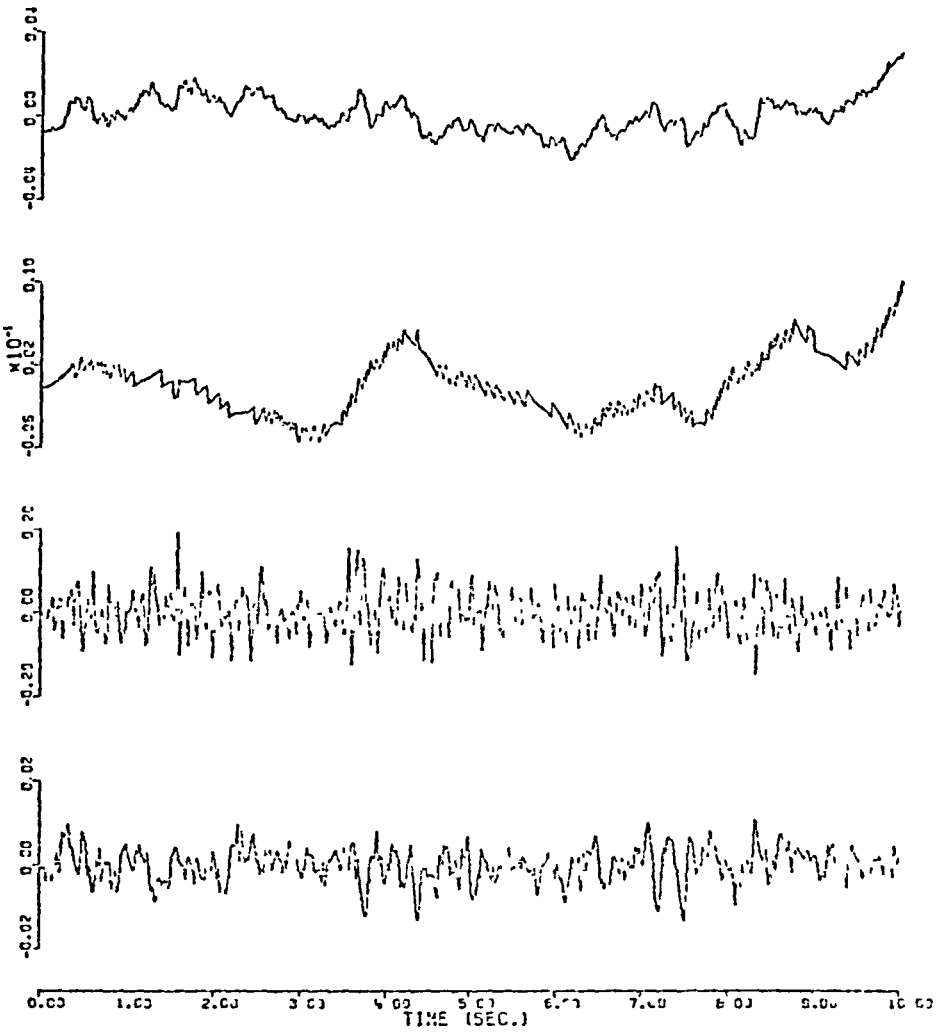

FIT ERROR : JETSTAR MANEUVER Y

Figure 4.7

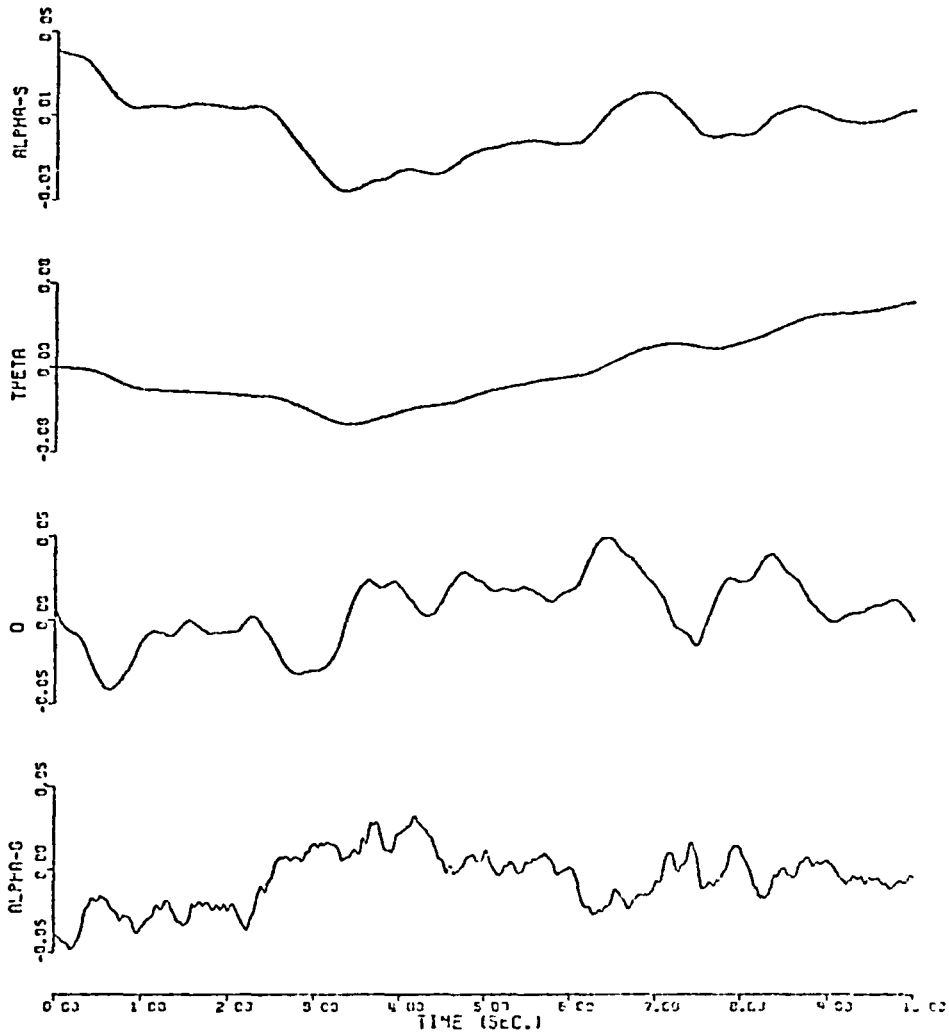

ESTIMATED STATE JETSTAR MANEUVER Y

Figure 4.8

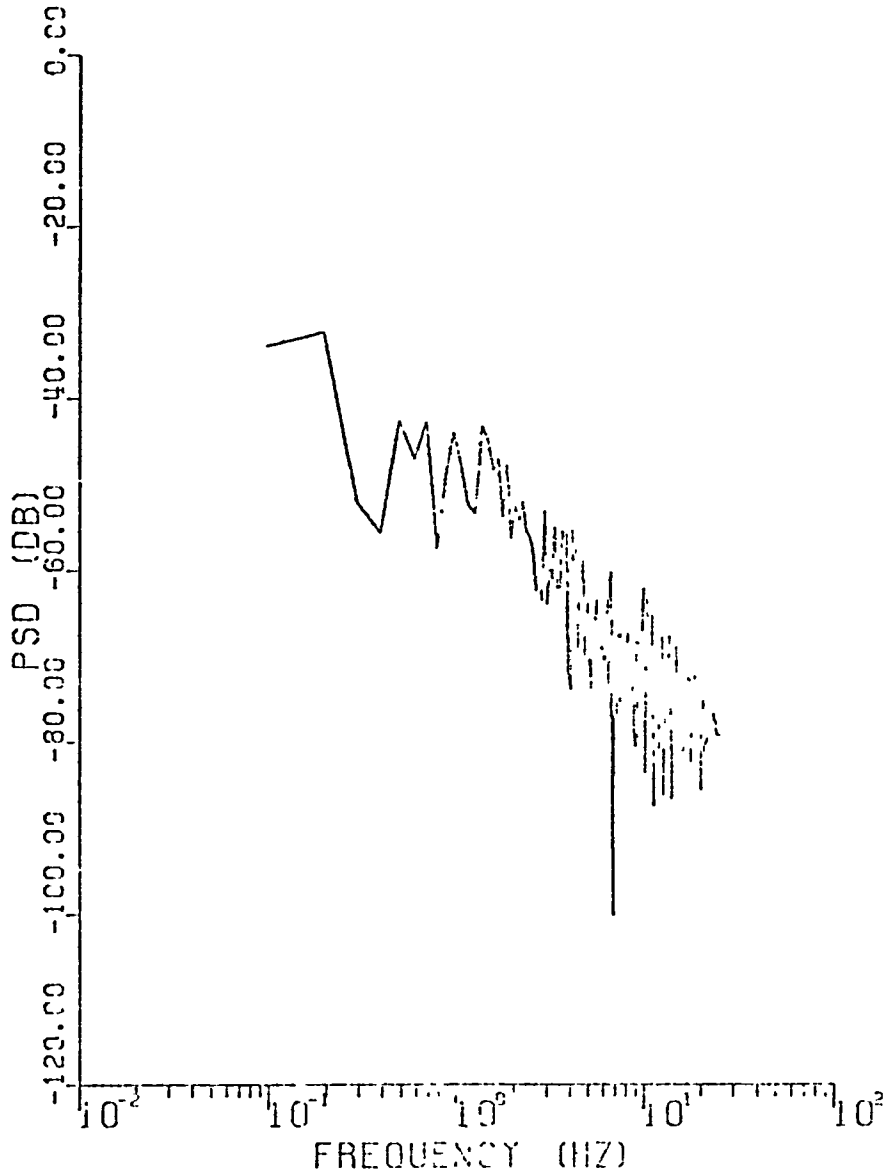

PSD OF EST TURBULENCE JETSTAR

Figure 4.9

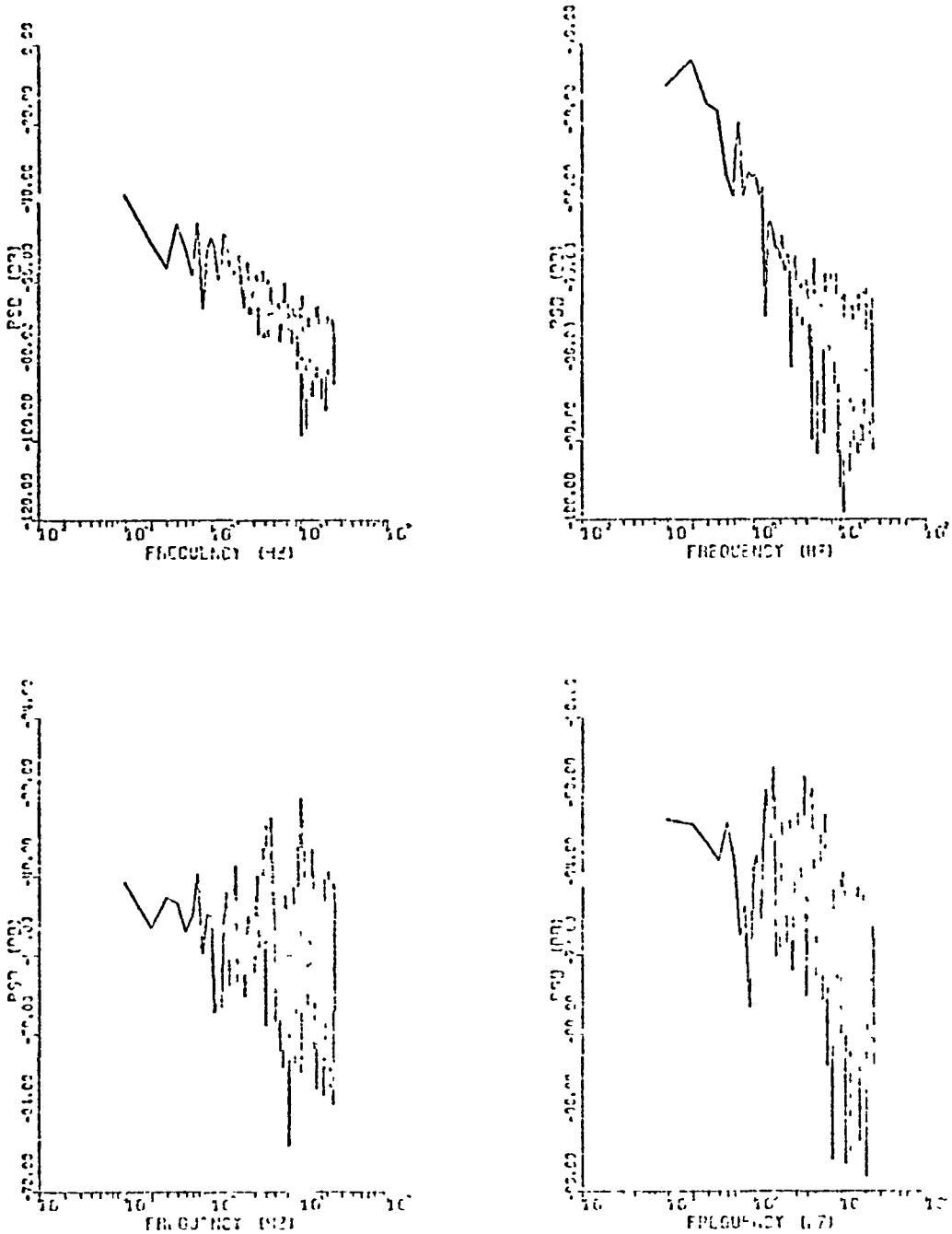

Figure 4.10

Parameter	Segment X	Maneuver A	Segment Y	Maneuver E
Z_α	- 1.41	-1.45	-1.38	-1.38
M_α	-9.42	-9.79	-7.34	-8.03
M_θ	-0.53	-1.43	-1.31	-1.83
M_{δ_e}	-6.04	-8.15	-10.49	-8.03
σ^2_{gust}	26.84	25.20	1177.5	305.98

T A B L E 4.1

Estimated Parameters: Dither Input and Gust

REFERENCES

1. K. W. Iliff: "Identification and Stochastic Control with Application to Flight Control in Turbulence": UCLA THESIS (UCLA-ENG-7340), May 1973.
2. L. W. Taylor: "The Application of Active Controls to Civil Transport Aircraft", MIT/NASA/AMES Workshop on System Rediability Issues for Future Aircraft; August 1975.

APPENDIX I

In this Appendix we examine a question basic to all digital computer processing of flight test data: whether the basic aircraft dynamics should be modelled as a continous-time process or a discrete-time process. We show that even though all digital computers sample the data before processing, the choice between the two models - continous-time vs. discrete-time is not clear-cut - that, in fact, for flight test data processing considered in this report, the continous-time model is more efficient, overall.

It is sufficient, for this purpose, to study the linear (Kalman) filtering problem. In order not to clutter the main thread of ideas with unnecessary mathematical details we shall only consider the case where the state-space dimension is one and there is only one observation. Thus let the system model be:

$$\dot{x}(t) = a\,x(t) + f\,n_s(t)$$

$$y(t) = c\,x(t) + g\,n(t)$$

where $n_s(t)$ is a white noise process with unit spectral density. The 3db signal bandwidth (two-sided) is then

$$\frac{2a}{2\pi}$$

We take a = -1, typical of the longitudinal short-period mode frequency. In

continous-time Kalman filtering theory we take n(t) to be white Gaussian. Let the spectral density of n(t) be unity, and let us take c = 1. Then the steady-state Kalman filter is given by:

$$\dot{\hat{x}}\,(t) \;=\; (a - p)\,\hat{x}\,(t) \;+\; p\,y(t)$$

where p is given by

$$p \;=\; -g^2 + \sqrt{g4 + f^2 g^2}$$

The main difficulty in applying the continuous-tire theory is that 'g' is essentially unknown, since 'white noise' is only a fiction, and what is really meant is that the noise-bandwidth is large compared to that of the signal. Now, if the time-history is long enough, we may allow 'g' to be a parameter to be chosen by 'minimising' (since we are taking c = 1):

$$\frac{1}{T} \int_0^T \left(y(t) \;-\; \hat{x}\,(t)\right)^2 dt$$

We may also estimate analytically the quantity:

$$E\;[(x(t) - \hat{x}(t)^2]$$

as a function of 'g' for assumed form of the spectral density of the noise n(t). Our first model for the spectral density is the band-limited versi

Case 1

$$p_{s_1}(\lambda) = \frac{\sigma^2}{2B} \qquad -B < \lambda < B$$

$$= 0$$

since this is not 'physically realizable', we choose next the more realistic:

Case 2

$$p_{s_2}(\lambda) = \frac{4\pi f_c \sigma^2}{(2\pi\lambda)^2 + (2\pi f_c)^2}$$

Here the 3-db break frequency is f_c Note that in eitner case the total power is σ^2. Since

$$x(t) - \hat{x}(t) = e(t)$$

satisfies:

$$\dot{e}(t) = -(1 + p/\varepsilon^2)\, e(t) - f\, n_s(t) + (p/\varepsilon^2)\, n(t)$$

we can calculate the filtering error

$$E\,[e(t)^2] = R_c$$

by integrating the spectral density:

for Case 1

$$= \frac{f^2 + \frac{p^2}{g^4} \quad P_{s_1}(\lambda)}{4\pi^2\lambda^2 + (1 + pc^2/g^2)^2}$$

and for Case 2

$$= \frac{f^2 + \frac{p}{g2}}{4\pi^2\lambda^2 + 1 + (p/g^2)} \cdot \frac{4\pi f_c \sigma^2}{4\pi^2\lambda^2 + 4\pi^2 f_c^2}$$

The results of calculations are shown in figures A-1 and A-2, which plot R_c versus g. Note that the optimal choice of g for Case 1 is

$$g^2 = \frac{\sigma^2}{2B}$$

while for Case 2 it is

$$\frac{\sigma^2}{\left(\frac{\pi}{2}\right)^2 f_c}$$

as may be expected intuitively more or less.

Let us now consider the situation we really want to study where the observation y(t) is sampled with sampling interval Δ. In most engineering treatments, we then proceed to write down the corresponding discrete-time version of the system model:

$$x_{n+1} = \bar{e}^{\Delta} x_n + \Gamma N_s(n\Delta)$$

where $N_s(\cdot)$ is a white noise (sequence) and

$$y_n = x_n + n(n\Delta)$$

where $$\Gamma = \sqrt{1/\Delta} \cdot \left(\int_0^{\Delta} e^{-s} ds \right) \cdot f$$

$$E[\, n(n\Delta)^2 \,] = \sigma^2$$

$$E[\, N_s(n\Delta)^2 \,] = 1$$

In the discrete-time Kalman filter the assumption is made that the noise samples $n(n\Delta)$ are uncorrelated, leading to the filter equations:

$$\hat{x}_{n+1} = (1 - k)\, \bar{e}^{\Delta} \hat{x}_n + k\, y_n$$

where

$$k = \frac{e^{-2\Delta} p + \Gamma^2}{e^{-2\Delta} p + \Gamma^2 + f^2}$$

$$p = \frac{e^{2\Delta}}{2} \left(-\zeta + \sqrt{\zeta^2 + 4 \Gamma^2 e^{-2\Delta} \cdot \sigma^2} \right)$$

$$\zeta = \Gamma^2 + \sigma^2 (1 - e^{-2\Delta})$$

The main point to be made is that the assumption of independence is incorrect for the aircraft data since the sampling rate of 50 samples/sec is 10 times as much as the Nyquist rate of the aircraft response. Hence the Kalman filter error variance will be larger than the nominal value p. The actual error variance

$$E[(x_n - \hat{x}_n)^2]$$

will depend upon the spectral density shape of the noise process. We shall calculate it for the sampled versions of Case 1 and Case 2. Thus

$$e_n = x_n - \hat{x}_n$$

satisfies:

$$e_{n+1} = e^{-\Delta} (1 - k) e_n - (1 - k) \Gamma N_\zeta (n\Delta) + k n (\overline{n+1}\Delta)$$

Let

$$R_d = E[\, e_n^2 \,].$$

Case 1

Let

$$\gamma = B\,\Delta$$

Note that $\gamma > \frac{1}{2}$ if the sampling rate is smaller than the Nyquist rate of 2B, and $\gamma < \frac{1}{2}$ otherwise. In particular

$$\gamma = 0.05$$

when the sampling rate is 10 times the Nyquist rate. We have

$$R_d = \frac{(1-k)^2\, \Gamma^2}{1-T^2} + \frac{k^2\, \sigma^2}{\pi\gamma\,(1-T^2)}\ \mathrm{Tan}^{-1}\ \left(\frac{1+T}{1-T}\ \mathrm{Tan}\ \pi\gamma\right)$$

where

$$T = (1-k)\, e^{-\Delta}$$

To show the difference between the use of the continous-time model versus the discrete, we have plotted in Figure A-3, the ratio of R_d to corresponding error for the continous model for $g^2 = \frac{\sigma^2}{2B}$, as a function of γ. Note

that as the sampling rate increases, the error on the discrete-model increases. The increase depends on the noise bardwidth B, increasing with B.

Similar calculations carried out for Case 2 are plotted in Figure A-4 where the continous-time model uses $g^2 = \frac{\sigma^2}{\pi f c}$. The curves are similar. Note that again the substantial increase in error for the discrite-time model for $\gamma = .05$, corresponding to the situation in our flight-test data.

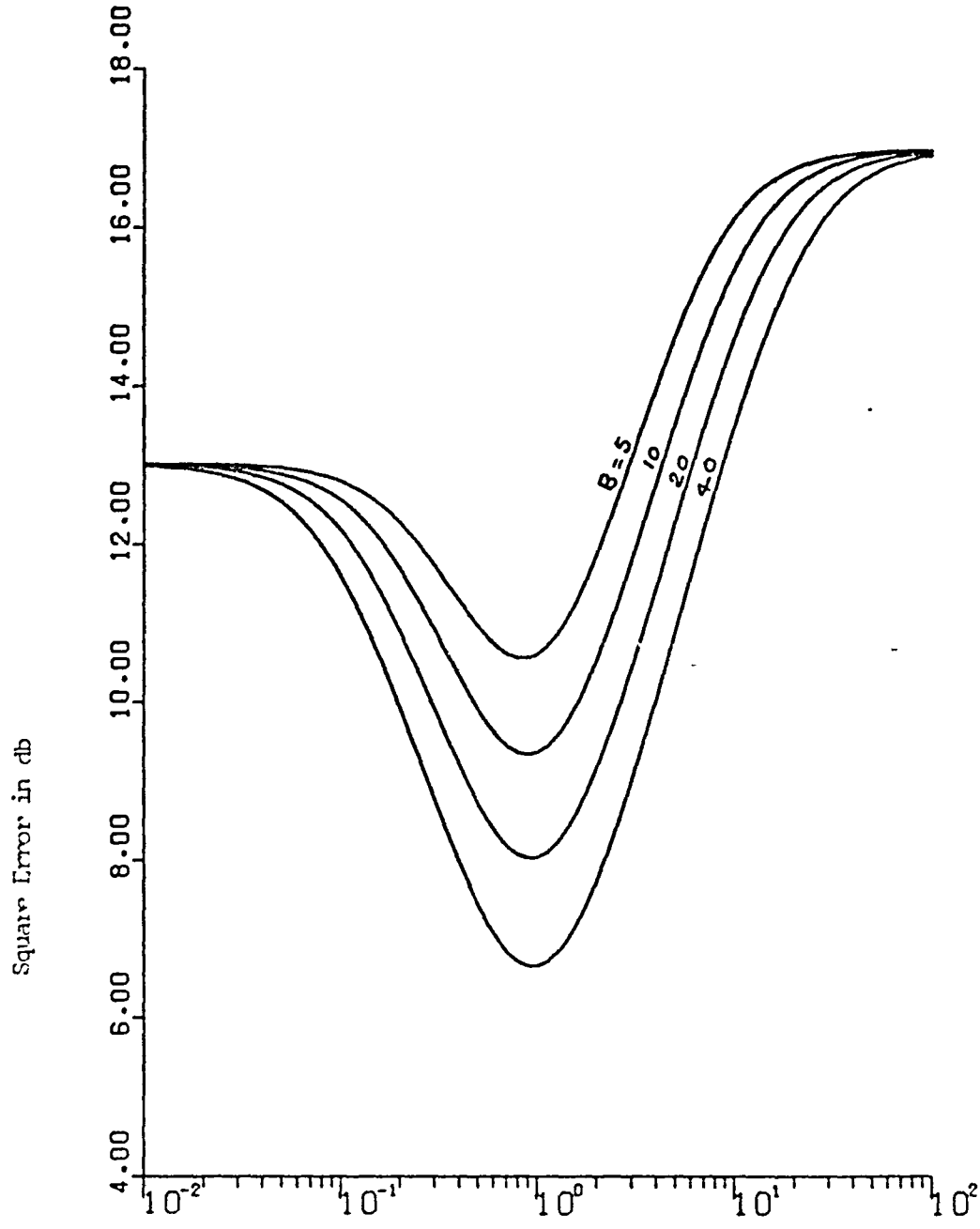

Fig.A.1: Effect of g on the Filtering Error (Case-I)

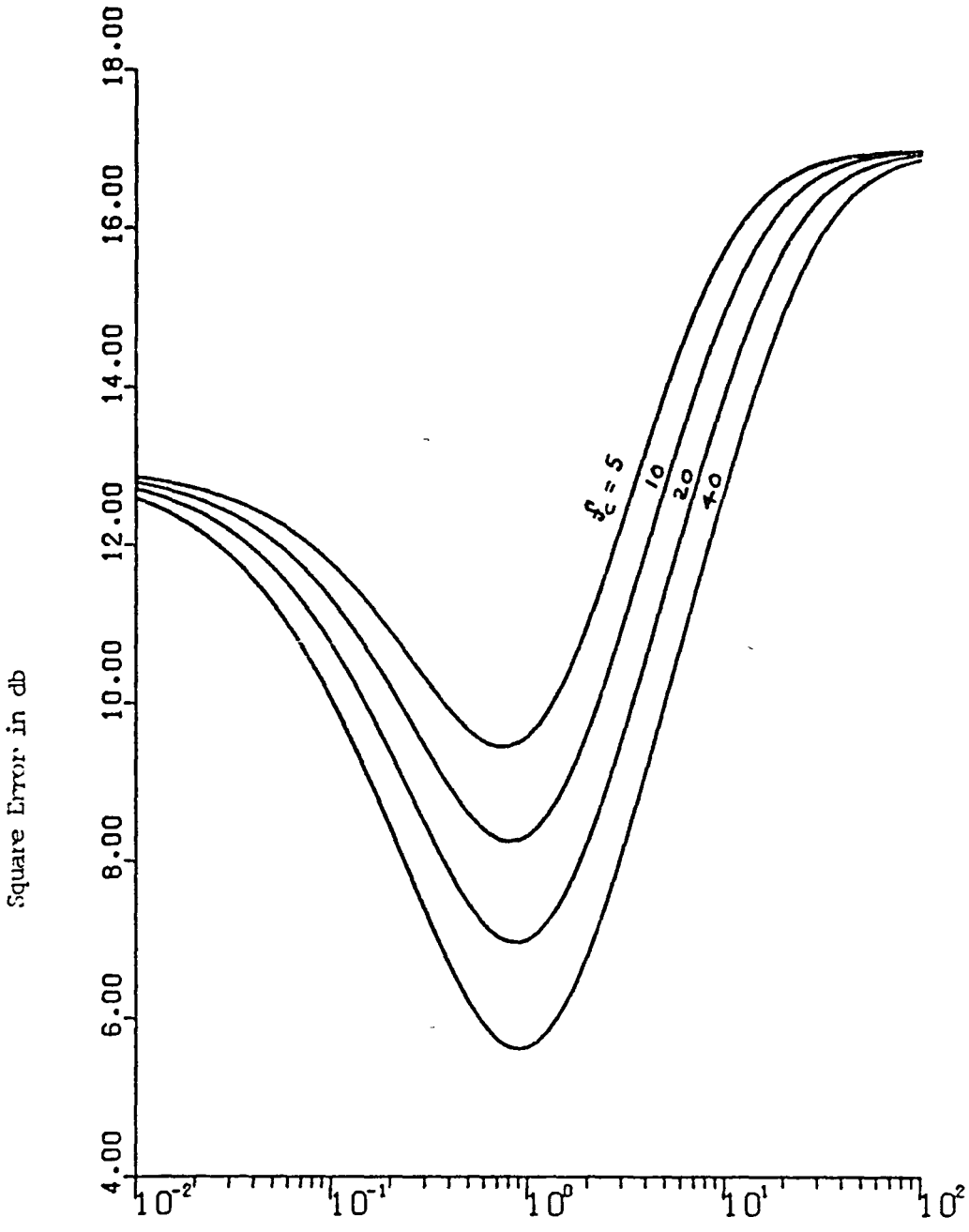

Fig. A.2: Effect of g on the Filtering Error (Case-II)

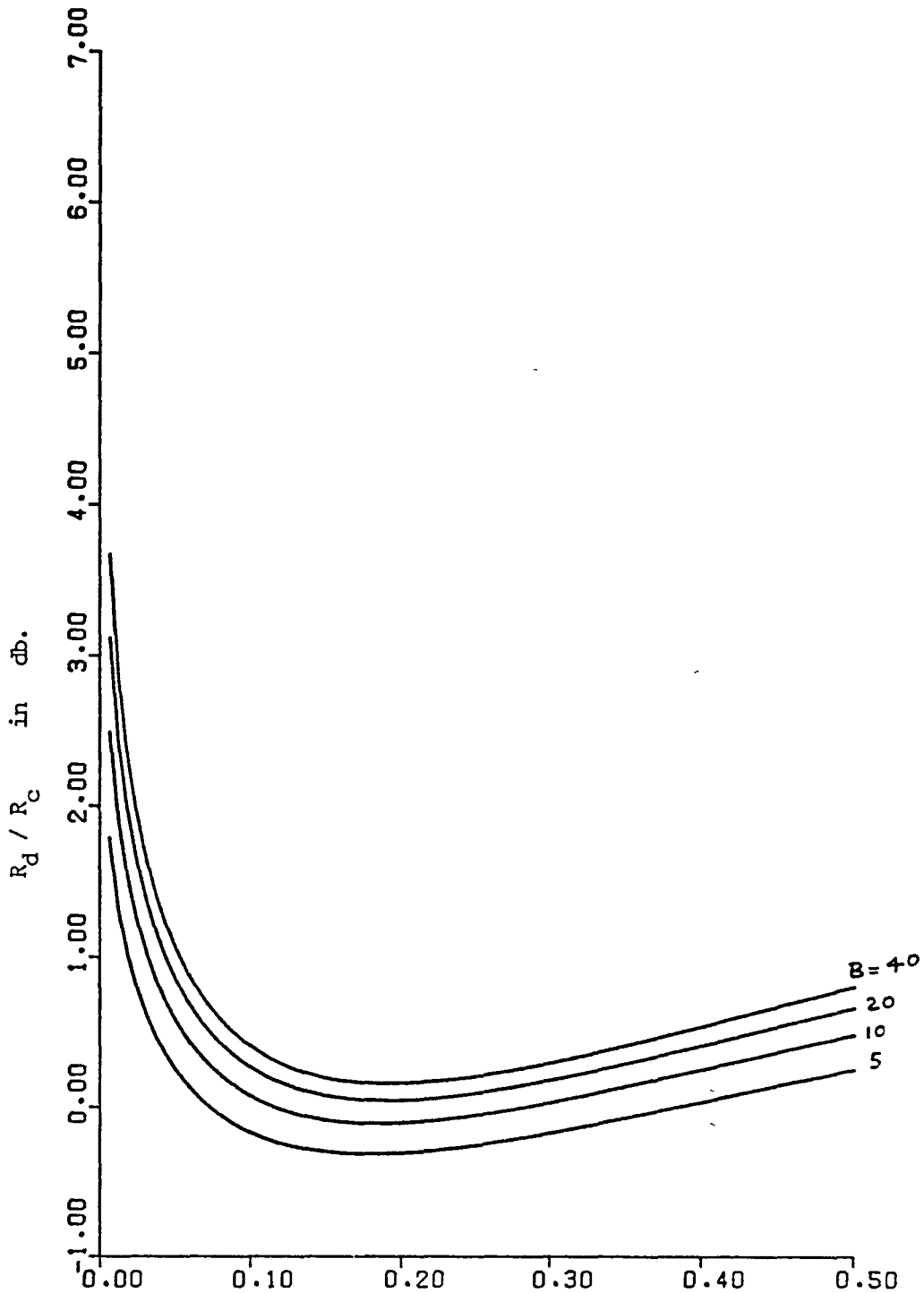

Fig. A .3: Ratio of Discrete Filtering Error to Continuous Time Filtering Error at $g = \frac{\sqrt{\alpha^2}}{2B}$ (Case-I)

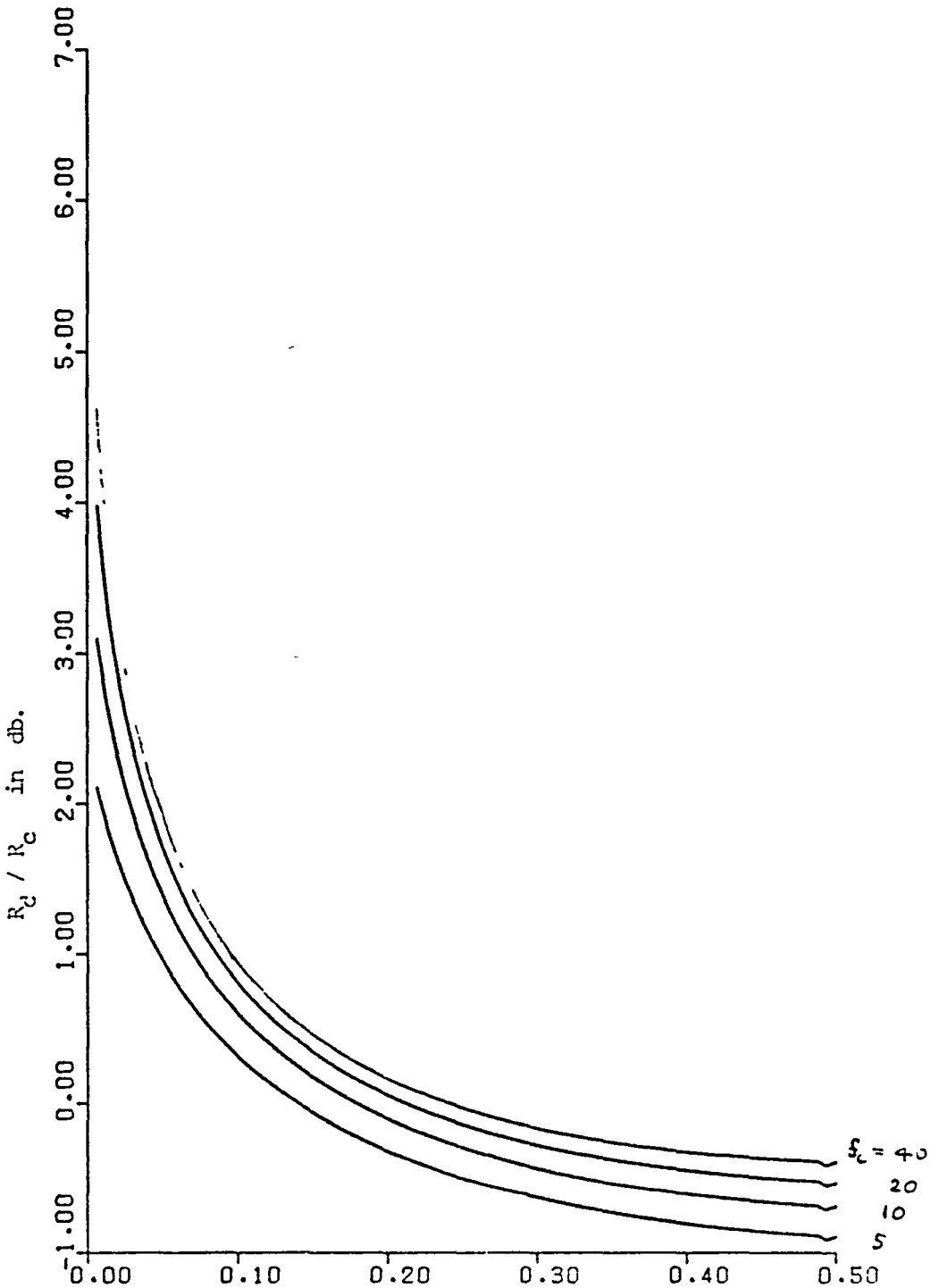

Fig.A .4 Ratio of Discrete Filtering Error to Continuous Time Filtering Error at $g = \sqrt{\frac{c^2}{\pi c}}$ (Case-II)

End of Document